Structural Design of the Transition Segment for an Onshore Wind Tower using different steel grades

Author: Muhammad Farhan

Supervisor: Prof. Carlos Alberto da Silva Rebelo

University: University of Coimbra

European Commission
ERASMUS
MUNDUS

University: University of Coimbra
Date: 31.01.2017

DEDICATION

Upon completion of my master's study of Sustainable Constructions under Natural Hazards and Catastrophic Events (SUSCOS) under Erasmus Mundus programme funded by European Parliament, this thesis is dedicated to all those who have helped, supported, shared joy and gone through difficulties with me during the last two-year period of study. This thesis is dedicated to my ***Parents*** *and* ***Teachers*** *who taught me the value of education and never failed to give me moral support in every step of my life for which I am now here at this stage and for teaching me that even the largest task can be accomplished if we have the right will and use our energies in the positive way. I am deeply indebted for their continued support and unwavering faith. I also hope that this thesis will be able to provide useful information to the exciting and upcoming hybrid onshore wind industry of my great enthusiasm.*

ACKNOWLEDGMENTS

The completion of this thesis would not have been possible without the guidance, help, patience and perseverance of number of people, who in one way or other extended their valuable assistance in the continuation and completion of this project. Most of all this piece of work would never been accomplished if it wasn't for the benevolence of one above all of us, the Most Merciful, Most Beneficial Allah, for answering my prayers and for giving me the strength.

This thesis work was completed within Institute for Sustainability and Innovation in Structural Engineering, Faculty of Sciences and Technology, University of Coimbra from where a lot of assistance and help is received. Professor Carlos Rebelo approval of this thesis task assignment to me as well as his guidance, explanation and clarification provided during the period of this work is very much appreciated. Mr. Mohammad Reza Shah Mohammadi fulfilment of supervision of this thesis has helped proceeding the thesis progress. In addition, Mohammad Reza Shah Mohammadi has provided much practical help, guidance in understanding whole work without which the thesis could not be completed in a smooth progress. Besides this they shared their knowledge unselfishly, so I may say that my expectations were even exceeded and I know the thesis could not be completed without their help. It has been for me an honour and privilege to work and learn from such experts, and I am sure it will help me a lot in the future.

ABSTRACT

With the emerging concept of sustainable constructions, the need to fight global warming has led to increased interest in renewable energies and consequently, wind industry is undergoing prosperous development and advancement which comes out as a call of global energy strategy and environmental issue. One of the most critical challenges for onshore wind turbine involves the optimal design of support structure including foundation and turbine tower. With the development of onshore wind industry heading for higher altitudes, new support structural concept might be proven to be more advantageous than conventional types when comparing in terms of cost, safety, innovative erection procedure, low maintenance and environmental aspects. In order to deal with such a problem a new hybrid tower solution was proposed. The solution is targeted at tall onshore applications which are more effective in energy generation in situations where wind shear profile is clearly benefiting higher turbines.

Hybrid lattice-tubular towers requires a transition piece which serves as a connection between lattice and tubular parts. As the transition piece is supposed to transfer all the dynamic and self-weight loads to the lattice and foundation, these structural elements present unique features and are critical components to design and ought to resist strong cyclic bending moments, shear forces and axial loads. Well-designed transition pieces with optimized ultimate state and fatigue capacities for manufacturing, contribute to the structural soundness, reliability and practicability of new onshore wind turbines hybrid towers.

This research mainly focuses on design and investigation of the transition piece for an onshore 5MW wind turbine hybrid tower as a reference. Using the simulated loads from an aero-elastic simulations and considering the geometrical, functional and mechanical requirements the transition piece was designed for ultimate limit state with considering nonlinearities and imperfections included into the finite element model. Different case studies were presented in this thesis with the aim to exploit different possibilities and broader the concept of research. Furthermore, analysing and comparing them on the basis of functionality and economics gives us greater sense of picking a viable option. In this research mainly the focus was to analyse the solution using a stiffener, transition piece using different grades of steel in different sections, using only mild steel grade and just utilizing high strength steel.

A simulation methodology for predicting the fatigue life of transition piece was used by performing elastic FEA analysis and importing the resulting stressses into the fatigue prediction software. A multi axial strain-life simulation is then performed to determine more realistic fatigue hot spots and life time of the transition piece. It is envisaged that more probabilistic approach should be used for fatigue life prediction, in which wind speed is constantly changing over service life as in this case only extereme wind conditions were studied.

TABLE OF CONTENTS

FIGURE INDEX

TABLE INDEX

Chapter 1 INTRODUCTION

1.1 Overview

In present era global warming has become the most talked environmental issue of today's life and is doubtlessly one the greatest concerns to the world. Once it became a priority issue, governments, corporations, and individuals from all around the world are debating the best and possible solutions and in order to encounter it and it's necessary to invest in the development and optimization of the use of renewable technologies. Renewable energy is the energy that relies on fuel sources that restore themselves over short periods of time and do not diminish such as the wind, sun, wave or tidal, the earth's heat (geothermal) and waste material (biomass).

Today, while energy production based on the burning of coal and oil or on the splitting of the uranium atom is meeting with increasing resistance, regardless of the various reasons, the re-emergence of wind power is an almost inevitable consequence. In today's world alternative energy resources are becoming increasingly more important considering the limited fossil fuel resources and the wild competition to obtain them[1].

It is worth noticing that wind is a clean and sustainable fuel source; and it does not create any greenhouse gases emissions or toxic substances. The fuel sources do not contribute to air or water pollution, and will never run out as it is constantly replenished by energy from the sun. Therefore, the wind energy market has a significant influence when it comes to energy installations. According with the EWEA, wind power was the renewable energy with the most capacity installed with a total of 12800 MW, an increase of 6.3% on 2014 installations, where 9,766 MW were onshore and 3,034 offshore. Wind power was the energy technology with the highest installation rate of 44.2 %, in 2015 as shown in **Figure 1.1**[2].

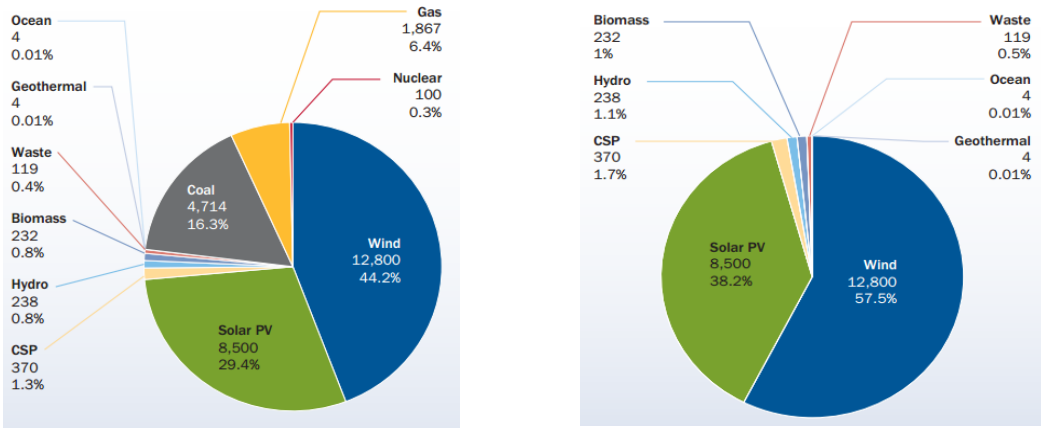

***Figure 1.1**:* Power Capacity installed a) Power Capacity installed in EU b) Renewable Power Capacity installed in EU [2]

Regarding the evolution of wind power installations in the EU it can be ascertained that it has been increasing over time. Annual installations of wind power have increased over the past 14 years, from 3.2 GW in 2000, to 12.8 GW in 2015, at an annual growth of 9.7%. As we can see in the **Figure 1.2**, a total of 141.6 GW is now installed in the European Union.

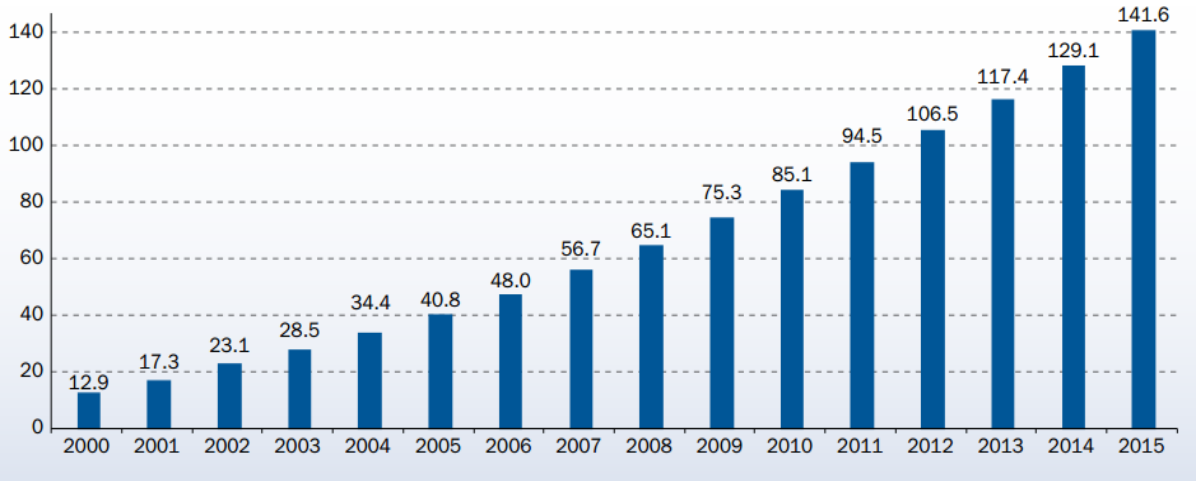

Figure 1.2: Cumulative Wind Power Installation in EU [2]

Across the world, many countries are installing a large quantity of wind turbines in order to achieve a higher percentage of electricity produced by this type of source. From the last 15 years, the global wind capacity installed is getting bigger each year, which shows the importance that this kind of energy type is having for all the countries. Popular Republic of China, Germany, USA and Latin America were the countries that got most installed capacity in the year of 2015 [3]. They are also the ones with higher cumulative capacity by December of the same year.

The world needs the development of wind energy among other renewable energies, because when the resources of fossil fuels run out, humanity will need electricity and renewable energy will be the only alternative. There is one forecast of which you can already be sure: someday renewable energy will be the only way for people to satisfy their energy needs. By that, new technologies and new ways of construction have to be investigated, in order to get the maximum of this resource. With the increase of the capacity of the turbines, from 0.5MW to around 7 MW, although turbines between the 2 and 5 MW of capacity are the most popular and common, the wind towers need to increase the structural strength and the stiffness that is required to support such turbines.

According to [1], the transportation and the erection procedure is developing into an increased problem for the last generation of multi-megawatt wind turbines. With heights of more than 100 meters, the required diameter at the tower base is more than 5 meters, which are not suitable for the road transportation. This problem becomes a strong incentive to find

innovative solutions in the tower design, for the wind energy continues to maintain the competitiveness in the future. Due to these upcoming challenges, the process of commercialising and monopolisation of wind turbines has driven governments and big companies to build bigger wind turbines which also helps other sectors to increase their productions. However, even though having the technology to build bigger parts or segments of towers is not enough to overcome some other problems explained before. Consequently, using smaller parts that can be assembled on site to build towers such as lattice towers was considered to be an option to avoid such problems. To have an opportunity to build higher lattice towers seems to be a good solution, yet the need to improve any invention persists. As well as the invention of different lattice towers, some inherent weaknesses of any structure like fatigue is still of a concern for such inventions.

1.2 Motivation

The overall motivation comes from the need of efficient and higher energy producing wind turbines. Currently for onshore installations the 2.5 MW wind turbines are economical. However, the quest of reaching higher capacity wind turbines is still there. For achieving higher capacity, higher wind speed is required with less turbulence. This can only be accomplished by building higher wind towers at the altitude of 150 to 220m. As the height increases the rated wind speed increases as well which can be make use of building innovative concepts wind turbines. However new concept brings new challenges with it. The assembly and maintenance are getting more difficult and expensive with the increase of the tower height. Because with the increase of tower height, the diameter of the tower on ground level increases. This brings to the major problem of transportation of the extra size tubular parts, very difficult and even in some places impossible due to road standard and logistics. However, it is not only the dimension but also the weight of the structure which cause road surface damage.

Since the exploitation of wind energy is rather mature, compared to other renewable energy facilities, various structural concepts have been presented and installed so far. The main difference of these concepts lies in the structure supporting (Tower), the wind energy converter itself and the design of the rotor blades. Depending on the site conditions, wind turbines are designed differently. The most innovative concepts in the construction and the material are usually applied on the supporting structure. In order to overcome the transportation and height limits, industry is moving towards building hybrid concepts of wind towers in order to achieve higher heights e.g. hybrid concrete-tubular tower and hybrid lattice-tubular tower. This thesis will be mainly focus on the later hybrid concept of wind towers. Many companies had already designed and implemented such type’s hybrid concepts like Suzlon Energy and Ruukki.

Which brings to another main parameter in the consideration that is when aiming higher altitude, you need bigger cranes to assemble whole wind tower. The cranes' costs exponentially increase with the increase of the cranes' size. So keeping in mind these constraints of transportation and lifting there was a need of novel concept of hybrid lattice/tubular tower which have an innovative solution for all these challenges to achieve higher height with less transportation and installation limits. The hybrid supporting structure consists of three main parts: Tubular tower as the upper section, lattice structure as the lower section and the transition piece which is the key component to connect the lower and upper section together. This thesis will mainly focus on designing transition piece.

1.3 Objectives

The inclusive objective of this thesis was to put a small effort in ongoing improvement of cost-effective wind technologies, which is to develop higher and more resistant towers to withstand stronger winds, which are located at high heights where the turbulence is comparatively less, and to take the advantage of more powerful turbines. So, increasing the hub height, the diameter of the tubular portion turns out to exceed the maximum allowed limit for the current transport. Therefore, the industry is demanding the development of a hybrid solution that corresponds in the design of a lattice segment, which should support the tubular part.

In this research the major objective will be the structural assessment, cost effectiveness and integrity of the new hybrid lattice-tubular tower solution corresponding to the transition piece which is employed as a connection between the lattice and the tubular tower. Transition piece is a critical design component which needs careful detailing. In order to ensure good behaviour of the hybrid tower, the transition segment has to ensure the correct transmission of the internal forces from the tubular tower to the lattice support structure. Due to the high level of bending moment, torsional moment and axial compression, the transition segment needs to have a high level of stiffness. So, it was then proposed the development of a unique solution for the transition segment as well as ensuring the proper transmission of efforts that could allow a new type of erection system for the tubular section by a slide procedure. Moreover, the transition piece should withstand the transient loads and equipment weight during self-lifting slide process. Although in this project, only the final stage of the transition segment was analysed. Construction phase and erection procedure were not objects of study during this project. Finally, the solution of transition piece was optimized by analyzing ultimate limit state and calculating possible fatigue life to ensure the structural reliability and feasibility of new onshore wind turbines hybrid towers.

1.4 Content of the thesis

The thesis is divided into six main chapters.

Chapter 1 provides the overview with statistical information as well as impacts of the wind power in the European Union and rest of the world, following with the motivation on basis of which this research is carried out by outlining the main objectives to be achieved.

Chapter 2 contains the state of the art describing how the wind turbines evolved over the period of time with general background information about previously installed wind towers and their types. Information about existing transition segments used in offshore with jacket foundations together with onshore new concepts on transition segments in hybrid lattice steel wind towers are summarized. Moreover, a theoretical background of fatigue is discussed with basic concepts and newly adopted procedure and algorithms used in fatigue analysis from FEA analysis are described.

Chapter 3 briefly presents the methodologies used for ultimate limit state, describing different types of analysis which are performed. Furthermore, frameworks used for plastic limit state and buckling limit state are discussed in detail. Lastly methodology used for calculation of fatigue life is explained pertaining to elastic FEA analysis.

Chapter 4 is divided into two main parts. In the first part all the requirements (geometrical, functional and mechanical) for the conceptual design of transition piece are presented which directly influences the design and implementation. In the second part different case studies were presented which will be further studied and analysed for ultimate limit state.

Chapter 5 explains into details all the steps and techniques used in 3D nonlinear finite element model of transition segment, modelled in ABAQUS program, with particular reference to some general issues in creating the model such as – boundary conditions, assembly and interactions, load point, element type, mesh size, material models etc. Furthermore, results from FEM analysis for all case studies are presented for plastic limit state. Case study 3 and 4 are further analysed for buckling limit state and fatigue life based on procedure described in methodology chapter.

In chapter 6, which is the last one, the main conclusions of the thesis are briefly underlined. Also, some ideas on the possible future work and the further development of this study are pointed out.

Chapter 2 STATE OF THE ART

If we don´t perceive from where we have come from, we cannot know where we are heading. So, when discussing and investigating wind towers and wind turbines, knowing the historical roots of wind power technology is an absolute need, because the successes and failures of the past will provide hints and clues for the future research and development. With this, the following state of art starts with a background on the origin for the use of the wind, in order to understand the present use for this resource.

2.1 The origin of Wind Mill

There is not any substantial proof about the historical origins of windmills, but some authors maintain that remains of stone windmills were found in Egypt, near Alexandria, with an estimated age of 3000 years. However, there are no certainties that the old empires such Greeks or Romans really knew and used windmills. The first reliable information a date forms 644 Anno Domini, and a later description of the year of 945, and describes a vertical axis windmill, see **Figure 2.1**, used for milling grain, from the Persian-Afghan border. Some centuries later, the Chinese were also using windmills to drains rice fields; the first known windmill in China is documented in 1219 A.D. It was a grain grinding mill, but it´s not possible to determine the year in which they started to use the wind as a power source to their activities.

Figure 2.1*:* Afghan wind will with vertical axis (oratoryorphanage.org)

The more traditional windmill with a horizontal axis was invented in Europe, independently of the existing vertical axis of rotation. The first information has its origin in 1180 in the Duchy of Normandy, which quickly spread to the North and East of Europe. In Germany, numerous post windmills could be found in the 13th century. In Holland, several improvements were made in the 16th century, leading to a new type of mill called “Dutch

Windmill". In this type of mills, the capacity of the tower cap to turn with the wind wheel permitted an increase of the applications for this type of structure.
In addition to the post windmills that were entirely made of wood, in the Mediterranean region, a traditional type of windmill, the so-called "Tower Windmills" make their appearance one or two centuries later. This type of mill mainly spread from the Southwest of France, to Greece and Italy, and are frequently referred as the Mediterranean type of windmill[1].

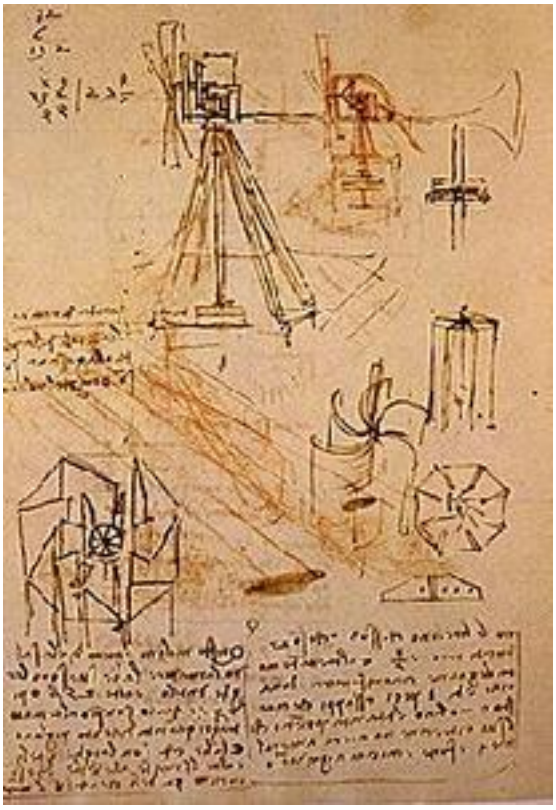

***Figure 2.2**:* Da Vinci's studies of a windmill (discoveringdavinci.com)

2.2 Technical Developments of windmills

In order to increase the performance of these types of structures, a systematic research and development were made, with an empirically founded evolution, based on experiment of new kinds of windmills and wind wheels. The first fundamental ideas concerning the design were raised in the Renaissance period, with Italian artists like Leonardo da Vinci and Veranzo, whose sketches and investigation, proposed various interesting design for vertical axis wind wheels shown in **Figure 2.2**. Only in the 17th and 18th century, wind technology was systematically considered for the first time. Names like Gottfried Wilhelm Leibniz (1646-1716), Daniel Bernoulli (1700-1782) and the mathematician Leonhard Euler (1707-1783), were the first to involve them in the matter, and to apply basic laws for the improvement of the sails for the windmills.

With new technologies and materials, this rudimentary wind turbine evolved until nowadays for a very complex machine, able to generate an amount of electricity that can sustain hundreds of houses. But, in order to get the most advantage of the wind, in a higher altitude, these turbines have to be assembled in a high tower, capable of supporting all the stresses, principally the wind and the self-weight. They have been in a constant development, such as the blades, and now, new types of tower are needed, in order to get a better performance of the existent technology.

2.3 Wind Power Turbine tower structures

The high tower is an essential part of the horizontal-axis turbine, a fact that can be positive and at the same time a disadvantage. The costs are, obviously, a disadvantage, which can grow up to 30% of the overall turbine costs[1]. As the height of the tower increases, transportation, erection and assembly become increasingly higher, but on the other hand, the energy yield also increases with the tower size.

The advantage of increased height was recognized and the old mill houses became slenderer and with an aspect of a tower. In average, the increase of 1 meter in the tower height brings a gain in the energy yield between 0.5% and 1%, depending on topographic conditions. So that, the optimum tower height can be determined from the point of economics, the increase in the cost of a higher tower must be compensated by an increase of the energy yield of the turbine. But, the previous choice must be what type of tower is better for the programmed installation. As a consequence of the development, designs and materials for towers increased in variety. Steel and concrete took the place of the wood, used to build the old windmills. In the early years, many designs and materials were tested in order to erect these towers, but the range of different types has narrowed to the most common, a free standing tubular steel tower, rarely made out of concrete.

Supporting structures for wind turbines are often tubular structures made of traditional structural materials, namely, steel and concrete. There are also hybrid concrete/steel wind turbine towers in which combination of concrete and steel tubes are used in the lower and upper part respectively. Most commonly pre-fabricated concrete segments and steel tubes with maximum diameter of about 4 m are transported by the truck to the site. Increasing requirements in efficiency and competiveness of wind turbines in generation of electrical energy lead to larger swept area, meaning the longer rotor blades, and higher hub height. Such developments, towers higher than 100 m were favourable for development of steel lattice towers[4] which leads to larger tower base diameter.

2.3.1 Concrete Tower

Wind towers can also be made of reinforced concrete. Despite the fact that concrete towers are not widely used, this type represents a good solution when towers need to be 100 m tall or more. Moreover, the increased steel price together with the development of new efficient

production techniques has led to an increased number of concrete towers. Concrete towers, like all other concrete structures, have reinforced steel and make use of bridge technology. Post-tensioned reinforcement can also be achieved and implemented in concrete wind towers. It is worth noting that concrete towers can be made in the following ways:

- Site-mixed concrete
- Prefabricated concrete towers

With the traditional reinforced-concrete type of construction, the concrete is either mixed in liquid form on site or delivered in special vehicles as is done in most cases today. The concrete is poured into a timber form into which the steel reinforcement has first been inserted in the form of a steel wire mat. In this formwork, the concrete hardens so that the required shape emerges when the boarding is removed[1].

***Figure 2.3**:* Concrete Tower for Wind Turbine (www.acciona-windpower.com)

A great stiffness and robustness associated with the low maintenance that is required by these towers represent the great advantages of this type of towers. The long construction period is doubtlessly the main disadvantage of these towers. Nevertheless, with the development of prefabricated parts it can be shortened. Combining a proper design and production in accordance with the today's rules/legislation, these towers do not need maintenance during their expected life cycle. However, a prototype of the Enercon E-112/60.114 with a total height of 124 m has already been built using this method **Figure 2.3**.

In a concrete tower the concrete proper only withstands pressure. The ability to absorb tension is provided primarily by pre-tensioned tendons, located in ducts in the concrete or

internal/external of the concrete walls. Making them internal or external enables easy inspection. There are also traditional un-tensioned reinforcement bars cast into the concrete shell, necessary to provide the compressive strength.

A concrete tower is clearly dimensioned by the extreme load case, since it has large margins towards fatigue. It is assumed that the concrete is pre-tensioned by the tendons to 20 MPa. In the extreme load case the pressure side is offloaded to close to zero whereas the tension on the other side is doubled. By increasing the thickness of the concrete cover it may be possible to increase the lifetime to e.g. 50 years. One concrete tower may then serve for two generations of machineries, with obvious economical savings **Figure 2.4**. Compared to steel towers, concrete towers are much heavier and takes longer time to erect. On the other hand, the concrete or the concrete elements, if made small enough, are not subject to transportation restrictions, as for the case with welded steel towers with large base diameters[4].

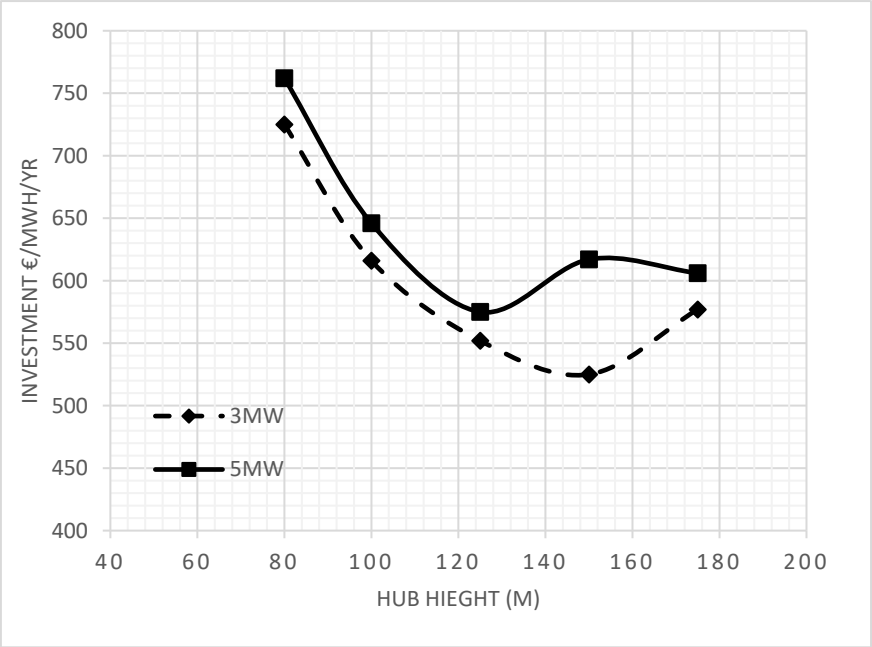

Figure 2.4: Summary of specific investment cost for 3 and 5 MW wind turbines furnished [4]

2.3.2 Welded Steel Tubular Towers

The welded steel shell tower today dominates the wind turbine market. Steel tubular wind towers are by far the most used in the onshore market of wind power. These towers are composed by 3-4 segments, which are individually transported and assembled on site using bolted connections. It consists of cylinders made of steel plate bent to a circular shape and welded longitudinally **Figure 2.5**. Transversal welds connect several such cylinders to form a tower section. Each section ends with a steel flange in each end. The sections are bolted to each other. The bottom flange is connected to the foundation and the top one to the nacelle.
In order to reduce the used material and achieve a greater efficiency the towers are conical: the diameter has its maximum value at the base decreases towards to the top. Furthermore,

increased wind power, i.e. turbine power, increases the loads, bending and torsional moments acting on the structure. In order to withstand the increased loadings, the dimensions of the tower must be increased, i.e. both diameter of the tube and the thickness of the plate, tube wall, must be increased, which lead to further implications[4].

A tower is primarily dimensioned against tension and buckling in the extreme load cases. Ideally the margin should be the same for both criteria, since increasing the diameter, with a corresponding reduction of plate thickness, increases the tension strength but reduces the buckling margin. Finally, the tower has to be checked against fatigue. According to BSK and Euro code connecting welds (transversal and longitudinal) and dimension changes flanges affects the strength in a negative way. Thus it is the welds and the geometry that primarily determine the fatigue strength rather than the quality of the steel. Therefore wind turbine towers mostly use ordinary qualities of steel. Ring flange connections result in high fabrication cost and long delivery times. Another disadvantage of such connections is their low fatigue resistance which is approximately 50 MPa

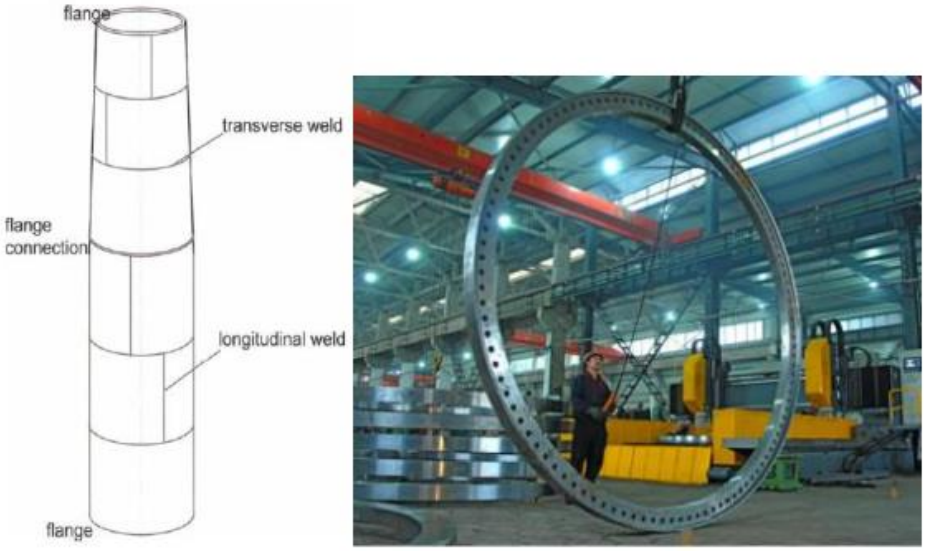

***Figure 2.5**:* Steel tubular tower in two sections and ring flange [4].

The bolted connection is achieved with a flange, which is welded to the top and bottom of the tubular segments and bolted traditionally **Figure 2.6**(a). However, a High-strength tower in steel for wind turbines (HISTWIN) is developing an innovative solution of assembling joints using friction connection with opened slotted holes which are currently under investigation **Figure 2.6**(b).

Due to transportation limitations the diameter may not exceed 4.5m [4] since it is the practical limit for the diameter of complete ring sections that can be transported along the public highway. Apart from that in terms of production, is difficult to have plates thicker than 50 mm, although steel tubular wind towers with 150 m of hub height have already been produced.

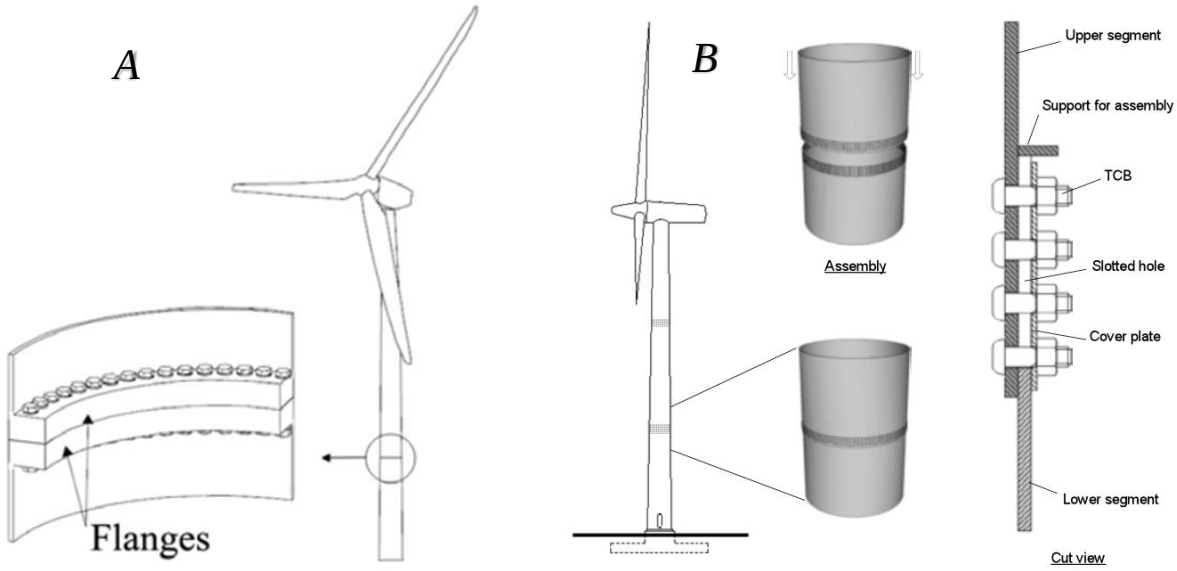

***Figure 2.6**:* Different methods for the assembly of the tubular segments A) Traditional welded flange bolted connection B) Friction connection (Histwin, 2012)

Wind towers are exposed to an extremely aggressive environment, especially those who are in coastal areas. To prevent corrosion a special sandblasting procedure is usually applied which consists of placing an epoxy resin coating to the tower surface. With regard to the tower foundation, it must comply with local rules and regulations; the foundation must be designed according to the local soil properties.

2.3.3 Lattice/Truss Tower

During the first years of commercial wind energy utilization, lattice towers were widely used in small turbines. As their sizes increased, steel tubular towers increasingly displaced the lattice towers. Recently, the interest in lattice towers has been rekindled, particularly in connection with large turbines with a hub height of 100m and more[1]. Steel lattice structure is a very well-known method that is used to build a wide range of tower types, such as energy transmission lines, and they were even used to support wind turbines in the beginning of wind energy exploitation.

Lattice towers have been used in large numbers for smaller wind turbines, especially in non-European countries. For larger turbines they have mainly been a choice when a stiff (under-critical) tower was needed. It is clear that they often are considerably lighter than towers based on other technologies. The physical background to this phenomenon is the large widths of the lower sections. The need for material to take strain or pressure is inversely proportional to the width. With a tubular section a thin-walled construction will finally meet with buckling, which restrains the maximum diameter. A lattice design does not buckle like a shell. The risk of buckling of the individual members is controlled by inserting numerous struts that give the lattice tower its characteristic look. The Finnish company Ruukki is

introducing a further developed design of lattice towers based on use of hexagonal steel profiles and high strength steel, enabling lower weights and better economy **Figure 2.7** [4]. Lattice towers, in forested areas represent a great solution, since the turbine for a better efficiency needs to be above of the tree line, due truss towers are proving to be a pronounced solution for very tall towers. The highest wind tower installed so far is a steel lattice tower, whose installation was completed in 2003, and it holds 160 m of hub height and is known as Fuhrländer Wind Turbine Laasow **Figure 2.7**.

Figure 2.7: Lattice tower by Fuhrlander on left and by Ruukki on Right (epoznan.pt)

Nowadays, the lattice tower has again become an alternative to the tubular-steel tower in the case of the very high towers required for large turbines sited in inland regions[1].

2.3.4 Hybrid Concrete-tubular steel towers

The idea behind building a hybrid concrete/steel tower is to use concrete in the wide lower part and steel in the upper part, where a conventional welded steel shell tower section may be designed without any risk of conflict with the transportation limitations. In reality it also makes it easier to design the concrete part and to get the Eigen-frequencies right. Nordex developed a new turbine N90/2500 (LS) that is supported by a 120 m hybrid concrete-steel. The bottom part is 60 m tall and is composed by several concrete parts where the lowest part has 8 m diameter and supports all steel tubular segments. The main disadvantage is the long construction time and the need for large cranes to assemble the towers[5]. GRI (Global Reporting Initiative) Hybrid Towers provide the wind industry with innovative solutions that address the challenges posed by new generations of turbines, based on proven reliability of steel and the capacity of precast concrete to solve the weaknesses that steel alone is unable to do. The precast concrete segments are transported individually, and when the foundation is completed they are assembled on site **Figure 2.8**. The steel tubular segments are assembled when the concrete part is completed.

***Figure 2.8**:* Crane assembling the precast concrete parts on left and on right side GRI hybrid concrete- steel wind tower (www.gri.com)

2.3.5 Hybrid Lattice Steel Tower

Use of hybrid towers is possible to achieve greater heights for the turbine shaft. This type of towers is composed of three parts, the lower lattice part fixed to the foundation and assembled at the installation site, a piece of tubular tower consisting of several parts bolted together, as happens in most tubular towers, and a transition piece which ensures the connection and transmission of efforts between the two main parts.

***Figure 2.9**:* Suzlon Energy 120m hybrid lattice-steel tower (www.suzlon.com)

A tower of this kind was installed at the wind farm in Gujarat, India by Suzlon Energy some years ago (**Figure 2.9**). It is expected that this new type of towers produces about 10 to 12% more energy, because gains against the normal towers more than 40 meters in total height, with a combined height of 120 meters against the 80 meters of most tubular towers, therefore an ideal bet for low wind areas, due to its superior performance, with a potential to be installed in all parts of the world, without having to look for places where the wind speed is high. These towers can be climbed from the inside, and have platforms inside the tubular part for maintenance and repair work, but also to maintain all the equipment necessary for its operation.

2.3.6 Increasing the height with different tower concepts

As we have seen before, in the initial phase of modern wind turbines and wind energy, the larger wind turbines were built with comparatively low towers. With more sophisticated technology and weaker inland wind regions, the height of the towers increased significantly, and now, towers with 100 meters or more were found to be a decisive factor for the more economical utilization of wind energy. On the other hand, with the raise of the high, the costs of the towers will naturally increase. However, the different types of tower show a different relation between the height and the cost, being some of them better for higher constructions than others.

The structural mass of self-supporting tubular steel constructions and the cost of this type of towers disproportionally increase with increasing height. Added to this is the fact that the tower base section size has already reached to the limit size for road transport of approximately 4.5 meters. To overcome this restriction, towers have started to be built from slim u-shaped shells, forming a polygonal section on the base of this structure. With this, the economical factor is maintained in towers up to 140 meters high, with the disadvantage of the increase in hand work on the construction site that comes with the assembly of the different plates that complete the section. Another aspect that we cannot forget is that these types of structures are heavier when compared to other type of steel structures, such as lattice types, which cause an initial investment higher than other designs. The lattice type of tower is more suitable for achieving heights above 100 meters, because the increase of the structure mass with the height is not very accentuated **Figure 2.10**. In general, this type of construction only has 60% of the mass of a tubular steel tower. However, economically that difference only represents about 20% due to the higher difficult of assembly, and more labour work.

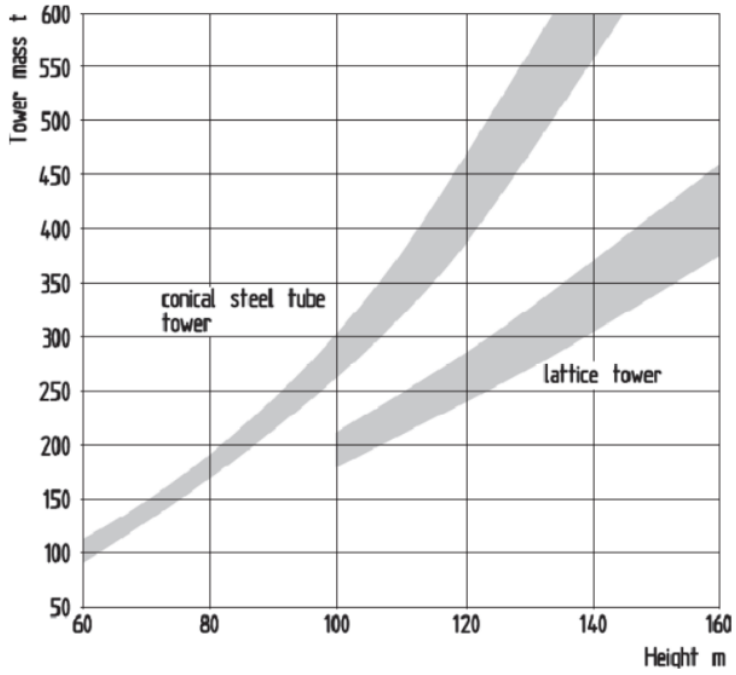

Figure 2.10: Increase of the structural mass with height [1]

The hybrid type seems to be the best way of construction, at least for towers height above 100 meters. There are a lot of hybrid towers installed, made from a pre-stressed concrete tower, assembled from pre-fabricated elements, which compound the base of the tower, with a tubular steel tower of about 25% of the total height **Figure 2.11**. These types of tower are being used by ENERCON, for towers with more than 100 meters.

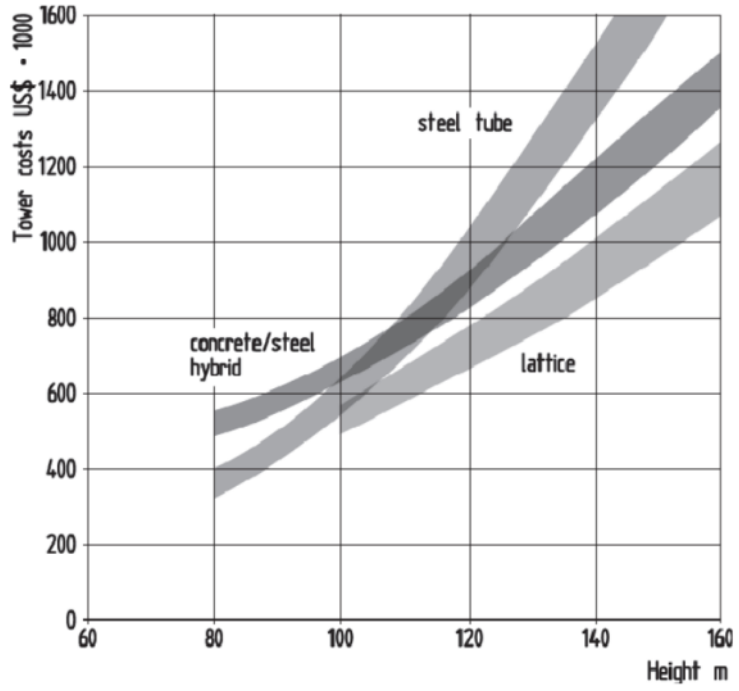

Figure 2.11: Tower costs in dependence of high for a 3 MW wind turbine [1]

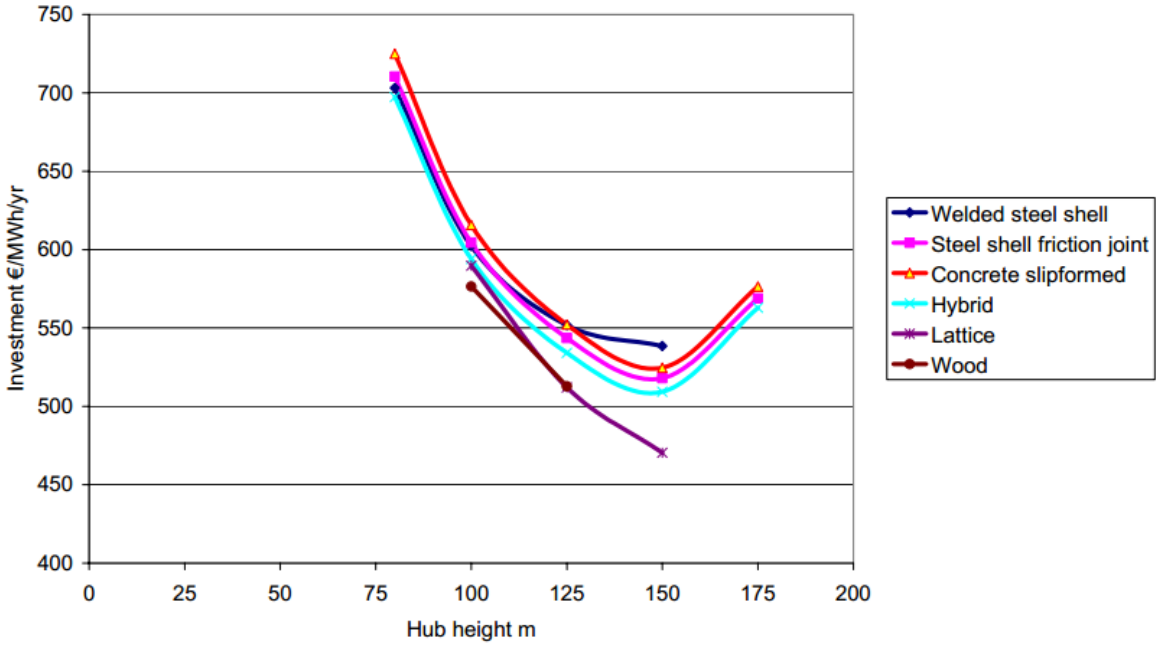

Figure 2.12: Tower alternatives for 3 MW wind turbines *(Vindforsk project)*

With this analysis, is possible to conclude that the best solutions for the wind towers are the lattice construction and the tubular steel towers. A hybrid solution between these two types seems a promising option for higher towers, because we can put together the better of each one of them, see **Figure 2.12**. A base from a lattice structure, whit higher hardness and a lower total mass, and an upper part made from a tubular part that can reach great heights. This is the study case in the master thesis, in order to perform an optimization for this new type of support for wind turbines.

2.4 Transition Piece/Segment

2.4.1 Introduction

The transition piece of a hybrid lattice-tubular onshore wind turbine shown in **Figure 2.13** serves as a reinforced part of the support structure that is connected to the wind turbine tower. These structural elements present unique features and are critical components of hybrid onshore wind turbines; design to resist strong bending moments, shear forces and axial loads coming from cyclic environmental loads such as wind loads acting during their complete design life. Well designed and manufactured transition pieces with optimized ultimate and fatigue capacities, contribute to the structural soundness and reliability of new onshore wind turbine hybrid towers.

A complex topology might meet all the requirements but it would make the manufacturing process and the transportation difficult. Although the design of transition pieces varies according to specific and individual project requirements including loading conditions, connecting structural dimension, the weight of rotor and nacelle, etc[6].The main goal of this project is to develop a conceptual design of transition piece in order to achieve a unique

solution for the transition segment for hybrid lattice-steel tubular towers. Offshore wind towers, using jacket foundations make use of a transition piece. This will be the basis for the design of an innovative solution that will allow the erection of tubular towers by slipping and, for this reason, avoiding the need for large cranes.

***Figure 2.13**:* CAD model of hybrid lattice-tubular wind turbine with transition segment (Bremerhaven prototype) [7]

2.4.2 Transition piece for early onshore wind turbine supported by lattice tower

Early development of onshore wind turbines has set up experience of how to deal with this transition piece. However, the dimension of the early turbines and their weigh cannot be compared with the multi megawatt requirement of present needs and even larger turbine units in future, not to mention whether complex functional requirements including the yaw control was taken into consideration or not in those early designs. A frame-cylinder system composed of an external steel frame of supports and an internal steel mono-column in the core is adopted in the small wind turbine of **Figure 2.14**(a). A single steel mono-column structure sitting on top of the lattice support structure and supporting the nacelle assembly is employed in the larger turbine of **Figure 2.14**(b). These concepts are somehow early prototypes for the transition piece design of the more recent hybrid offshore wind turbine support structures.

***Figure 2.14**:* Example of Lattice Tower for Onshore Wind Turbines [8]

2.4.3 Jacket Foundations

Offshore wind turbines are constituted by an upper part, which is a tubular steel tower, and a bottom part that supports the upper part; the two segments are connected by a transition piece. The structure of the bottom part can be:

- Monopile (**Figure 2.15**A)
- Tripod (**Figure 2.15**B)
- Space frame or jacket foundations (**Figure 2.15**C)
- Gravity base (**Figure 2.15**D)

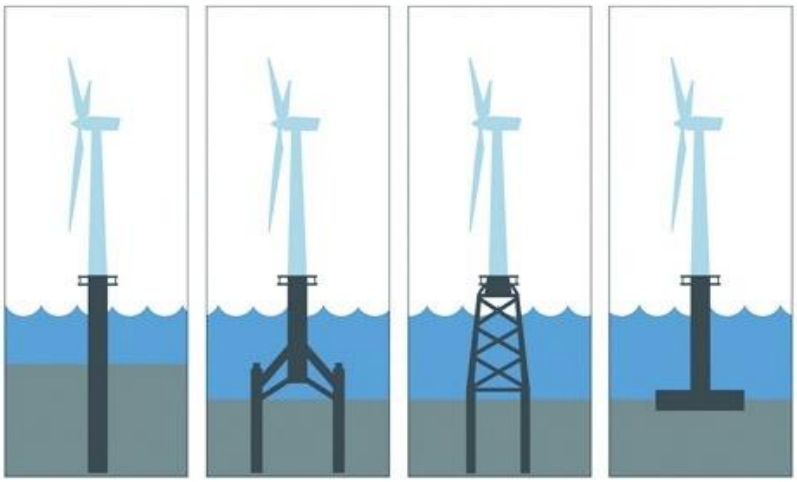

***Figure 2.15**:* Different base structures for the support of offshore towers A) Monopile; B) Tripod; C) Jacket; D) Gravity base (www.theengineer.co.uk)

A jacket foundation is similar to a lattice tower. All its members have small diameter steel circular hollow sections in a "X" configuration, which ensures a high stiffness and robustness that, in turn, withstands rough weather conditions. According with DTU (Technical University of Denmark) department of wind energy, jacket foundations can be applicable at large depths, between 60 and 70 meters. The components of a standard jacket foundation are presented in **Figure 2.16**.

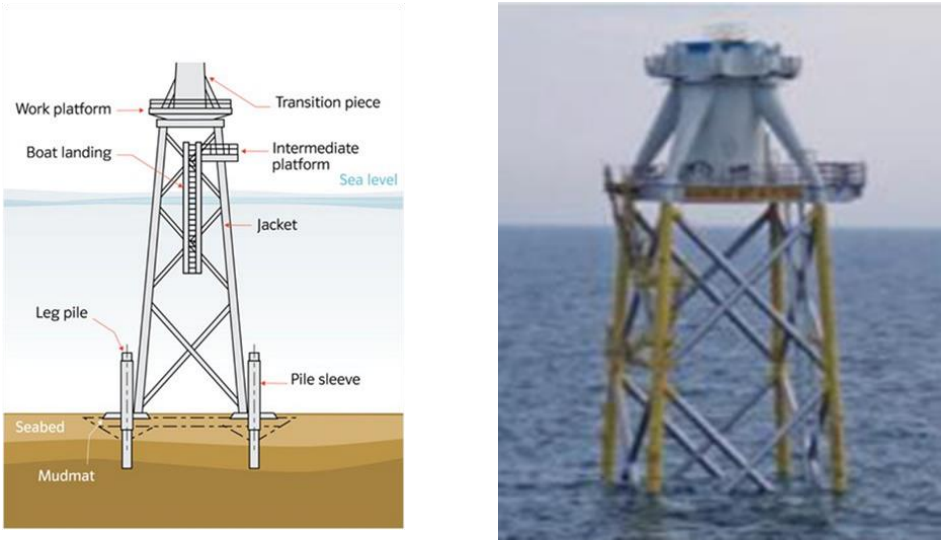

***Figure 2.16**:* Standard jacket foundation components and transition piece detail [6]

2.4.4 Hybrid Lattice-Steel Tubular tower

As mentioned in the section 2.3.5, hybrid lattice-steel tubular towers are relatively new and under development. Nevertheless, there were already some developments regarding the transition piece. In [9] a transition segment (**Figure 2.17**) with a diameter of 4500 mm, total height of 9120 mm (by overlapping two segments of 4560 mm) and whose connection with the chords members (legs of the lattice) was provided by a gusset plate was presented. The two overlapped pieces are divided in 8 parts and connected by flanges and the same gusset plate that connects the chords members of the lattice.

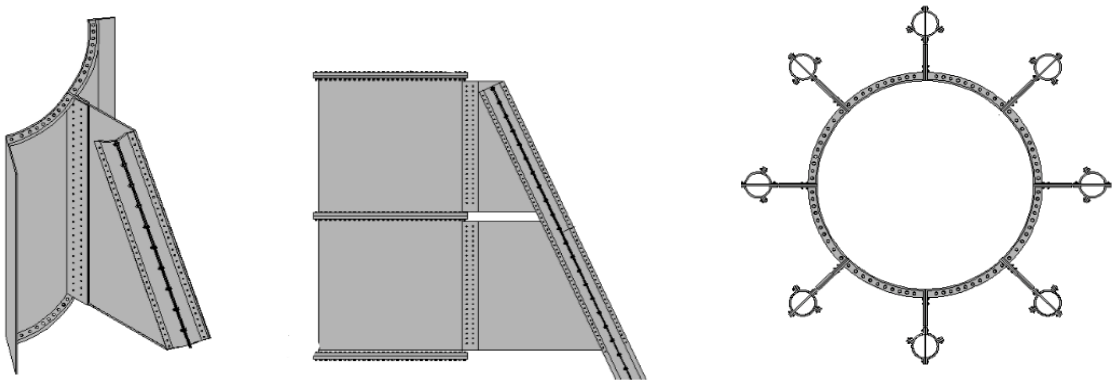

***Figure 2.17**:* Transition piece adapted from [9]

Additionally, there are several industrial Research and Development projects and registered patents which are only in the research stage Geodome Ltd developed an offshore transition piece for 6MW wind turbines **Figure 2.18**(a). The aim of the design was the reduction of structural weight and fabrication costs while the fatigue life exceeds 25 years. The transition pieces are designed for jacket structures utilized for 20m and 60m water depth[10].
SeaPlace did a full scope study on jacket structures **Figure 2.18**(b) and related areas like lifting, life cycle assessment and transition piece design basis for GL Structure Validation[11].

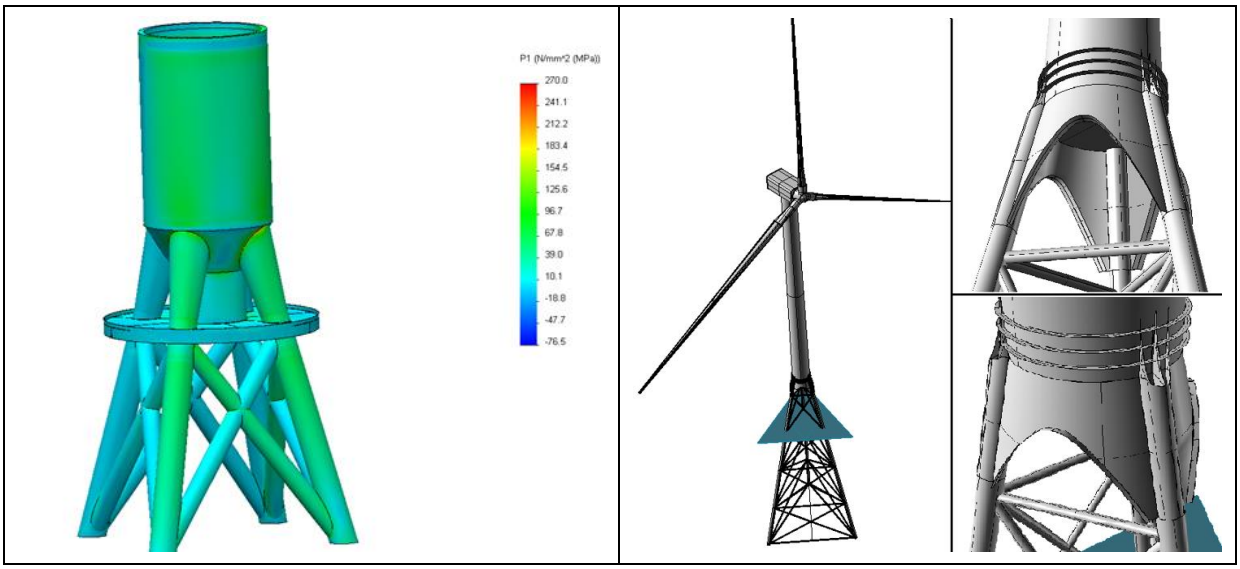

Figure 2.18: Concepts of transition piece under research [10], [11]

Moreover, with recent advances in wind technology offshore structures new and different concepts were idealized (**Figure 2.19**). The conceptual model presented on Chapter 4 was conceived through the different concepts presented.

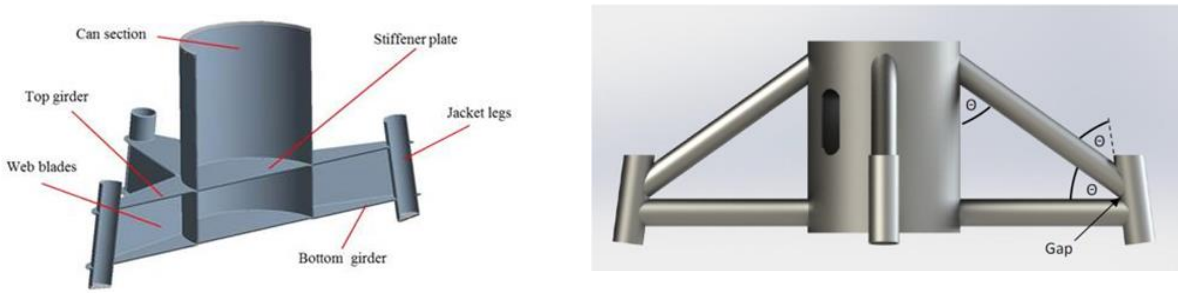

Figure 2.19*:* Concepts of transition piece [9]

2.4.5 Summary of Transition Piece Designs

Although designs of the transition piece vary according to specific and individual project requirements including the site and loading condition, connecting structural dimension, the

rotor nacelle assembly weight, etc. there are some general types of the transition piece design for selection and consideration[6].

Frame-Cylinder: This design is composed of a steel frame of bracings in the outside and a steel cylinder structure in the core. Both early onshore lattice tower supported wind turbine (**Figure 2.14**) and recent hybrid offshore wind turbine (**Figure 2.16**) have applied this design concept. From a structural characteristics point of view, this combination of an external frame system and an internal cylinder structure will increase the strength and the robustness of the transition piece. The bracing legs are designed to allow for convenient connection with the lattice substructure and the internal cylinder structure is employed for connection with the upper tower, through the application of a specific flange connection.

Steel Cone: Repower wind turbine used further steel cone type of transition piece. It consists of a conical shell and combines the half clinging legs to the main body. In comparison with previous shell frame structure, a reduction of material cost might be achieved through the elimination of the bracing legs. However, the larger dimension of the cone structure will lead to more material and higher cost. It can be seen in **Figure 2.20**(a); the transition piece has the form of a truncated cone with a height of 7 m. Moreover, AMBAU GmbH[12] constructed a 14 m high cone-shaped shell transition piece with 200 tones weight for the “Baltic2” wind farm **Figure 2.20**(b).

(a) (b)

Figure 2.20: (a) Transition piece for Repower jacket [7] (b) Ambau GmbH transition piece with Conical shell (www.ambau.com)

Concrete block: The concrete block transition piece was only proposed in the research stage and is not realized yet. The cost efficiency might be an advantage of such a design in many places. Nevertheless, a heavy concrete block changes the dynamic response of the whole supporting structure. Therefore, the dynamic behavior must be carefully adopted corresponding to the whole supporting structure, dynamic properties and the wind turbine.

A heavy design like the concrete block might be a good option for a hybrid concrete-tubular tower but should be avoided for a lattice-tubular structure due to the high self-weight, this lead to higher axial and overturning bending with a minor displacement. Moreover, the transportation and in-situ construction are much more difficult and time-consuming.

All of the above-mentioned design concepts are either actually in developing process or only studied for onshore lattice-tubular tower supported wind turbines and hybrid offshore wind turbines. In order to design a transition piece for a hybrid high rise supporting structure, several ideas will be proposed. Due to high loads, high strength steel will be taken into account for more investigation. Moreover, all the existing concepts are so huge which create challenges for transportation and installation; therefore, a compact and stiff transition piece will be proposed. On the other hand, the transition piece mass and stiffness significance on overall tower dynamic behavior will be investigated.

2.5 Theoretical Background of Fatigue

2.5.1 Introduction

Fatigue is caused by the repeated application of loads to a structural part which forms into gradual crack growth due to repeated stresses. Fatigue cracks usually initiate from the surface of a component (**Figure 2.21**). This is crack initiation. The crack may then propagate in a direction perpendicular to the direct stress. This is crack propagation. Finally, the component may fracture.

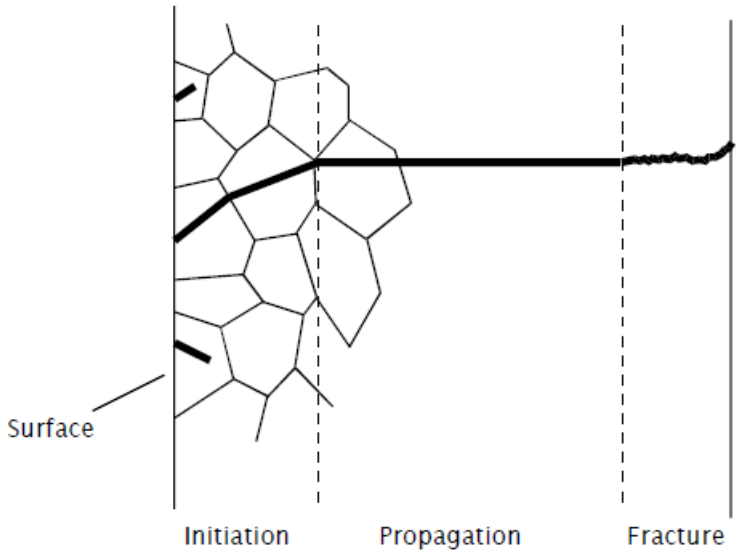

Figure 2.21: The three stages of fatigue failure [13]

Modern fatigue theories provide separate analyses for each phase. Crack initiation theories are based on the assumption that fatigue cracks are initiated by the local strains and stresses on the surface of a component. Crack propagation theories re late crack growth to the stresses

in the component. Final fracture is analysed using fracture mechanics. Earlier theories treated the whole of the fatigue life as a single entity, and related fatigue life to the calculated engineering stresses in the component. Much current research is attempting to describe the whole fatigue process by the study of crack propagation from very small initial defects[13].

2.5.2 Basics of Fatigue

Metals when subjected to repeated cyclic load exhibit damage by fatigue. The magnitude of stress in each cycle is not sufficient to cause failure with a single cycle. Large numbers of cycles are therefore needed for failure by fatigue. Fatigue manifests in the form of initiation or nucleation of a crack followed by its growth until the critical crack size of the parent metal under the operating load is reached leading to rupture. Behaviour of metal under cyclic load differs from that under monotonic load. New cracks can nucleate during cyclic load that does not happen under static monotonic load. Importantly, fatigue crack nucleates and grows at stress levels far below the monotonic tensile strength of the metal. The crack advances continuously by very small amounts, its growth rate decided by the magnitude of load and geometry of the component. Also the nucleated crack may not grow at all or may propagate extremely slowly resulting in high fatigue life of the component if the applied stress is less than the metal fatigue limit. However, maintaining that condition in actual working components with design constraints and discontinuities calls for limited service loads which may be an impediment. Therefore, fatigue cracks in most cases are permissible but with proper knowledge of fracture mechanics about the allowable or critical crack size. The component under cyclic load can work satisfactorily for years, albeit with hidden crack growth, but ruptures suddenly without any pre-warning. Such characteristics make cyclic load more dangerous than monotonic load[14].

As stated before, fatigue life until failure consists of two periods: the crack initiation period and the crack growth period as shown in **Figure 2.22**. Differentiating between the two periods is of great importance because several surface conditions do affect the initiation period, but have a negligible influence on the crack growth period. The stress concentration factor, *Kt*, is the important parameter for predictions on crack initiation. The stress intensity factor, *K*, is used for predictions on crack growth[15].

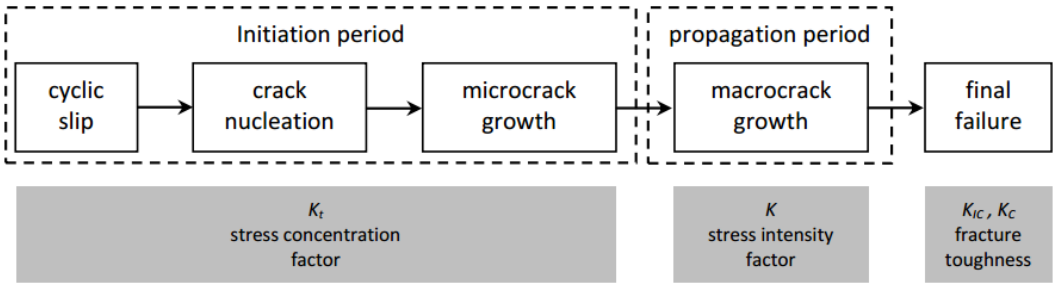

Figure 2.22: Fatigue life stages [15]

2.5.2.1 Types of Fatigue Loads

Fatigue load cycles can be of constant amplitude or variable amplitude type. Rotating machines operating at same conditions usually work under pre-calculated constant amplitude load cycles whereas wind turbines aircrafts and ships are subjected to variable amplitude load cycles due to unpredictable and fluctuating wind or sea gusts. Some common types of load cycles are illustrated in **Figure 2.23**[14]. Important fatigue terms are presented.

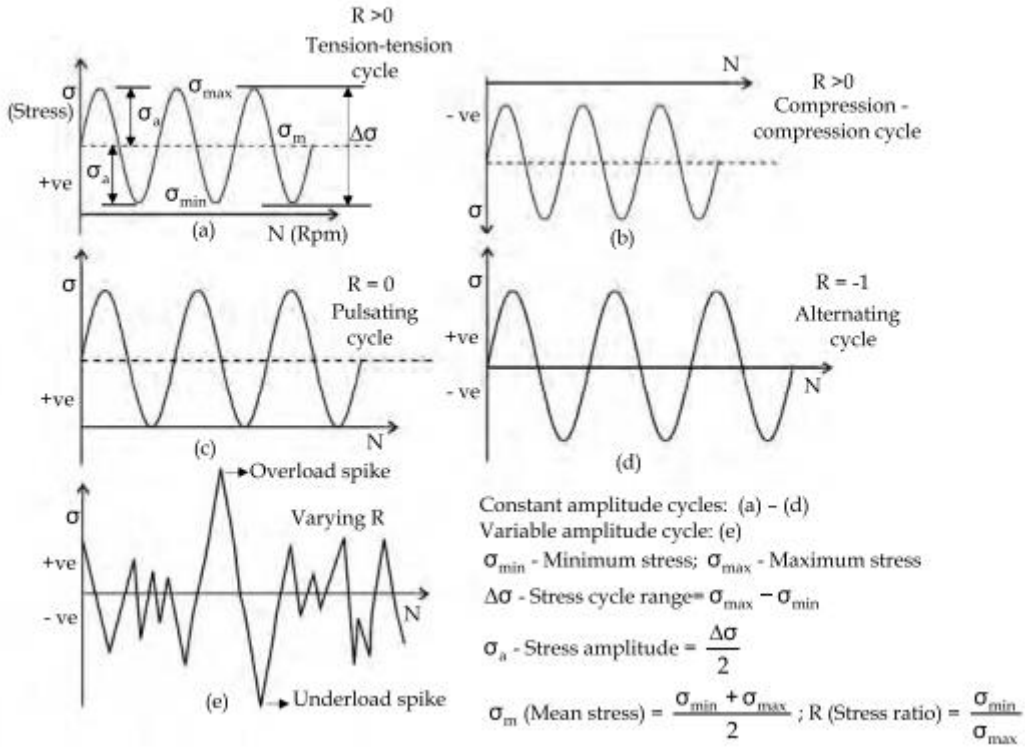

***Figure 2.23**:* Types of Fatigue cycles [14]

2.5.2.2 Factors Influencing Fatigue life

The factors influencing fatigue life prediction of materials and structures are as follow:

1) Environment: Corrosive and aqueous environments promote crack initiation and increase crack growth rate although crack tip blunting and closure due to accumulation of environmental products at crack tip may dip crack growth rate to some extent. But the overall effect of such environments is to enhance crack growth rate. Under high temperature too, fatigue resistance in most metals generally diminishes with increase in crack growth rate due to the effect of creep.

2) Microstructure of Metals: Large grains metals have low yield strength and reduced fatigue limit and vice-versa. However, at higher temperatures, the coarse grained metal is seen to show better fatigue properties. Barriers to crack growth in the form of precipitates, impurities, grain boundaries, etc. improve fatigue properties. Phase transformations occurring during cyclic loading can also influence the fatigue life.

3) Manufacturing process: Fatigue properties are better in the direction of forging, extrusion and rolling and are lower in the transverse direction. Some specific processes like shot peening, cold rolling etc. and other hardening/heat treatment methods that induce compressive residual stresses reduce the chances of crack initiation and enhance the fatigue properties. Tensile residual stresses on the other hand promote crack initiation. Other manufacturing processes like forming, drawing, forging, extrusion, rolling, machining, punching etc., that produce rough surfaces, decrease fatigue life. A rough surface possesses more crack initiation sites due to unevenness and asperities. Polished and ground surfaces on the other hand have excellent high fatigue life due to minimum asperities.

4) Structure/Component geometry: Discontinuities such as holes, notches and joints, that are the source of stress risers, facilitate crack initiation. Fatigue life of a notched component is less than that of an un-notched one when subjected to similar loads.

5) Loading Condition: A multiaxial load reduces fatigue life in comparison with uniaxial loads except in the case of pure torsional loading. Mean stress also influences fatigue life. Positive tensile mean stress reduces fatigue life whereas negative mean stress may increase it. The influence of mean stress is more significant in low strain or high cycle fatigue regime[14].

2.5.3 Fatigue Life Prediction methods

In this section an overview is given of different fatigue life prediction models. Since it falls beyond the scope of this study to provide a general overview of all existing fatigue modelling techniques, this overview is limited to stress-life, local strain models and multi-axial fatigue models. These techniques can be grouped into the following categories:

- Fatigue life prediction using stress life (S-N) curves
- Local Strain models
- Multiaxial models

The stress-life approach was the first fatigue prediction technique to be developed. This technique is generally used to predict the total life of a component. Local strain models, however, only consider the crack initiation life. This approach can be used when crack initiation dominates the total fatigue life. On the other hand, fracture mechanics only deals with the crack propagation stage. When both the crack initiation and propagation stage of a component are important, local strain models can be used in conjunction with fracture mechanics to predict the total fatigue life by simply adding the calculated number of cycles in the two stages.

Multiaxial fatigue models take into account the multiaxial stress or strain distribution at notches or crack tips and can either be based on a stress or strain based approach or can be

based on energetic criteria. Depending on the criterion, the models predict fatigue crack initiation, propagation or total fatigue life.

2.5.3.1 Stress life approach

2.5.3.1.1 S-N curves

The stress-life approach is the oldest among the fatigue analysis techniques. This method was developed by Wohler and is based on experimental observations. The mathematical relations of this approach are derived from the so-called ***S-N*** curve or Wohler curve of. This curve is obtained by subjecting a number of test specimens to fatigue tests at different stress levels. During a single test, the load is fluctuated with constant amplitude until failure occurs. How failure is defined, depends on the test specimen. For standardized strip- or bar-like specimens, failure means commonly total fracture of the specimen, while for tubular specimens a through wall crack is generally considered as failure. The resulting number of load cycles to failure ***N*** corresponding with a certain stress amplitude S_a is then plotted in the ***S-N*** curve. The number of cycles ***N*** is plotted on the horizontal axis, which is conventionally put in logarithmic scale. The stress amplitude on the vertical axis can be either logarithmically or linearly plotted.

A typical example of an ***S-N*** curve is shown in **Figure 2.24**. It starts as a sloping curve changing into a horizontal asymptote with the number of cycles to failure becoming infinite. The stress level corresponding to the asymptote is referred to as the ***fatigue limit***. Since stresses below the fatigue limit would never result in fatigue failure, tests are generally stopped when a certain number of cycles are reached, for example at $2x10^6$ cycles.

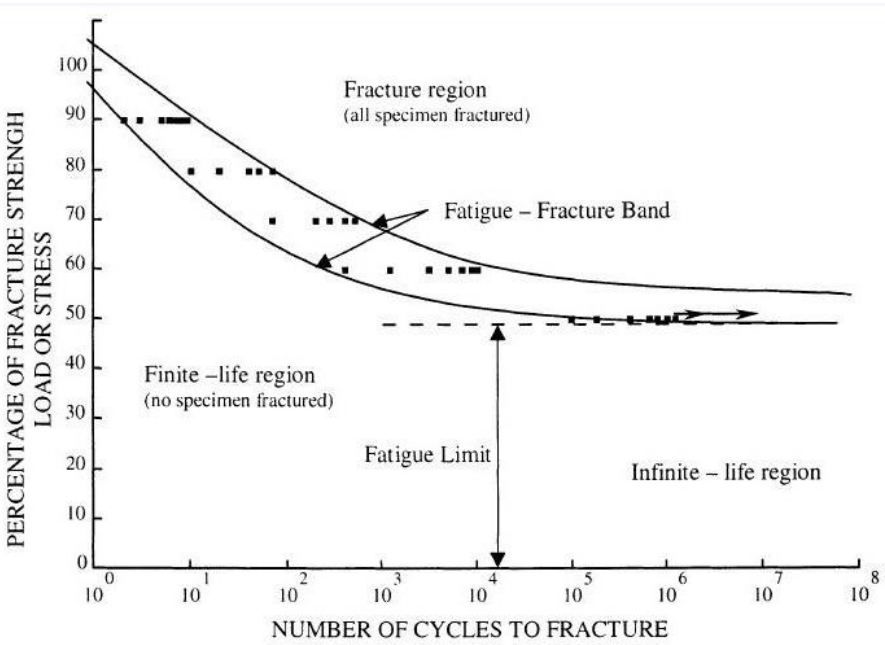

Figure 2.24: Typical S-N curve of a medium-strength steel (From ASM Atlas of fatigue curves, pg.28)

Fatigue test data are prone to scatter, due to the nature of the fatigue mechanism. Nevertheless, the data can be embedded in a certain fatigue- fracture band wherein the probability of failure changes from a low probability next to the finite-life region, to a high probability next to the fracture region. Typically, a mean curve for the finite-life region with a 50 % probability of failure is used according to the Basquin relation [16].

$$S_{a^k} \times N = constant \qquad 2.1$$

For design purposes a probability of failure of 50% is obviously unacceptable. For this reason, design curves are used which are obtained by subtracting two times the standard deviation from the mean curve which corresponds to a probability of failure of 4.55%.

The stress amplitude to which the fatigue life is related to is generally a nominal stress, since it is derived from the forces applied in the experimental test setup. This has the advantage of avoiding complex stress analysis evaluate the test specimens. However, this means that results obtained for a specific component cannot easily be extended to a modified component. Additionally, ***S-N*** curves are obtained from constant amplitude tests whereas in practice most components are subjected to variable amplitude stresses. To use ***S-N*** data for practical load histories, the cumulative fatigue damage model of Miner can be used:

$$D = \sum_i \frac{n^i}{N^i} \qquad 2.2$$

Miner postulated that fatigue damage accumulates linearly. When a component is subjected to n_i stress cycles at a stress which has N_i cycles to failure, then a fraction of n_i/N_i of the total life is consumed. The damage accumulated over the cycles at different stress levels is summed up to give the total damage ***D***. The component would fail if ***D*** becomes one. Miner's theory assumes that damage can be superimposed, that the appearing damage is irreversible and that there is no interaction between different stress levels in the sense that it is unimportant in which order the component experiences the stress cycles.

2.5.3.1.2 Mean Stress Effect

Fatigue tests can be carried out with a fully reversible load with zero mean stress or with a fluctuating load with a certain pre-stress. To make the test conditions clear, a load ratio R as defined in **Figure 2.25**, should be mentioned with every S-N curve. Additionally, S_a is the alternating stress, S_m is the mean stress S_{min} and S_{max} are respectively the minimum and maximum applied stress, as shown in Figure.

Many ***S-N*** curves are given for a fully reversible fatigue load with zero mean stress or load ratio ***R*** = -1. In order to compare data obtained in tests conducted at a different load ratio, the Goodman Eq. (3.3) can be used to correct the mean stress effect.

$$\frac{S_a}{S_f} = 1 - \frac{S_m}{\sigma_{UTS}} \qquad 2.3$$

With this equation the fatigue stress S_f as would occur for a fully reversible fatigue load can be calculated from the applied stress amplitude S_a taking into account the ratio between the applied mean stress S_m and the material's tensile strength σ_{UTS}.

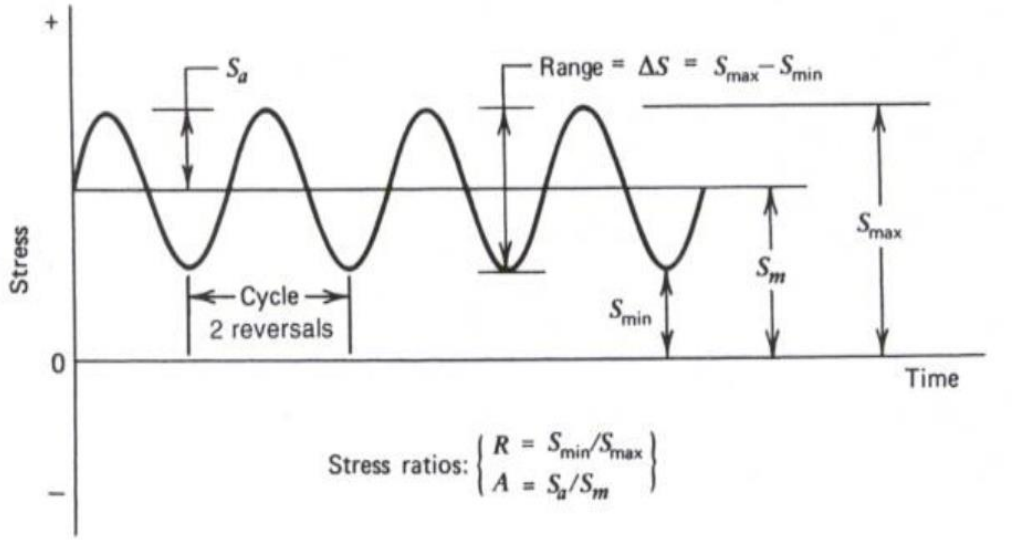

Figure 2.25: Stress definitions [13]

2.5.3.1.3 Stress Concentrations

To determine the fatigue life of a machined component, the fatigue data of standard test specimens can be used. However, a real-life component has an arbitrary size with a certain stress concentration, an arbitrary surface finish and an arbitrary loading mode, while standard test specimens have prescribed dimensions and a polished surface. To take all these differences into account, the fatigue stress of the machined component $S_{f,\,comp}$ can be estimated from the fatigue stress of a standard component S_f by introducing a number of correction factors:

$$S_{f,comp} = k_a k_b k_c \frac{S_f}{K_f} \qquad 2.4$$

In this equation k_a is a correction factor for the loading mode, since the fatigue behaviour of a component is different when the loads are applied e.g. in tension or bending mode. The factor k_b deals with the size effect, which takes into account that the effect of fatigue failure on small standardized specimens can be different from the effect on a bigger structure; k_c is a surface roughness factor that allows relating the results of polished standard specimens to machined parts with a higher surface roughness. Finally, K_f is the fatigue notch factor. This can be calculated from the geometrical stress concentration factor K_t by Eq. (2.6) with q the notch sensitivity factor.

$$K_f = 1 + q(K_t - 1) \qquad 2.5$$

When using this technique to evaluate threaded connections based on experimental data of the pipeline steel, one should consider that the factors k_a, k_b, k_c and q are all given by empirical relations or charts, which means that each single factor is subjected to a certain amount of uncertainty. Additionally, the input for these relations or charts requires measurements of local parameters such as surface roughness and root radii. Next to this, selecting a certain uniaxial loading mode from a complex stress distribution might be an oversimplification. Due to these assumptions and the scatter of every factor, the calculated life might differ significantly from the real behaviour of the connection.

2.5.3.2 Local Approach

Fatigue design philosophy has evolved from fatigue limit and infinite life criteria to approaches based on finite life behaviour. The local approaches use fatigue damage parameters to correlate fatigue test results, especially for crack initiation life. In order to predict the fatigue life under a specified condition, different fatigue damage parameters have been proposed to correlate fatigue life[17]. The local approaches are generally divided into two categories, i.e., stress-based and strain-based when stress and strain is independently used as the fatigue damage parameter. Models to account for the stress level effect referring to the stress-based and strain-based methods have been proposed by different authors. These models are presented in the following.

2.5.3.2.1 Stress Based Method

The stress-life method uses the alternating stress amplitude to predict the number of cycles to failure [17]. This method is based on comparing the stress amplitude to stress amplitude versus fatigue life curve *(**S**-**N** diagram).* The ***S**-**N*** curves are based on empirical formulas derived from experimental data. The stress-life method is generally only used for high cycle fatigue, because under low cycle fatigue the stress-strain relationship becomes nonlinear. Similar to ***S**-**N*** curves, the relation between stress amplitude, $\Delta\sigma/2$, and the number of cycles to failure [16].

$$\frac{\Delta\sigma}{2} = \sigma'_f \times (N_f)^b \qquad 2.6$$

Where σ'_f the fatigue strength coefficient, and 'b' is is the fatigue strength exponent. For many loading cases, the mean stress is not zero. Although the stress level effect is often neglected in fatigue life calculations for welded details, the high residual stresses in such details tend to obliterate any possible effect of applied stress level. However, in non-welded details, the effect of stress level must be accounted for in the fatigue life calculations.

Morrow [18] proposed a correction to account for mean stress effect as follow:

$$\frac{\Delta\sigma}{2} = (\sigma'_f - \sigma_m) \times (N_f)^b \qquad 2.7$$

Where σ_m the mean stress and the other variables are are the same as for Equation (7). The effect of the tensile mean stress is thus equivalent to a reduction of the fatigue strength coefficient. The model assumes that a given combination of stress amplitude, $\Delta\sigma/2$, and mean stress, σ_m is expected to have the same fatigue life as fully reversed stress amplitude of $\left(\frac{\Delta\sigma}{2}\right)_{-1}$, where:

$$\left(\frac{\Delta\sigma}{2}\right)_{-1} = \frac{\frac{\Delta\sigma}{2}}{1-\frac{\sigma_m}{\sigma'_f}} \qquad 2.8$$

The Morrow correction for stress-based method was found to work reasonably well for structural grades of steels.

2.5.3.2.2 Strain based Approach

The strain-based approach to fatigue problems is widely used at present. Strain can be measured and has been shown to be an excellent quantity for correlating with low-cycle fatigue. For example, gas turbines operate at fairly steady stresses, but when they are started or stopped, they are subjected to a very high stress range. The local strains can be well above the yield strain, and the stresses are more difficult to measure or estimate than the strains. The most common application of the strain-based approach, however, is in fatigue of notched members. In a notched component or specimen subjected to cyclic external loads, the behaviour of material at the root of the notch is best considered in terms of strain. As long as there is elastic constraint surrounding a local plastic zone at the notch, the strains can be calculated more easily than the stress [19]. This concept has motivated the strain-life design method based on relating the fatigue life of notched parts to the life of small, un-notched specimens that are cycled to the same strains as the material at the notch root. Since fatigue damage is assessed directly in terms of local strain, this approach is called the "local strain approach". A reasonable expected fatigue life, based on the nucleation or formation of small macro-cracks, can then be determined if one knows the local strain-time history at a notch in a component and the un-notched strain-life fatigue properties of the material. The remaining fatigue crack growth life of a component can be analysed using fracture mechanics concepts.

For engineering materials at room temperature, cyclic hardening or softening usually takes place rapidly at first and then approaches to a stable condition. The stable cyclic stress versus strain curve is often defined using the Ramberg-Osgood equation [20]. The curve can be determined from several companion specimens cycled at various constant strain amplitudes or from a single specimen in conformity with the incremental step test method.

The total strain amplitude in **Figure 2.26** can be resolved into elastic and plastic strain components from the steady-state hysteresis loops. At a given life, N_1, the total strain is the sum of the elastic and plastic strains. Both the elastic and plastic curves can be approximated

as straight lines. At large strains or short lives, the plastic strain component is predominant, and at small strains or longer lives the elastic strain component is predominant.

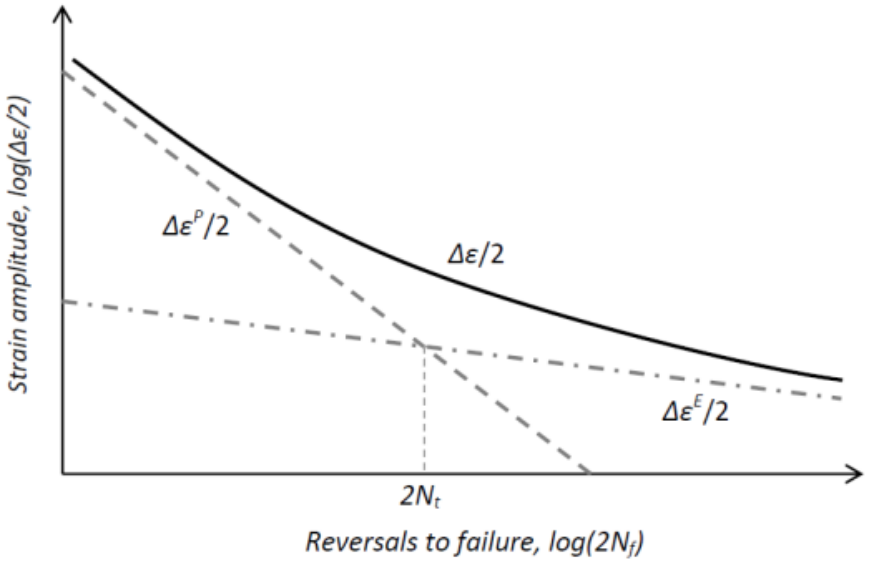

***Figure 2.26**:* Strain-life curves showing total, elastic, and plastic strain components [15].

Basquin's equation [16], proposed in 1910, which represent the elastic component of the strain amplitude, $\frac{\Delta\varepsilon^E}{2}$ can obtained as follow:

$$\frac{\Delta\varepsilon^E}{2} = \frac{\sigma'_f}{E}(N_f)^b \qquad 2.9$$

The plastic strain amplitude, $\frac{\Delta\varepsilon^P}{2}$ versus fatigue life can also be linearized on a logarithmic scale for low cycle fatigue. The relationship between the plastic strain amplitude and fatigue crack initiation life can be expressed in the following form which is known as Manson-Coffin [21] relationship proposed in the early 1960s:

$$\frac{\Delta\varepsilon^P}{2} = \varepsilon'_f(N_f)^c \qquad 2.10$$

Where $\varepsilon'_f$the fatigue ductility coefficient, and 'c' is is the fatigue ductility exponent, both determined experimentally. By adding the elastic and plastic components of strain amplitude, given respectively by equations 2.9 and 2.10, the relationship between the total strain amplitude, $\frac{\Delta\varepsilon}{2}$ and the fatigue life can be expressed as:

$$\frac{\Delta\varepsilon}{2} = \frac{\Delta\varepsilon^E}{2} + \frac{\Delta\varepsilon^P}{2} = \frac{\sigma'_f}{E}(N_f)^b + \varepsilon'_f(N_f)^c \qquad 2.11$$

The life at which elastic and plastic components of strain are equal is called the "transition fatigue life", ***2Nt.*** This is the life at which the elastic and plastic strain-life curves intersect.

In strain-controlled cycling with a mean strain usually results in a mean stress, which may relax fully or partially with continued cycling, as shown in **Figure 2.27**. This relaxation is

due to the presence of plastic deformation, and therefore, the rate or amount of relaxation depends on the magnitude of the plastic strain amplitude.

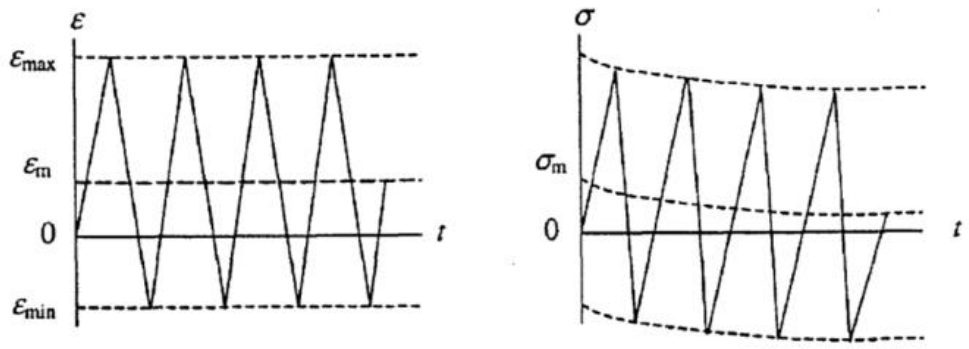

***Figure 2.27**:* Mean stress relaxation under strain-controlled cycling with a mean strain[19]

As a result, there is more mean stress relaxation at larger strain amplitudes. Mean strain does not usually affect fatigue behaviour unless it results in a non-fully relaxed mean stress. Since there is more mean stress relaxation at higher strain amplitudes due to larger plastic strains, mean stress effect on fatigue life is smaller in the low-cycle fatigue region and larger in the high cycle fatigue region. The inclusion of mean stress effects in fatigue life prediction methods involving strain-life data is more complex. Several models dealing with mean stress effects on strain life fatigue behaviour are discussed in. One method, often referred to as "Morrow's mean stress method", replaces σ'_f with $(\sigma'_f - \sigma_m)$ in Equation 2.11, such that [18]:

$$\frac{\Delta\varepsilon}{2} = \varepsilon_a = \frac{(\sigma'_f - \sigma_m)}{E} \times 2(N_f)^b + \varepsilon'_f (N_f)^c \qquad 2.12$$

An alternative version of Morrow's mean stress parameter where both the elastic and plastic terms are affected by the mean stress is given by Manson:

$$\frac{\Delta\varepsilon}{2} = \varepsilon_a = \frac{(\sigma'_f - \sigma_m)}{E} \times 2(N_f)^b + \varepsilon'_f \left(\frac{(\sigma'_f - \sigma_m)}{\sigma'_f}\right)^{\frac{c}{b}} 2(N_f)^c \qquad 2.13$$

Another equation suggested by Smith, Watson, and Topper [22] based on strain-life test data obtained with various mean stresses, is:

$$\sigma_{max}\,\varepsilon_a = \frac{(\sigma'_f)^2}{E} \times 2(N_f)^{2b} + \sigma'_f \varepsilon'_f 2(N_f)^{b+c} \qquad 2.14$$

Where $\sigma_{max} = \sigma_m + \sigma_a$ and ε_a is the alternating strain. This equation 2.14 is based on the assumption that for different combinations of strain amplitude,ε_a and the mean stress σ_{max}, the product $\sigma_{max}\,\varepsilon_a$ remains constant for a given life.

2.5.3.3 Multiaxial Fatigue Approach

When dealing with structures subjected to complex load cases, the above mentioned fatigue analysis approaches, might not give accurate results since they consider the dynamic loads to be uniaxial. Even in situations where the global acting stress is purely uniaxial, the local stress situation around notches or irregularities can be multiaxial. To describe such load cases more accurately, multiaxial fatigue models were developed.

The origin of multi-axiality in stress is dependent on various parameters such as type of loading, complex geometry of the mechanical parts, residual stresses or pre-stresses, etc. In order to estimate fatigue strength of the components, many multiaxial fatigue criteria have been proposed in the literature for metals. From technical point of view, multiaxial criteria for prediction of fatigue strength of mechanical components may be categorized into three main groups, namely stress based criteria, strain based criteria and energy based approaches. As for the stress criteria proposed by Susmel and Lazzarin, McDiarmid, Crossland and so on, are based only on stress and are suitable for high cycle fatigue when the deformation is elastic or the plastic strain is small. The strain criteria such as the Brown–Miller model, Fatemi–Socie, Li–Zhang and Wang–Brown model, are appropriate for such cases in which there is significant plasticity. The energy based multiaxial criteria such as the Smith–Watson–Topper model, Glinka and Varani-Farahani include both stress and strain terms[23].

Multiaxial fatigue criteria, from another point of view, can be categorized as those criteria which use the critical plane concept and those do not use this concept. In the multiaxial fatigue criteria based on critical plane, initially a material plane on which a combination of some stress components has the maximum value has been determined. Then, fatigue parameters as combinations of the maximum shear strain or stress and normal strain or stress on the critical plane have been calculated. The criteria will be checked then on this plane. Like to classical models, critical plane models can be stress-, strain- or energy-based. The concept of critical planes was primarily proposed by Brown and Miller. Brown and Miller proposed a strain-based parameter that considers that fatigue life to be a non-linear function of strain. The critical plane of this parameter is the plane of maximum shear strain. Firstly, the history of strain on the critical plane is analysed; and then strain parameters are used to quantify the damage parameters on the critical plane. Various terms have been proposed for different materials and experimental results[24]. Socie proposed that the fatigue life criterion should be based on a physical mechanism. Socie modified the SWT parameter for a material with tensile-type failures, by taking the view that crack growth is perpendicular to the maximum tensile stress.

The energy criteria have been used in conjunction with the critical plane approach, as proposed by Liu, and Glinka. Varani-Farahani (VF) proposed critical plane based energy parameters that are weighted by axial and shear fatigue properties of the material. In fact, many efforts have been made to evaluate the performance of multiaxial fatigue criteria for

various materials, notched and unnoticed components, different loading conditions and stress (and strain) states by several authors such as Papadopoulos *et al.*, Sonsino, Brown and Miller, You and Lee, Macha and Sonsino, Wang and Yao, Chakherlou and Abazadeh, Varvani-Farahani *et al.*, and Jiang *et al*. However, due to the complexity of this challenging problem and its practical application, much additional studies are still needed to evaluate the accuracy and reliability of the multiaxial fatigue criteria in design, life estimation, and failure assessment particularly for practical specimens.

2.5.4 Fatigue Analysis from Finite Element Analysis

Finite element models are used to analyze engineering components. The results may include stresses, strains, temperatures, deflections and frequency response. These results can be used for fatigue analysis.

Many fatigue analyses use the stress results from a linear elastic FEA. A linear analysis assumes a linear relationship between load and response. An elastic analysis assumes that the material stress-strain behavior is elastic, with no allowance for yielding. There are many different element formulations, and no general description will apply to all elements.

Three basic types of element are used for stress analysis - shell elements, tetrahedral elements and hexagonal (brick) elements. Tetrahedral and hexagonal elements are solid three dimensional elements. Engineering components produced by casting, forging and machining may be modelled using solid elements. Shell elements are thin, and are used to model thin walled structures fabricated from sheet and plate, for example. The different types of elements may be mixed in the same model.

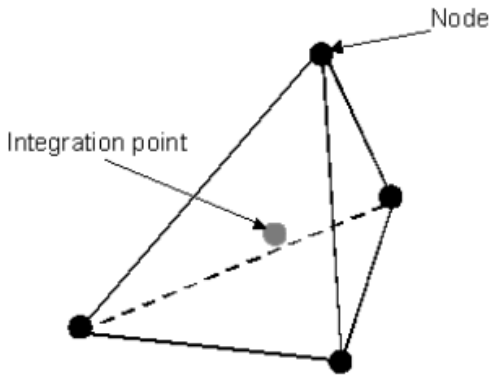

Figure 2.28: 4 node tetrahedral element [13]

Figure 2.28 shows a tetrahedral element with a node at each corner. The separate elements in a finite element model will usually be linked together at the nodes. The stresses in the element may be calculated at one or more points inside the element, called integration points, or Gauss points. Nodal stresses are calculated by extrapolating the internal integration point stresses to the nodes of the element.

The nodal stresses for solid elements are calculated as a full stress tensor, consisting of three direct stresses and three shear stresses, usually orientated on the global axis system for the model. Standard equations can be used to resolve the stresses into the plane of the surface of the element, to produce the two in-plane direct stresses and the in-plane shear stress. The out-of-plane direct stress will also be calculated. This should be approximately zero on the surface of the component. A significant out-of-plane stress is an indication of inadequate meshing. The stress tensor for a shell element will be the two in-plane direct stresses and the in-plane shear stress.

The finite element load case will consist of linear elastic FEA solution for the stresses at each node, calculated for single or multiple applied loads. At each node, the elastically- calculated stress tensor is multiplied by the load history to give a time history of the stress tensor **Figure 2.29**.

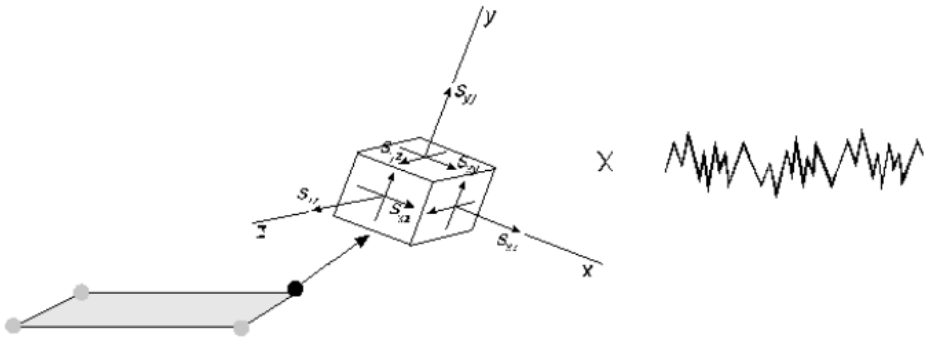

***Figure 2.29**:* Multiplying the unit load tensor by the time history of loading[13]

If $S_{i,j}$ is one component of the stress tensor from the unit load linear elastic FEA, and $P(t)$ is the time history of loading then the time history of the stress component $S_{i,j}(t)$ is:

$$S_{i,j}(t) = S_{i,j} \times P(t) \qquad 2.15$$

For the multiple loads each load has its own time history. The FE analysis is used to calculate the unit load stresses for each load applied separately. Consider a component with two applied load histories $P(t)$ and$Q(t)$. The FEA results will have a set of stresses for a unit load *P*, and set of stresses for a unit load *Q*.

If the elastically calculated stress tensor at a node is $S_{i,j}^{P}$ for unit load *P*, the stress tensor can be multiplied by the load-time history$P(t)$, to produce the time history of the stress tensor $S_{i,j}^{P}(t)$.

$$S_{i,j}^{P}(t) = S_{i,j}^{P} \times P(t) \qquad 2.16$$

This is calculated for each of the six components of the unit load stress tensor (S_{xx}^{P},S_{yy}^{P},S_{zz}^{P},S_{xy}^{P}, S_{yz}^{P} and S_{xz}^{P}) to produce six time histories.

If the elastically calculated stress tensor at a node is $S_{i,j}^{Q}$ for unit load *Q*, the stress tensor can be multiplied by the load-time history$Q(t)$, to produce the time history of the stress tensor $S_{i,j}^{Q}(t)$.

$$S_{i,j}^{Q}(t) = S_{i,j}^{Q} \times Q(t) \quad 2.17$$

The stresses are then added together point by point to give the stress-time history for both load histories applied simultaneously.

$$S_{i,j}^{(t)} = S_{i,j}^{P}(t) + S_{i,j}^{Q}(t) \quad 2.18$$

The common algorithms used in this thesis from fatigue analysis using Finite Element Analysis are:

i. Uniaxial stress life
ii. Uniaxial Strain life
iii. Brown Miller Analysis

2.5.4.1 Uniaxial Strain life

Uniaxial strain algorithm is mainly used for analyzing uniaxial stresses. Elastic stresses are required from an elastic FEA analysis. Uniaxial stresses rarely occur in practice, and the multi-axial algorithms are strongly recommended[25]. The elastic-plastic strain amplitude is used to calculate the fatigue life. Morrow, Smith-Watson-Topper, Walker or no mean stress correction can be used. The strain-life equation with no mean stress correction:

$$\frac{\Delta\varepsilon}{2} = \frac{\sigma_f'}{E}(2N_f)^b + \varepsilon_f'(2N_f)^c \quad 2.19$$

The strain-life equations with morrow mean stress correction:

$$\frac{\Delta\varepsilon}{2} = \frac{(\sigma_f' - \sigma_m)}{E}(2N_f)^b + \varepsilon_f'(2N_f)^c \quad 2.20$$

The strain-life equations with Smith-Watson-Topper mean stress correction:

$$\frac{\Delta\varepsilon}{2}(\sigma_{max}) = \frac{(\sigma_f')^2}{E}(2N_f)^{2b} + \sigma_f'\varepsilon_f'(2N_f)^{b+c} \quad 2.21$$

Although these strain-life algorithms are intended for uniaxial stress states, *Fe-safe* use multiaxial methods to calculate elastic strains from elastic FEA stresses, and a multiaxial elastic-plastic correction to derive the strain amplitudes and stress values used in these equations.

2.5.4.2 Uniaxial Stress life

Uniaxial stress algorithm is mainly used for analyzing uniaxial stresses. Elastic stresses are required from an elastic FEA analysis. For this analysis the stress amplitude is used to calculate the fatigue life. The fatigue life curve can be an S-N curve or a stress-life curve derived from local strain materials data. When using the local strain materials data, the life curve is defined by the equation:

$$\frac{\Delta\sigma}{2} = \sigma_f'(2N_f)^b \qquad 2.22$$

And a multiaxial cyclic plasticity correction is used to convert the elastic FEA stresses to elastic-plastic stress-strain. Otherwise the life curve is defined by the S-N values defined in the materials database, and the plasticity correction can be optionally performed.

2.5.4.3 Goodman and Gerber mean stress corrections

As each stress cycle is extracted, the stress range and mean stress for the cycle are calculated. If S_{max} is the maximum stress in the cycle and S_{min} is the minimum stress in the cycle. The stress range is $S_{max} - S_{min}$, the stress amplitude is $(S_{max} - S_{min})/2$ and the mean stress is$(S_{max} + S_{min})/2$.

For Goodman and Gerber mean stress corrections, the stress amplitude and mean stress are used to calculate the equivalent stress amplitude S_{a0} at zero mean stress. The endurance for the cycle is calculated using this stress amplitude. This method allows the Goodman and Gerber mean stress corrections to be used for endurances other than the endurance limit. In *Fe-safe*, the Goodman diagram is implemented as shown by the full line in **Figure 2.30**. This means that no allowance is made for possible beneficial effects of low compressive mean stresses, nor is any allowance made for possible detrimental effects of high compressive mean stresses.

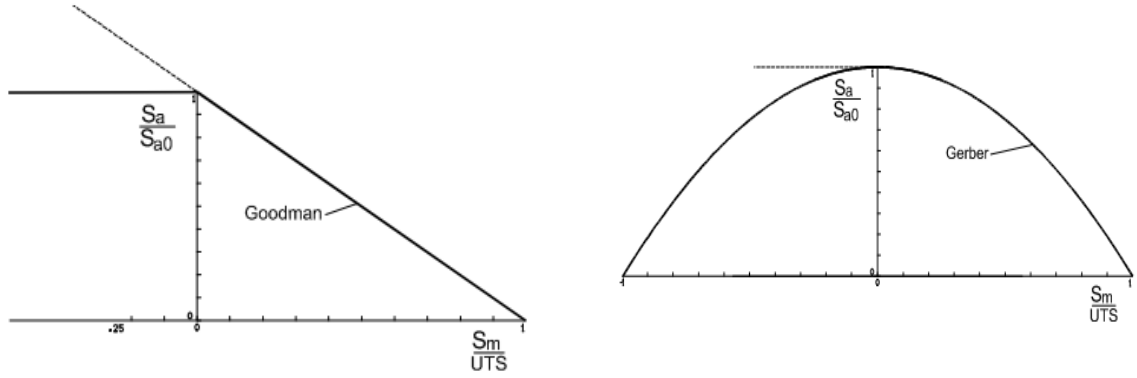

(a) (b)

***Figure 2.30**: a)* Goodman mean stress correction *(b)* Gerber mean stress correction [13]

2.5.4.4 Brown Miller combined strain criterion

The Brown-Miller equation proposes that the maximum fatigue damage occurs on the plane which experiences the maximum shear strain amplitude, and that the damage is a function of both this shear strain and the strain normal to this plane.

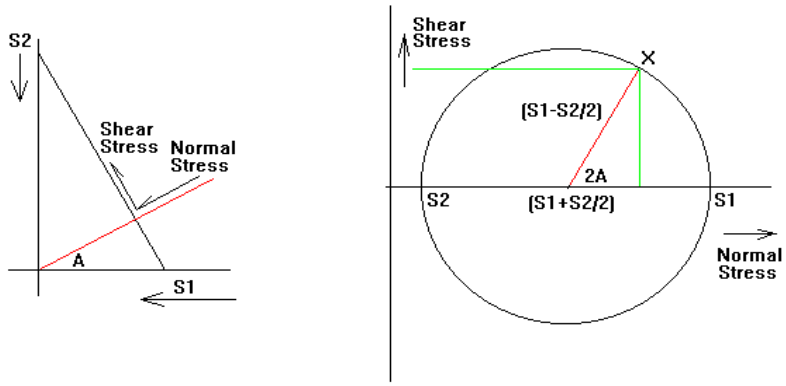

Figure 2.31: Representation of normal and shear plane (www.uwgb.edu/dutchs/structge/mohrcirc.htm)

This is a critical plane multi-axial fatigue algorithm, using planes perpendicular to the surface, and at 45° to the surface. Stress results from an elastic FEA are required. A multi-axial elastic-plastic correction is used to calculate elastic-plastic stress-strains from the elastic FEA stresses.

On each of three planes, fatigue lives are calculated on eighteen subsidiary planes spaced at 10 degree increments. On each plane:

- The principal strains are used to calculate the time history of the shear strain and the strain normal to the plane
- fatigue cycles are extracted and corrected for the effect of the mean normal stress
- the fatigue life is calculated.

The fatigue life is the shortest life calculated for the series of planes. This algorithm uses the strain-life curve defined by the equation:

$$\frac{\Delta\gamma}{2}+\frac{\Delta\varepsilon}{2}=1.65\frac{\sigma_f'}{E}(2N_f)^b+1.75\varepsilon_f'(2N_f)^c \qquad 2.23$$

For the Morrow Mean Stress correction equation is modified as:

$$\frac{\Delta\gamma}{2}+\frac{\Delta\varepsilon}{2}=1.65\frac{(\sigma_f'-\sigma_m)}{E}(2N_f)^b+1.75\varepsilon_f'(2N_f)^c \qquad 2.24$$

This analysis can also be used for fatigue analysis of elastic-plastic FEA analysis. The Brown Miller algorithm is the preferred algorithm for most conventional metals at room temperature[25].

2.5.4.5 Critical Plane Analysis

For many components subjected to combine direct and shear stresses, the phase relationship between the stresses is not constant. Examples are rotating shafts in bending with torsion forces applied at a frequency different from the rotational frequency. Machine tools, and powered axles with ABS braking or traction control, are examples. In these cases, it is not obvious which plane will experience the most severe combination of strains and hence the highest fatigue damage. **Figure 2.32** shows an idealized time history of bending and shear strains from a powered railway axle with traction control experiencing wheel slip. The cyclic bending strains are caused by the rotation of the axle. The shear strain cycles at a higher frequency as the traction control repeatedly applies and removes power to the axle. The angle 0 of the maximum principal strain to the axis of the axle is also shown.

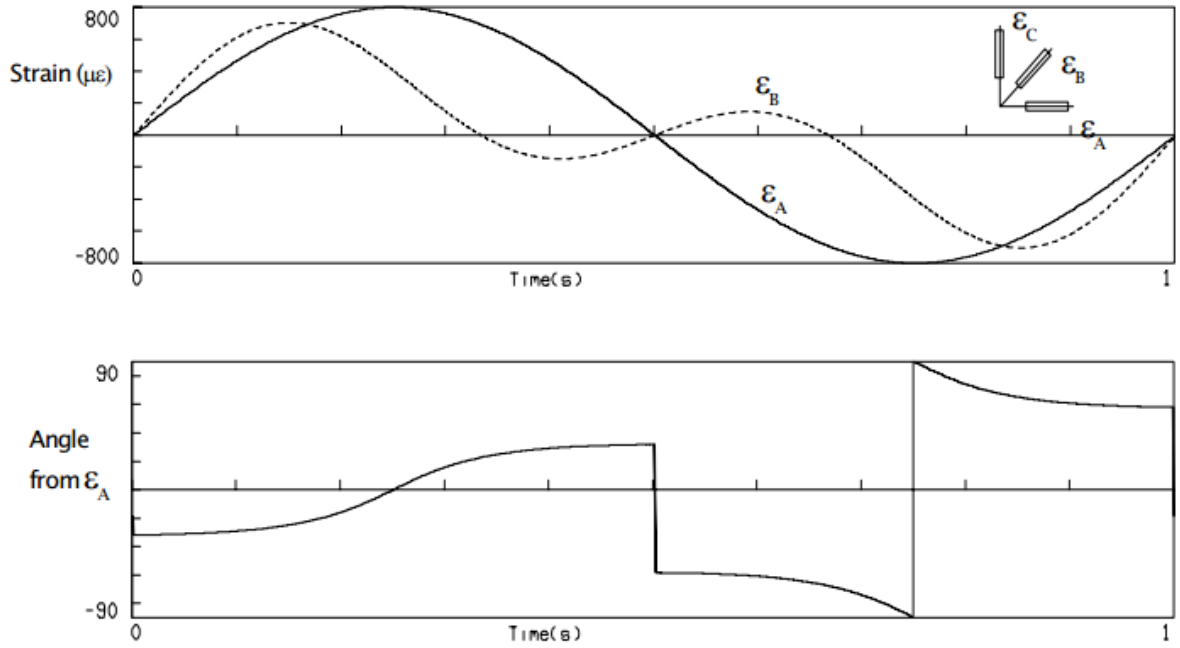

Figure 2.32: Direction of Principal and shear strains on an axle [13]

In this case it is not obvious which plane experiences the largest strain cycles. If a fatigue analysis was carried out using the principal strain-life method, the plane on which the principal strain acts changes its orientation throughout the loading cycle, as shown in Figure. The plane of maximum shear strain is at 45° to the principal strain plane.

Critical plane methods resolve the strains onto a number of planes, and calculate the damage on each plane. This form of analysis must be applied for criteria such as principal stress/strain, maximum shear stress/ strain, and the Brown-Miller criterion, for complex strain signals with varying phase relationships.

Chapter 3 METHODOLOGY

In this chapter, the design methodology of the transition segment is explained briefly. Mainly the methodology is divided into three parts according to Ultimate limit state i.e. Plastic Limit State (LS1), Buckling Limit State (LS3) and Fatigue Limit State (LS4). Moreover, the flowchart is described in detail with all steps which are completed for ultimate limit state according to Euro code EN1993 Part 1-3 (plastic limit state, buckling limit state and fatigue life calculation methodology) are explained in detail.

3.1 Ultimate limit State

3.1.1 Plastic Limit State (LS1)

The ultimate limit state where the structure develops zones of yielding a pattern such that its ability to resist increased loading is deemed to be exhausted by yielding of the material. The resistance offered by the structure at the plastic limit state is closely related to a small deflection theory plastic limit load or plastic collapse mechanism. Tensile rupture phenomenon may occur when the shell wall experiences gross section tensile failure, leading to a possible separation of the shell parts.

3.1.2 Cyclic Plasticity Limit State (LS2)

The limit state of cyclic plasticity should be taken as the condition in which repeated cycles of loading and unloading produce yielding in tension and in compression at the same point, thus causing plastic work to be repeatedly done on the structure, eventually leading to local cracking by exhaustion of the energy absorption capacity of the material. The natures of the loads arising from operation of the turbine are highly cyclic. Low cycle fatigue is rarely present in steel tubular towers for wind energy converter that's why this state will not be considered in the analysis.

3.1.3 Buckling Limit State (LS3)

According to the same standard, LS3 is the ultimate limit state where the structure suddenly loses its stability whether under membrane compression or shear. It leads either to large displacements or to the structure being unable to carry the applied loads.

3.1.4 Fatigue Limit State (LS4)

The limit state of fatigue should be taken as the condition in which repeated cycles of increasing and decreasing stress lead to the development of a fatigue crack.

3.2 Type of Analysis

According to EN 1993-1-6, buckling is an ultimate limit state where the structure suddenly loses its stability under membrane compression and/or shear. It leads either to large displacements or to the structure being unable to carry the applied loads. It is one of the most

important part of analysis in thin walled members, which nowadays are used in several practical applications. The wide application of shell structures is sustained by the following favourable factors [26].

i. Efficient load carrying performance;
ii. High strength vs. weight ratio; shell structures may be optimal structures;
iii. High values from an architectural point of view, once they can be easily integrated in urban and landscape areas.

However, shell structures are very slender structures and very sensitive to initial imperfections, which brings issues that must be considered when predicting the overall behaviour. By that, is important to have in account that the buckling resistance can be significantly lower than the theoretical buckling load, calculated from EN1993-1-3. The EN1993-1-6 shows a sequence of analysis to be performed. This sequence tries to systematize the various levels of analysis. Several types of analysis can be conducted following the structure complexity and regarding the failure mode that is considered:

3.2.1 Linear Elastic Shell Analysis

Linear analysis (LA) is applied to the perfect structure as a linear elastic eigenvalue calculation. It predicts the behaviour of a thin-walled shell structure on the basis of the small deflection linear elastic shell bending theory, related to the perfect geometry of the middle surface of the shell.

3.2.2 Linear Elastic Bifurcation Analysis (LBA)

An analysis that evaluates the linear bifurcation eigenvalue for a thin-walled shell structure on the basis of the small deflection linear elastic shell bending theory using geometrical stiffness matrices, and certain load conditions, related to the perfect geometry of the middle surface of the shell. It is used to determine the critical stress and the buckling shape. It should be noted that, where an eigenvalue is mentioned, this does not relate to vibration modes.

3.2.3 Geometrically Nonlinear Analysis (GNA)

An analysis based on the principles of shell bending theory applied to the perfect structure, using a linear elastic material law but including nonlinear large deflection theory for the displacements that accounts full for any change in geometry due to the actions on the shell. A bifurcation eigenvalue check is included at each load level.

3.2.4 Materially Nonlinear Analysis (MNA)

Analysis based on shell bending theory applied to the perfect structure, using the assumption of small deflections, but adopting a nonlinear elasto-plastic material law.

3.2.5 Geometrically and Materially Nonlinear Analysis (GMNA)

GMNA analysis is based on shell bending theory applied to the perfect structure, using the assumptions of nonlinear large deflection theory for the displacements and a nonlinear elasto-plastic material law. A bifurcation eigenvalue check is included at each load level.

3.2.6 Geometrically and Materially Nonlinear Analysis with Imperfections included (GMNIA)

An analysis with imperfections explicitly included, based on the principles of shell bending theory applied to the imperfect structure (i.e. the geometry of the middle surface includes unintended deviations from the ideal shape), including nonlinear large deflection theory for the displacements that accounts full for any change in geometry due to the actions on the shell and a nonlinear elastoplastic material law. The imperfections may also include imperfections in boundary conditions and residual stresses. A bifurcation eigenvalue check is included at each load level.

3.3 Design Methodology for LS1 and LS3

The design methodology for plastic and ultimate limit state is illustrated in **Figure 3.1**.

A parametric study was performed for the design of transition piece based on thickness of Transition Piece Shell and Chords. The plastic limit state (LS1) was verified according to the standard EN1993-1-6 6.3[27]. For design by global numerical analysis, according to EN1993-1-6 4.1.1 (6), either a MNA or GMNA should be performed when checking LS1. Considering the high complexity of the geometry for achieving accurate and realistic results, a GMNA (Geometrically and Materially Nonlinear Analysis) was performed. In order to verify LS1, Von Mises design strength has to be higher than the Von Mises stress distribution on the transition segment parts. If the Von Mises stress is higher than yield strength than the thickness of the transition piece has to be changed and the procedure is repeated.

The buckling limit state (LS3) was verified according to the standard EN1993 Part 1-6 section 8.7. According to standard, for the design by global numerical analysis a Geometrically and Materially Non-linear Analysis with Imperfections included (GMNIA) has to be performed. For GMNIA analysis firstly, an LBA (linear bifurcation analysis) is needed to obtain Eigen mode-affine shapes of imperfections with real load analysis. Furthermore, imperfections are applied to the succeeding model using shape from LBA and amplitudes of imperfections calculated according to same standard. Once obtained the Eigen mode shape for the critical mode, it is then necessary to estimate the magnitude of the imperfections to apply for the following model to determine the imperfect elastic-plastic buckling load. The second step consists in calculating the magnitude of the imperfection for the post-buckling analysis, the amplitude of the adopted equivalent geometric imperfection form should be taken as dependent on the fabrication tolerance class **Table 3.1**.

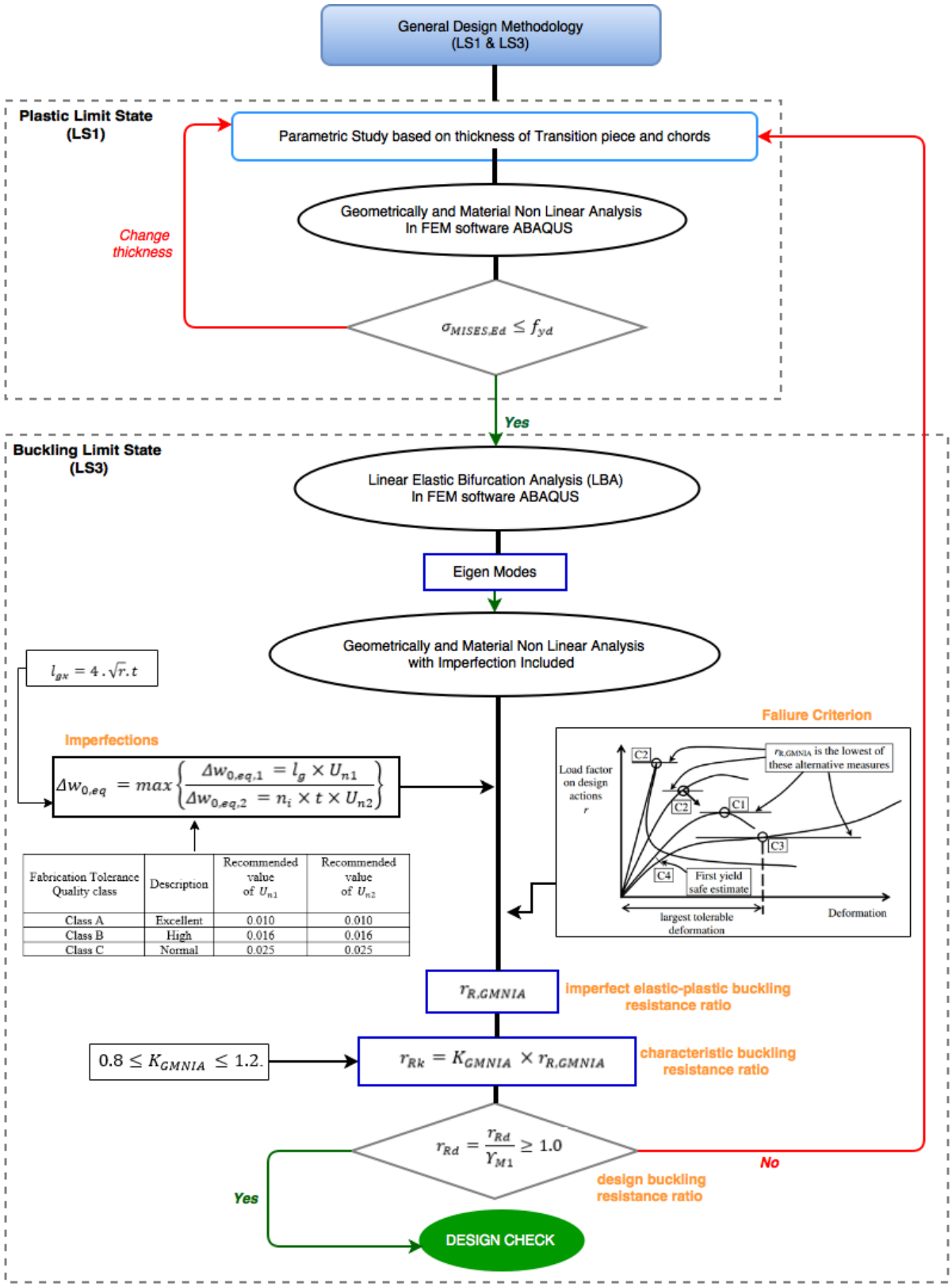

Figure 3.1: Design of Transition Segment *(LS1 & LS3)* Flowchart

The maximum deviation, $\Delta w_{0,eq}$ of the imperfection from the perfect structure shape should be estimated by the following formula:

$$\Delta w_{0,eq} = max\left\{\begin{matrix}\Delta w_{0,eq,1} = l_g \times U_{n1} \\ \Delta w_{0,eq,2} = n_i \times t \times U_{n2}\end{matrix}\right\} \quad 3.1$$

***Table 3.1**:* Recommended values for dimple imperfection amplitude parameters U_{n1} and U_{n2}[27]

Fabrication tolerance quality class	Description	Recommended value of U_{n1}	Recommended value of U_{n2}
Class A	Excellent	0,010	0,010
Class B	High	0,016	0,016
Class C	Normal	0,025	0,025

According to the EN1993 Part 1-6 wherever meridional compressive stresses are present, including across the welds, measurements should be made in both the meridional and circumferential directions **Figure 3.2**, using the gauge length l_{gx} given by:

$$l_{gx} = 4 . \sqrt{r}. t \quad 3.2$$

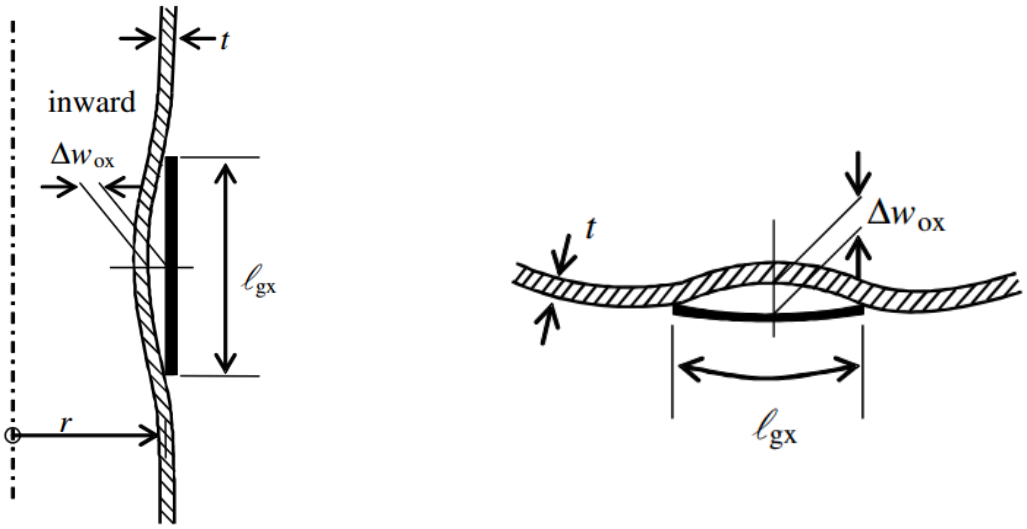

(a) (b)

***Figure 3.2**:* Measurements of depths of initial dimples *(a)* Measure on meridian *(b)* First measurement of circumferential circle [27]

The imperfection is calculated and applied to the succeeding model for post buckling analysis and curve should be obtained between load point factor and deformation measured at load point. According to the EN1993 Part 1-6 section 8.7.2 the imperfect elastic-plastic buckling resistance ratio $r_{R,GMNIA}$ should be found as lowest factor r_R obtained from the following three criteria C1,C2 and C3 as shown in the **Figure 3.3**.

Criteria C1: The maximum load factor on the load-deformation-curve (limit load);

Criteria C2: The bifurcation load factor, where this occurs during the loading path before reaching the limit point of the load-deformation-curve;

Criteria C3: The largest tolerable deformation, where this occurs during the loading path before reaching a bifurcation load or a limit load.

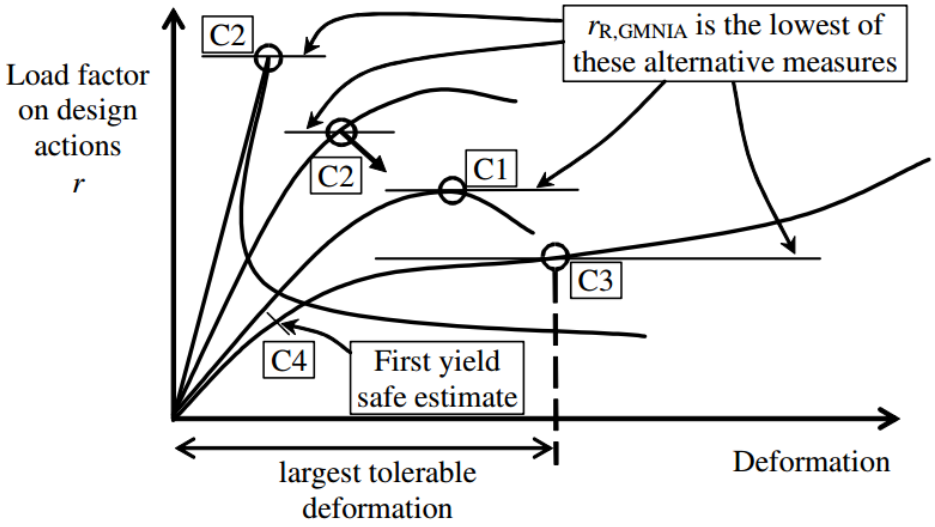

***Figure 3.3**:* Definition of buckling resistance from Global GMNIA analysis [27]

The characteristic buckling resistance ratio $r_{R,k}$ should be found from the imperfect elastic-plastic buckling resistance ratio$r_{R,GMNIA}$, adjusted by the calibration factorK_{GMNIA}. The design buckling resistance ratio $r_{R,d}$ should then be assessed using the partial factor γ_{M1}, according with the following equations:

$$r_{Rk} = K_{GMNIA} \times r_{R,GMNIA} \quad 3.3$$

$$r_{Rd} = \frac{r_{Rd}}{\gamma_{M1}} \quad 3.4$$

The verification is given as:

$$r_{Rd} \geq 1 \quad 3.5$$

The calibration factor K_{GMNIA} is obtained as follows:

$$K_{GMNIA} = \frac{r_{Rk,known,check}}{r_{R,GMNIA,check}} \; or \; \frac{r_{R,known,check}}{r_{R,GMNIA,check}} \quad 3.6$$

If the test results are used to determine K_{GMNIA}, and if it exceeds 1 then it should be adopted as:

$$K_{GMNIA} = 1.0 \quad 3.7$$

If the established theory results are used to determine K_{GMNIA}, then the obtained value must lie inside the range:

$$0.8 < K_{GMNIA} > 1.2 \qquad 3.8$$

3.4 Methodology for the Fatigue Life Estimation

The complexity and dynamics of wind loads interacting with a turning rotor are leading to forces and moments that act simultaneously and independently in the three spatial directions. It is not definitely assessable which of the load components are design driving for the structural components those are subject to the fatigue strength verification. Therefore, all load components have to be considered equally. At the same time the phase relationship is vitally important. Hence, the conventional approach using load spectra for the fatigue verification will fail in most cases.

Due to the large number of load cycles the wind turbine is exposed to a multiaxial stress condition and to verify the transition piece a multiaxial based fatigue approach is appropriate for the accurate life estimation. In this thesis a multiaxial fatigue based software package ***Fe-Safe*** is used for fatigue life estimation of the transition piece.

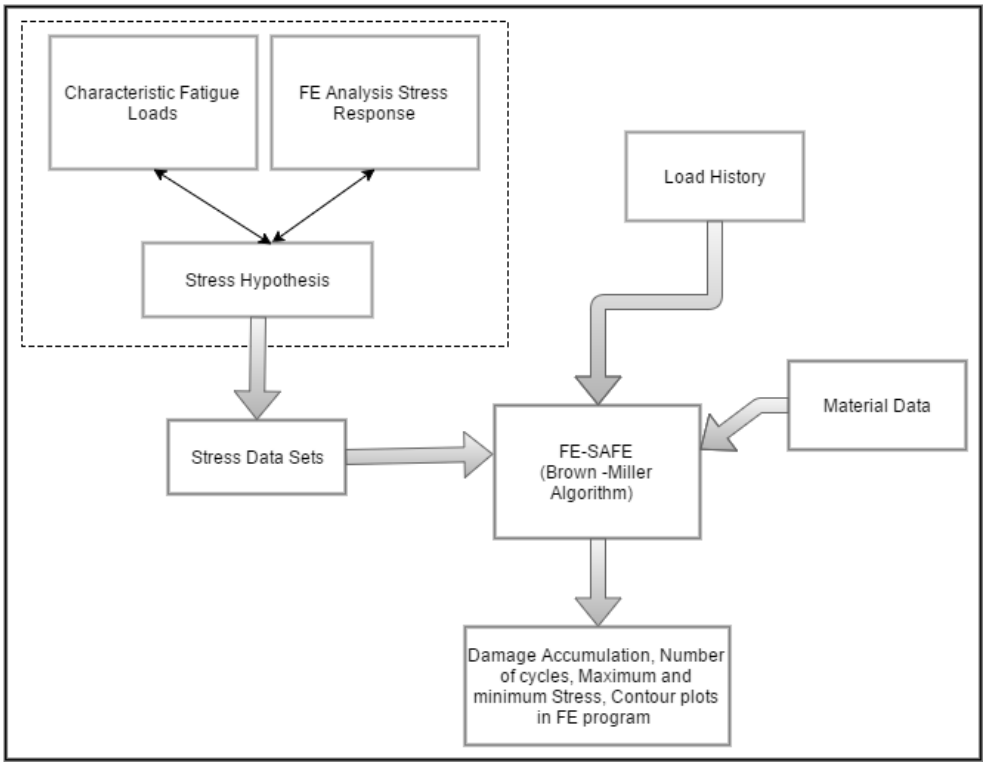

Figure 3.4: Fatigue Analysis procedure *(Flowchart)*

The methodology depicted in **Figure 3.4** for analysis can be divided in two parts: the determination of stresses under characteristic fatigue loading and determination of damage and total life using Fe-Safe tool. The stress data sets calculated on each element of the structure using any FEM software is imported into the Fe-Safe, in case of multiaxial loading each load history is applied on respective stress data set and material properties are assigned to different groups of structure to be analysed. Algorithm should be indicated for the analysis; usually for multiaxial fatigue analysis Brown-Miller with Morrow mean stress correction is used. The fatigue life for each node is calculated as:

i. The stress tensors are multiplied by the time history of the applied loading, to produce a time history of each of the 6 components stress tensor;

ii. The time histories of the in-plane principal stresses are calculated;

iii. The time histories of the three principal strains are calculated from the stresses;

iv. A multiaxial cyclic plasticity model is used to convert the elastic stress-strain histories into elastic plastic stress-strain histories;

v. A ‘critical plane’ method is used to identify the most damaging plane by calculating the damage on planes at 10° intervals between 0° and 180° in the surface of the component;

vi. For each of the critical planes, strains are resolved onto the three shear planes (1-2, 2-3 and 1-3);

vii. The time history of the damage parameter (which in this case, using the Brown-Miller algorithm, is the shear and normal strain) is cycle counted;

viii. Individual fatigue cycles are identified using a ‘Rain-flow’ cycle algorithm, the fatigue damage for each cycle is calculated and the total damage is summed;

ix. The plane with the shortest life defines the plane of crack initiation, and this life is written to the output file.

Chapter 4 CONCEPTUAL DESIGN OF TRANSITION SEGMENT

Design of transition piece can only be possible after understanding all the requirements that this component should meet. Previous experience and existing design models can be referred to but a good design should always be able to look into the specific characteristics of each individual project. The project on which this thesis or study is based on also have some unique requirements. After the outcome of a conceptual design model, further analysis of different case studies will be made in order to ensure every detailed requirement. A suitable conceptual model should take into consideration the following aspects:

4.1 Geometrical requirement

The transition piece is employed as a connection between the lattice support structure and the tubular part of the tower. The major challenges or parameters which effect and govern the geometrical shape of transition piece in this thesis are transportation and assembling the whole structure which are described in detail below:

4.1.1 Transportation

The main motivation of the undergoing project is to increase the height of conventional wind turbines to harness more energy with less turbulence in wind speed. Due to which a hybrid high rise onshore structure is proposed because hybrid lattice/tubular tower solution can be used to reach higher altitude with less transportation installation limits, which consist of three main parts tubular part, lattice part and transition piece. The transportation of lattice part is solved as it will be transported in pieces and bolted on site. Regarding tubular part of wind turbine, transportation limit is illustrated in **Figure 4.1**. It shows that the maximum diameter of 4.3 m being transported to the site and if the size will be increased up to 5 m or more then the road width will be blocked by the tower logistic process which should be avoided. However, it is not only the dimension but also the weight of the structure which cause road surface damage. So, the solution for transition piece should be an innovative hybrid solution which can be transported in parts and can be assembled on site.

4.1.2 Lifting Mechanism

The other parameter which effects the design of transition piece is the lifting procedure opted in this unique project. In usual assembling of wind turbines, the parts of the tubular tower are lifted by a crane as shown in the **Figure 4.2** and bolted together towards the whole length of wind turbines which are usually 80-120 meters tall. But in this project increasing the length of the turbines is the main goal to utilize higher altitude, stronger winds with less turbulence. And the problem which happens when aiming higher altitude is the cost of the tubular tower assembly using the cranes. The cranes' cost exponentially increases with the increase of the cranes' size.

***Figure 4.1**:* Transportation of section of tubular tower
(http://piximus.net/vehicles/transportation-of-the-giant-wind-turbine)

***Figure 4.2**:* Conventional lifting procedure of tubular tower segments by Crane
(http://www.siemens.com)

So the lattice part will be assembled first, then the Transition piece is connected to the lattice part and the tubular parts of the tower will be jacked up from the lattice part by a hydraulic machine and finally, the whole tower will be connected to the Transition piece to ensure the transmission of loads. Leaving up with some constraints which are considered for the design of transition segment which are:

i. Diameter of the transition piece should be greater than largest diameter of tubular tower so that they can slide up easily from the inside during the jacking process.

ii. There should not be any obstruction or cross stiffeners inside the transition piece which can hurdle the jacking process of tubular parts.

Various structural profiles which can meet the above mentioned geometry characteristics suffice but for simplicity, with consideration of manufacturing, transportation, assembly and structural cost, the existing frame-cylinder concept and the cone-strut concept seem to have more advantages than the others **Figure 4.3**. The cone-strut concept is not studied in this thesis; the main focus for the further research will be on frame-cylinder type of transition piece.

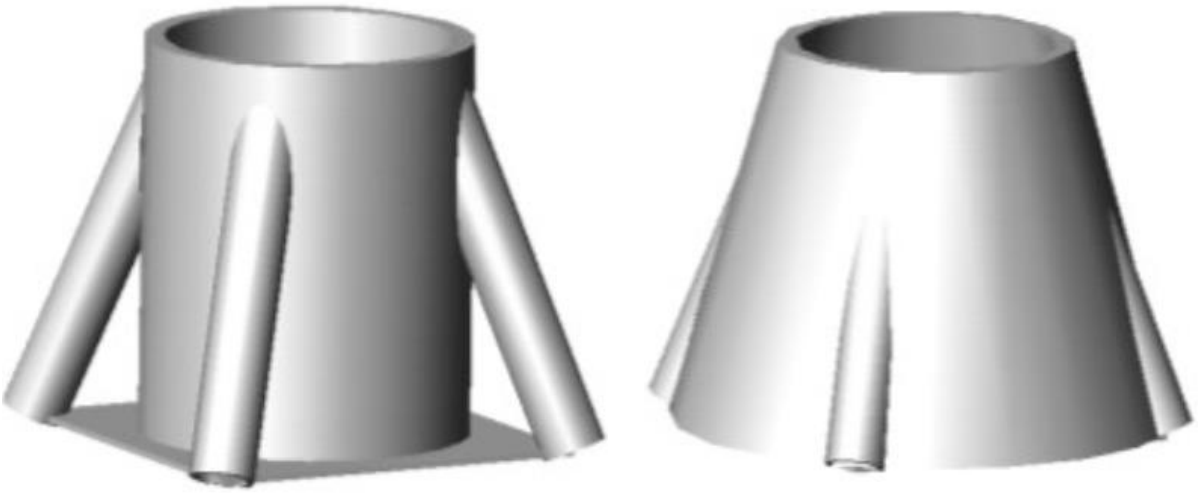

(a) (b)

***Figure 4.3**:* Various Geometrical Models for Transition Piece (a) frame-cylinder (b) cone-Strut [8]

4.2 Functional Requirement

In addition to the geometrical challenge, the transition piece should also be able to meet a number of functional requirements. Transition piece is a critical design component which needs careful detailing. Several authors have previously shown lattice support structure design proposals, but this transition structure was often only sketched and not realistically designed.

In order to ensure good behaviour of the hybrid tower, the transition segment has to ensure the correct transmission of the internal forces from the tubular tower to the lattice support structure. Due to the high level of bending moment, torsional moment and axial compression, the transition segment needs to have a high level of stiffness. Design of Transition piece vary according to specific and individual project requirements including the site and loading conditions, connecting structural dimensions, turbine weight, material cost etc. The main body geometry, the transition piece/lattice connection, transition piece/tubular connection are the parameters which grantee the maximum load transfer and resistance.

4.3 Mechanical Requirement

4.3.1 Connection with the lattice support structure

Connections are generally not the part of the study but for representing the original structure and transferring of loads they have to be part of study. Connection between the lower lattice support structure and the transition piece can normally be made through the welding of the lattice legs and the respective bracing legs of the frame cylinder system. Welding should ensure a sufficient strength which is able to transfer the loads from the transition part to the lattice support structure. On the other hand, sufficient fatigue strength of the connections is also a big challenge. In this case of hybrid design transition piece, a hexagonal shaped plate is employed covering the lattice top and can also be used as the service platform. The placement of a hexagonal plate on top of lattice support structure will be able to connect the structural components of the lattice top bracings and the six legs, which helps increasing the plane stiffness of the whole support structure. Furthermore, this hexagonal plate also provides foundation for the sitting of the cylinder and six chords of the transition piece.

4.3.2 Connection with the tubular part of tower

Connection between the transition piece and the upper tubular tower assembly is usually made through the connection of the ring flange and the cylinder component of the transition piece. But in this unique case the main connection is required on the bottom level of transition piece.

This was achieved like after jacking the last tubular part, ring flange level will be maintained with the bottom level of hexagonal plate. A covering plate will be inserted at the bottom of both hexagonal plate and ring flange of the tubular part covering both them effectively. Then the connection between them will be achieved through proper bolting ensuring the loads can properly propagate through the connection. The bolting will be done similarly as ring flange connection. First bolted connection will be between ring flange of the tubular part and covering plate. Then second bolted connection will be between ring flanges of transition piece going through hexagonal plate and connected to covering plate as shown in the **Figure 4.4**. The bolting should ensure a sufficient level of strength due to the existence of the highly complex loading conditions to be transferred at this crucial conjunction.

Secondly there will be an upper connection between transition piece and tubular part to keep the gap filled on the upper end of transition piece so the super structure will be in place while in operating condition. At this stage the details about upper connection are unclear. So in the design another covering plate is added on the top to insure the correct transmission of loads.

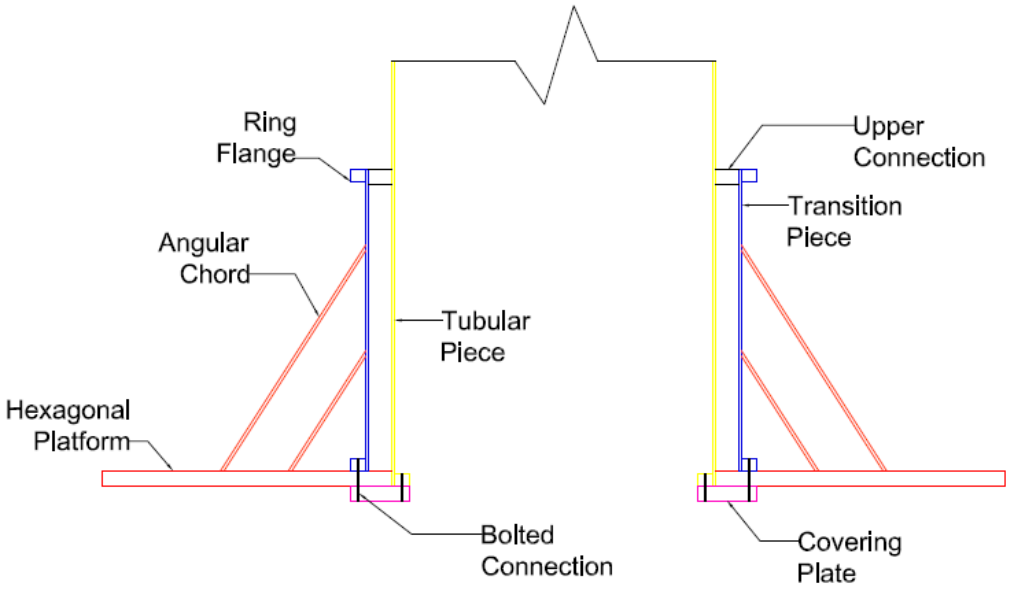

***Figure 4.4**:* Section View of Transition Segment depicting the connection of TP to lattice and tubular part

4.4 Case Studies

Based on all these project centred requirements and constraints different solutions are proposed following a conventional trial and error design methodology i.e. starting from a draft solution that is constantly improved until the design requirements are completely satisfied. Furthermore, for a detailed design of transition piece, we also need to include a realistic model of the lattice part and for that in every analysis one level of lattice part is incorporated in the model to have more detailed results. Different case studies presented in this thesis are:

1) Hybrid Transition Piece with Internal Stiffener (Case Study#1)

2) Circular Transition Piece using different grades of steel in sections (Case Study#2)

3) Circular Transition Piece using grades S690 steel in all sections (Case Study#3)

4) Circular Transition Piece using grades S355 steel in all sections (Case Study#4)

The aim of presenting different solutions of Transition segment is to exploit the possibilities and broader the concept of research. Furthermore, analysing and comparing them on the basis of functionality and economics gives us greater sense of picking a viable option. In this research mainly the focus was to analyse the solution using a stiffener, transition piece using different grades of steel in different sections and transition piece using only one grade of steel also utilizing high strength steel.

4.4.1 Case Study#1 (Hybrid Transition Piece with Internal Stiffener)

In this case study Conceptual Model of Hybrid Transition as seen in **Figure 4.5** is comprised of 10 main parts:

i. Transition Piece Shell
ii. Chords
iii. Flanges for Transition Piece
iv. Tubular Tower Shell
v. Flanges for Tubular Tower Shell
vi. Covering Plate
vii. Platform
viii. Columns
ix. Diagonals
x. Internal Stiffener

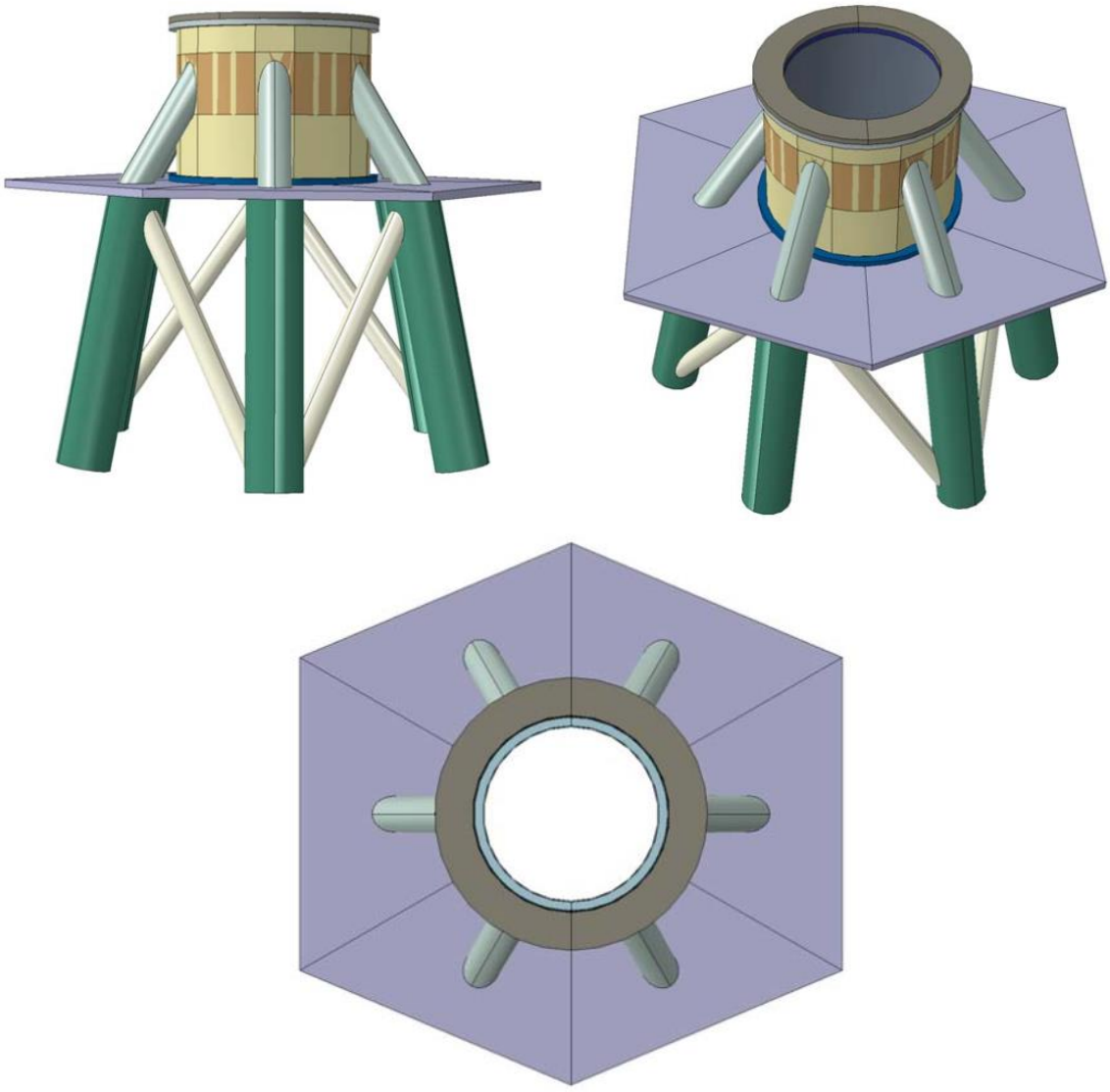

Figure 4.5: Different views of conceptual model of transition segment from Case Study#1

The Transition Piece shell is composed of two pieces, a plate and an arc plate, which are repeated 6 times each other. This reduces the complexity of the welding where the chords meet the Transition Piece Shell. The dimensions can be seen in **Table 4.1**. The two parts are welded together making a nearly perfect cylinder of 4 m high and with a diameter 5 m. Tubular tower shell is perfect cylinder of 4.2 m as it is representing a tubular part of the tower with a diameter of 4.3 m. Transition Piece Shell is connected with Ring flanges as welded connection from top and bottom on the outer face of transition piece. Tubular tower shell (tubular part of tower) is also connected with Ring flanges as welded connection from top and bottom on the inner face of the tubular ring. Both Ring flanges for outer and Tubular tower shell have same dimensions: height 150mm and width 200mm. The chords members that have a cross section of 800x40mm are welded to the plates making with the vertical an angle of 33º and from the bottom chords are welded to the platform making an angle of 57º. Furthermore, the chords are separated by an angle of 60° from top the view.

Table 4.1: Geometric Properties of Transition Piece Shell for Case Study#1

Transition Piece Shell			
Plates		Arc Plates	
b (mm)	950	L (mm)	1667.4
h (mm)	4000	r (mm)	2500
t (mm)	35	t (mm)	35
n	6	n	6

Once the circular hollow section (chords) is cut with an angle of 33º from upwards and 57º from downwards, it will take the form of an ellipse from both sides. The elliptical tube will then connect the Transition Piece Shell from top and to platform from bottom, making a proper transmission of the forces. Platform provides enough rigidity to the transition segment by connecting it to the sub-structure which in this case is lattice part of tower. It has a peculiar hexagonal shape as of lattice structure with dimensions as 12×12m and thickness of 200mm.

A covering plate of 200mm is provided on the bottom of Tubular tower shell which connects Tubular tower shell with platform and interims with transition piece serves as a basis of connection at the bottom part, while at the top it covers both Transition Piece Shell and Tubular tower shell which serves as a surface for load application as well as a connection between transition segment and tubular part to remain intact.

A circular internal stiffener of 50mm thickness is provided additionally on the internal surface of Transition Piece Shell in the vicinity of chords for adding more stiffness to the Transition Piece Shell. A cross-section view of transition piece is shown in the **Figure 4.6** for the better understanding of connection between all parts. A summary of dimensions of all parts incorporated in super structure are given in the **Table 4.2**.

Table 4.2: Overall Geometric properties of all parts in assembly of transition piece concerning Case Study#1

Transition Piece Shell	
Diameter (mm)	5000
Thickness (mm)	35
Tubular tower shell	
Diameter (mm)	4300
Thickness (mm)	34
Chords	
Diameter (mm)	800
Thickness (mm)	40
Hexagonal Platform	
Length (m)	12
Width (m)	12
Thickness (mm)	200
Flanges (Outer and Tubular tower shell)	
Width (mm)	200
Height (mm)	150
Covering Plate	
Width (mm)	750
Thickness (mm)	200
Internal Stiffener	
Length (mm)	1500
Thickness (mm)	50

Substructure is composed of 6 angular columns arranged in hexagonal shape with a plane angle of 12.2251º. The distance between the two parallel columns is 8 m. Bracing type K is used between the columns of lattice part. The details about the substructure is given in the **Table 4.3**.

Table 4.3: Geometric properties of substructure

Lattice Structure				
	D (mm)	t (mm)	No.	L
Bracing	560	18	6	8050
Column	1350	35	6	7000

The connection between the tubular tower and the transition piece is made through bolted flange connection. It is important to mention that the connections were not objective of study in this project. Moreover, the introduction of holes for the bolts on the model has a significant

increase of computation effort. Thus the bolts will not be considered. The same type of connection will be used to link the lattice structure to the transition segment.

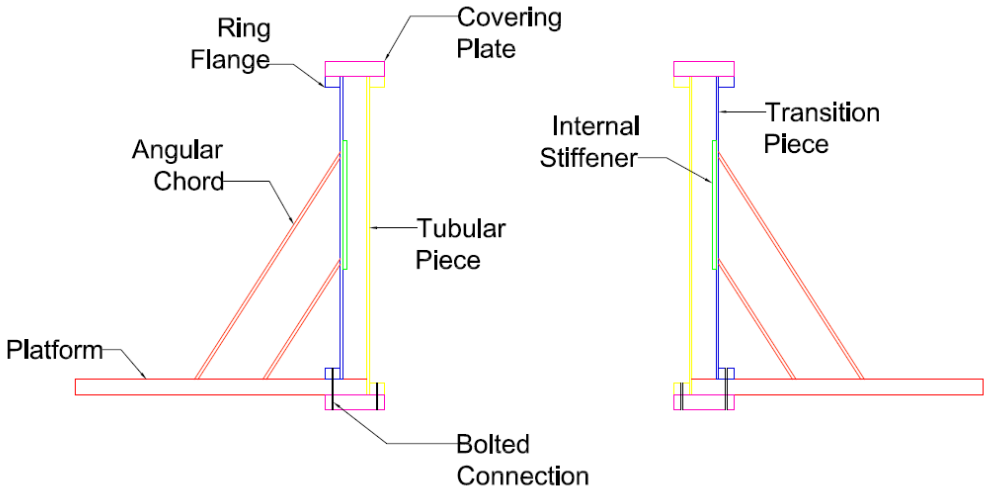

***Figure 4.6**:* Section View of Transition piece for Case Study#1

4.4.2 Case Study#2 (Circular Transition Piece using different grades of steel in Transition Piece Shell)

In this solution of Conceptual Model of Circular Transition Piece seen in **Figure 4.7** has nine main parts:

i. Transition Piece Shell
ii. Chords
iii. Flanges for Transition Piece Shell
iv. Tubular tower shell
v. Flanges for Tubular tower shell
vi. Covering Plate
vii. Platform
viii. Columns
ix. Diagonals

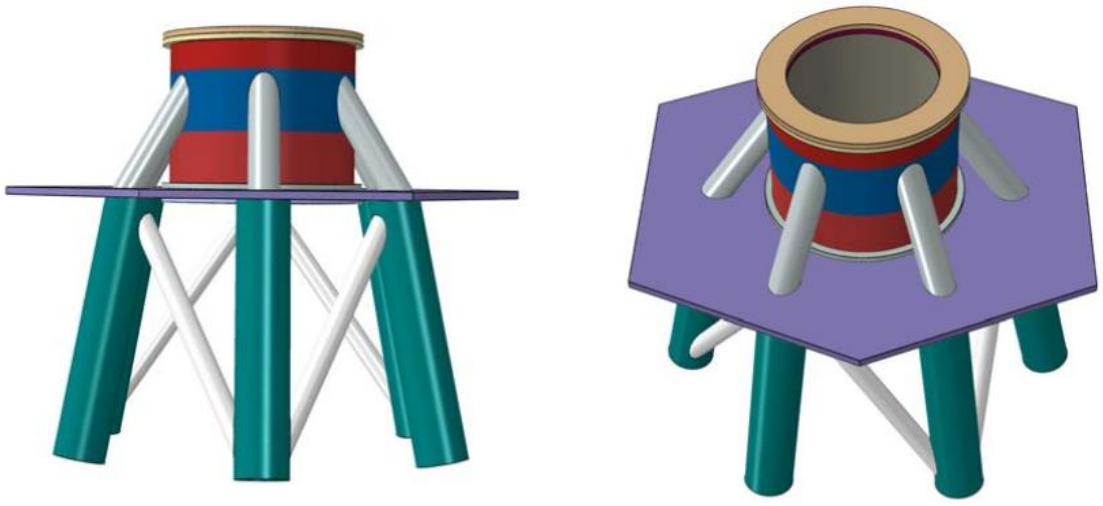

***Figure 4.7**:* Different views of conceptual model of transition segment from Case Study#2

The Transition Piece Shell is composed of three pieces of circular rings upper, lower and middle. The three circular rings are welded together making a perfect cylinder of 4m high and with a diameter of 5m. This reduces the complexity of the welding. The dimensions can be seen in **Table 4.4**.

Table 4.4: Geometrical properties of Transition Piece Shell for Case Study#2

Transition Piece Shell					
Upper		Middle		Lower	
height	900mm	height	1600mm	height	1500mm
thickness	35mm	thickness	50mm	thickness	35mm

The assemblage and construction of other parts are exactly the same as described in previous solution like boundary condition, load point and interactions everything is same for this solution too. The main difference between previously described and this solution lies only in Transition Piece Shell, there is no internal stiffener in this solution and three circular rings are used instead of hybrid ring which was composed six of plates and arcs. The upper and lower ring is composed of thinner thickness with a lesser yield strength steel grade while middle ring is thicker with high yield strength steel grade. The three sections have less height so that they can be transported easily and on the site for assembly they can be either bolted or welded together.

4.4.3 Case Study #3 (Circular Transition Piece using grade S690 steel in Transition Piece Shell)

In this solution of Conceptual Model of Circular Transition Piece **Figure 4.8** has nine main parts which are listed as:

i. Transition Piece shell
ii. Chords
iii. Flanges for Transition Piece shell
iv. Tubular tower shell
v. Flanges for Tubular tower shell
vi. Covering Plate
vii. Platform
viii. Columns
ix. Diagonals

The Transition Piece Shell is composed of three pieces of circular rings upper, lower and middle. The three circular rings are welded together making a perfect cylinder of 4m high and with a diameter of 5m. This reduces the complexity of the welding. And this solution represents the applicability of using just high strength steel on transition piece. The dimensions can be seen in **Table 4.5**.

***Table 4.5**:* Geometrical properties for Transition Piece Shell from Case Study#3

Transition Piece Shell					
Upper		Middle		Lower	
height	900mm	height	1600mm	height	1500mm
thickness	40mm	thickness	40mm	thickness	40mm

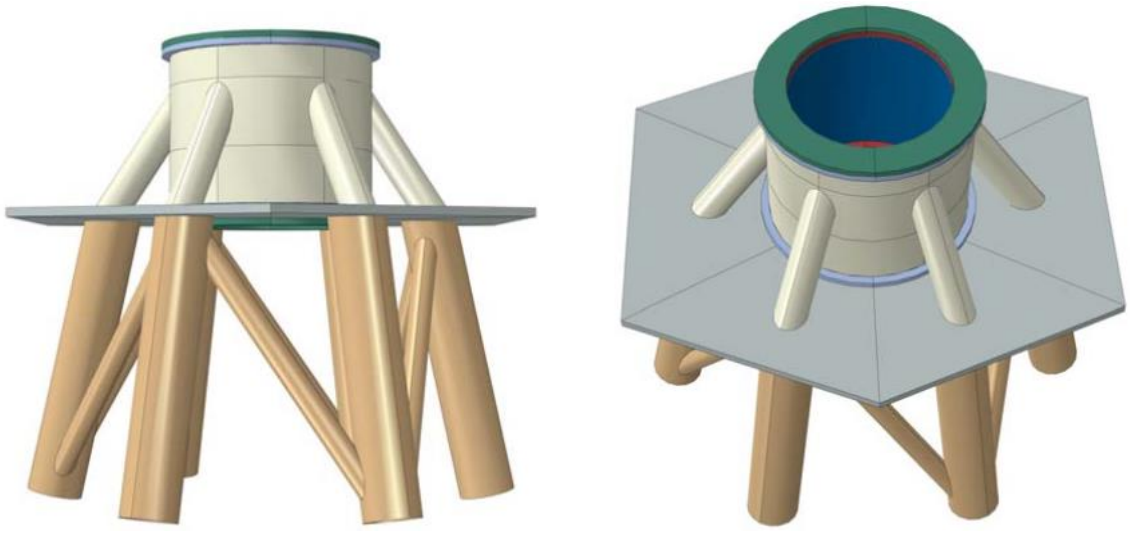

***Figure 4.8**:* Different views of Transition Segment from Case Study#3

The assemblage and construction of other parts are exactly the same as described in previously mentioned solutions like materials, boundary condition, load point and interactions everything is same for this solution too. The main difference between previously described and this solution lies only in Transition Piece Shell, there is no internal stiffener in this solution and three circular rings are used instead of hybrid ring. All sections of Transition Piece Shell are composed of same thickness with a same yield strength steel grade. The three sections have less height so that they can be transported easily and on the site for assembly they can be either bolted or welded together.

4.4.4 Case Study #4 (Circular Transition Piece using mild steel S355 in Transition Piece Shell)

Conceptual Model of Hybrid Transition piece using mild structural steel S355 **Figure 4.9** has nine main parts:

i. Transition Piece Shell
ii. Chords
iii. Flanges for Transition Piece Shell
iv. Tubular tower shell

v. Flanges for Tubular tower shell
vi. Covering Plate
vii. Platform
viii. Columns
ix. Diagonals

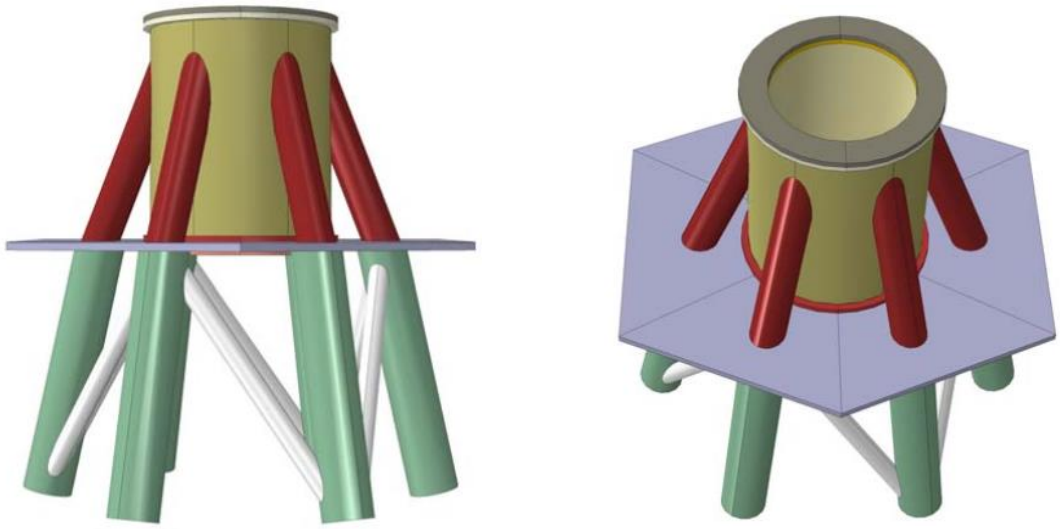

***Figure 4.9**:* Different views of Transition Segment from Case Study#4

The Transition Piece Shell is composed of three pieces of circular rings upper, lower and middle. The three circular rings are welded together making a perfect cylinder of 6m high and with a diameter of 5m. And this solution represents the applicability of using just mild structural steel on transition piece. The dimensions can be seen in **Table 4.6**.

***Table 4.6**:* Geometrical properties for Transition Piece Shell from Case Study#4

Transition Piece Shell					
Upper		Middle		Lower	
height	900mm	height	3000mm	height	2100mm
thickness	45mm	thickness	45mm	thickness	45mm

The chords members that have a cross section of 1000x35mm are welded to the Transition Piece Shell making with the vertical an angle of 21º and from the bottom chords are welded to the platform making an angle of 69º. Furthermore, the chords are separated by an angle of 60° from top the view.

Chapter 5 FINITE ELEMENT ANALYSIS OF THE TRANSITION SEGMENT

In previous Chapter 4 it was defined that what are the governing factors and requirements for the design of transition segment and case studies of different solutions were indicated. Now each solution will be analysed in detail by performing, a finite element analysis (FEA) on software package *ABAQUS* according to Euro code EN1993-1-6 [27] European standard. Such standard takes into account the requirements for the design against Ultimate Limit. So, all the solutions proposed will be checked for Plastic Limit State, Buckling Limit State and Fatigue Limit State subsequently.

5.1 General Numerical Model

5.1.1 Assembly and Interactions

After creating each part separately in *ABAQUS*, to create whole model as one, all the parts had to be assembled on assembly module. The **Figure 4.5**, **Figure 4.7**, **Figure 4.8** & **Figure 4.9** in sections 4.4.1,4.4.2, 4.4.3 & 4.4.4 shows only the model geometries, where all the part instances are assembled generating the whole transition segment. Although all the part instances are in the correct position on the assembly section but it is necessary to model the interaction between all the elements for *ABAQUS*, to recognize the model as one segment and for transfer of forces from one part to the other effectively.

For that purpose, *Tie* constraints are defined between surfaces. A surface-based tie constraint can be used to make the translational and rotational motion as well as all other active degrees of freedom equal for a pair of surfaces. By default, nodes are tied only where the surfaces are close to one another. One surface in the constraint is designated to be the slave surface; the other surface is the master surface. Nine *tie* constraints had to be created to simulate the interaction of the assembly which are as:

i. Interaction between top of chords and outer surface of Transition Piece Shell
ii. Interaction between bottom of chords and upper surface of platform
iii. Interaction between top of columns and lower surface of platform
iv. Interaction between the flanges connected to transition piece and outer surface of Transition Piece Shell
v. Interaction between the flanges connected to tubular part and outer surface of Tubular tower shell
vi. Interaction between the lower surface of platform and upper surface of covering plate
vii. Interaction between the lower surface of covering plate and upper surface of outer and Tubular tower shell flanges

viii. Interaction between outer surface of stiffener and inner surface of Transition Piece Shell

ix. Interaction between the lower surface of transition piece and upper surface of platform.

5.1.2 Boundary Conditions

In order to model accurately the transition piece, there was an effort to replicate the boundary conditions on the real structure by adding one extra level of the lattice part of wind turbine, on the model. Therefore, at the bottom end of the column a reference point (RP) was made for each support. Furthermore, coupling constraint was created in order to have a control point of that region. The surface-based coupling constraint in *ABAQUS* provides coupling between a reference node and a group of nodes. So, all translations and rotations were restrained on the reference point. This procedure can be seen on **Figure 5.1** and it was repeated six times, for the all supports.

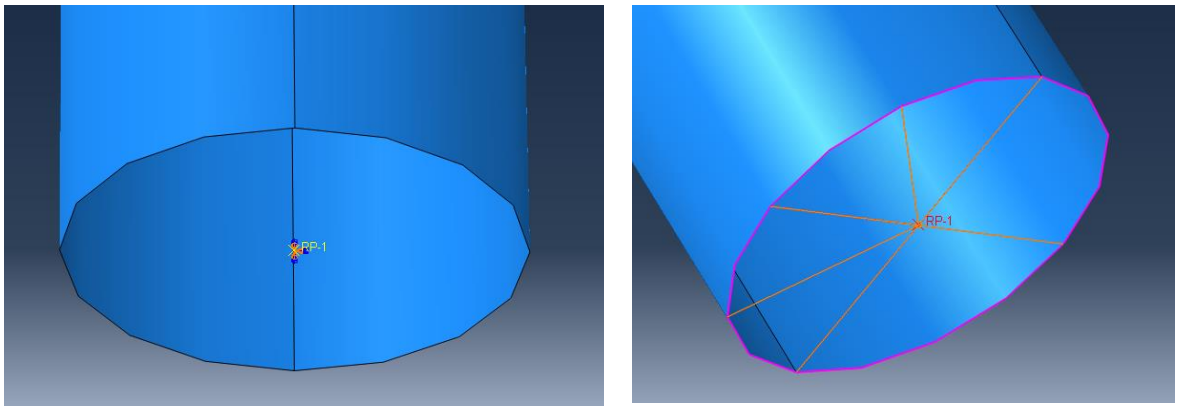

***Figure 5.1**:* Boundary Conditions for support

5.1.3 Application of Load

For the application of load in *ABAQUS* the same procedure that was done before for the boundary conditions was repeated, since it is the same type of connection. A reference point was created (RP-7), which was named as load point (LP), as shown in **Figure 5.2**, and then coupling constraint was created for the load point with the upper surface of covering plate, which applies the load simultaneously on both Tubular tower shell and Transition Piece Shell, but in reality the load is just because of Tubular tower shell (tubular tower with nacelle) which was modelled too by applying load on just upper flange of Tubular tower shell but the stresses comes out to be more or less same. This system of loading (applying load simultaneously on inner and Transition Piece Shell) is applied because it gives more stress on Transition Piece Shell/transition piece which is the main focus of this study.

ABAQUS has no inbuilt unit system. Caution is highly recommended when using consistent units as SI-system. In this project, the SI-mm system was used as shown in **Table 5.1**.

***Table 5.1**:* Units *SI* system used in *ABAQUS*

ABAQUS		
Quantity	SI (m)	SI (mm)
Length	m	mm
Force	N	N
Mass	Kg	Tonne (10^3 kg)
Time	s	s
Stress	Pa (N/mm^2)	MPa (N/mm^2)
Energy	J	mJ (10^{-3} J)
Density of Steel	7850 kg/m^3	7.85E-09 tonne/mm^3
Acceleration of Gravity	9.81 m/s^2	9810 mm/s^2
Young's Modulus of Steel	210E9 Pa	210E3 MPa

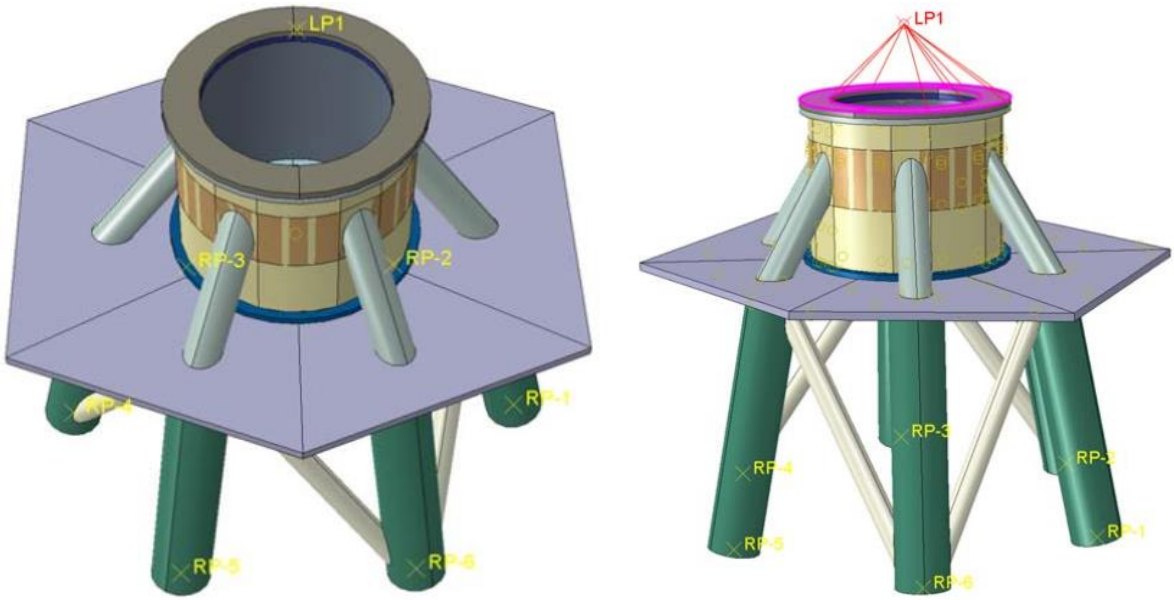

***Figure 5.2**:* Reference Load Point and coupling constraint

***Table 5.2**:* Design Load values [28]

LOADS input in ABAQUS		
Load Vector	Magnitude	Units
Fx	1.0650E+06	N
Fy	1.0650E+06	N
Fz	-4.8790E+06	N
Mx	8.9126E+10	N*mm
My	1.2328E+11	N*mm
Mz	3.9660E+09	N*mm

5.1.4 Mesh Study

In order to ensure adequate results from *ABAQUS* simulation a refined and good quality mesh should be used. However, the computer resources required to perform the finite element analysis increase with the level of the mesh refinement. Since the Transition Piece Shell is the most critical part a mesh convergence study was done for this part. A linear analysis was performed using a standard general procedure. Mesh study was conducted using two types of elements:

1. Tri-dimensional solid elements
2. A 3-node triangular basic shell element.

5.1.4.1 Tri-dimensional solid elements

In this type, finite element mesh is exclusively constituted by tri-dimensional solid elements. The element type of C3D8R was adopted, due to the high dimension of the model. A different type of solid element such as C3D8, C3D20 or C3D20R would increase exponentially the computation effort. Since the model has a complex shape, given by a lot of partitions (see **Figure 5.3**) in all part instances were created in order to have a structured mesh technique. Same ULS loads were applied at the load point. The criterion to stop the mesh refinement was that the difference should be very lower then compared to the previous mesh size. The **Figure 5.4** shows the stress distribution versus number of elements. Moreover, **Table 5.3** reviews the mesh convergence study and held not only the different global mesh sizes but also the criteria used to stop the mesh refinement.

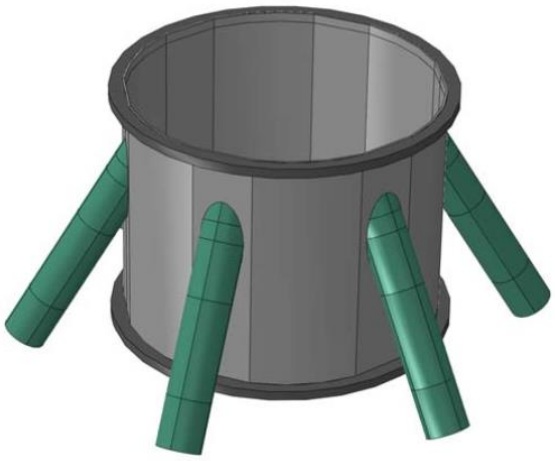

Figure 5.3: Transition piece used for mesh study

Table 5.3: Mesh Convergence study using tri dimensional Solid Elements

	Global Size	Total Elements	Maximum Stress	Error (%)
Mesh#1	100	8409	2872.42	0.222112
Mesh#2	80	13056	2878.8	-21.2394
Mesh#3	50	34644	2267.36	1.222567
Mesh#4	40	57978	2295.08	-0.36426

Mesh#5	30	105952	2286.72	-1.88173
Mesh#6	23.5	178323	2243.69	-22.5682
Mesh#7	23	313753	1737.33	1.619151
Mesh#8	22	343526	1765.46	-0.19768
Mesh#9	21.5	358578	1761.97	-0.09705
Mesh#10	21	374373	1760.26	-0.07953
Mesh#11	20.5	389806	1758.86	-0.02274
Mesh#12	20	424850	1758.46	

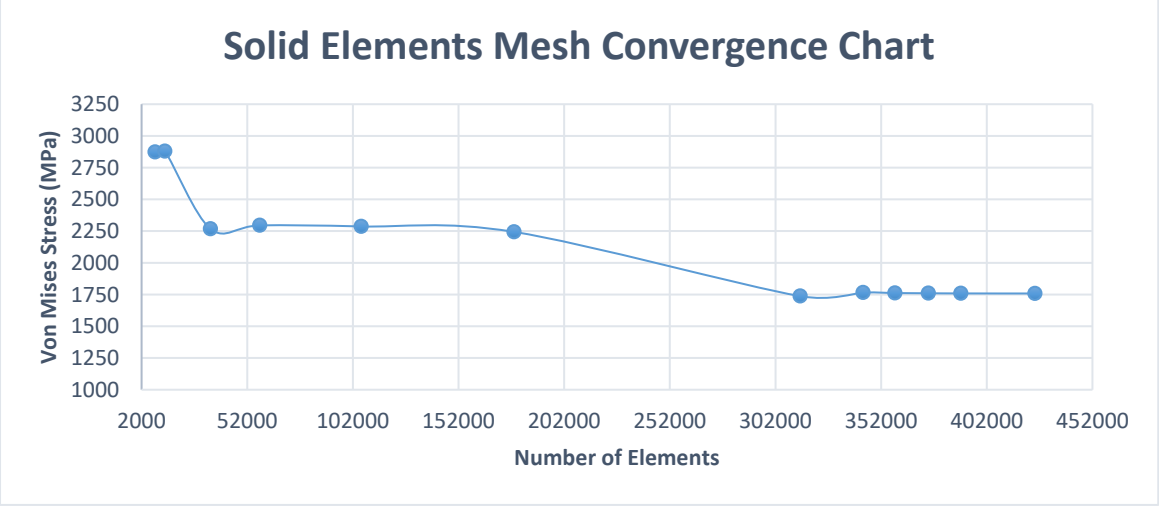

Figure 5.4: Mesh convergence Study for Solid elements

5.1.4.2 A 3-node triangular basic shell element

In this type, finite element mesh is constituted by tri-nodal triangular shell elements. The element type S3 was adopted. Since the model has a complex shape, given by a lot of curves free tri mesh technique was used. Same ULS loads were applied at the load point. The criterion to stop the mesh refinement was that the difference should be very lower then compared to the previous mesh size. The **Figure 5.5** shows the stress distribution versus number of elements. Moreover, **Table 5.4** reviews the mesh convergence study and held not only the different global mesh sizes but also the criteria used to stop the mesh refinement.

Table 5.4: Mesh Convergence study using A 3-node triangular shell Elements

	Global Size	Total Elements	Maximum Stress	Error
Mesh#1	100	15074	1627.67	0.014745
Mesh#2	80	23788	1627.91	5.587532
Mesh#3	60	43754	1718.87	3.015935
Mesh#4	50	61410	1770.71	2.644137
Mesh#5	40	99894	1817.53	1.804097
Mesh#6	30	180176	1850.32	1.911021
Mesh#7	28	205957	1885.68	0.840546

Mesh#8	26	246192	1901.53	0.911897
Mesh#9	25	265620	1918.87	1.056872
Mesh#10	24	286558	1939.15	0.745172
Mesh#11	21	355869	1953.6	0.112613
Mesh#12	20	434626	1955.8	

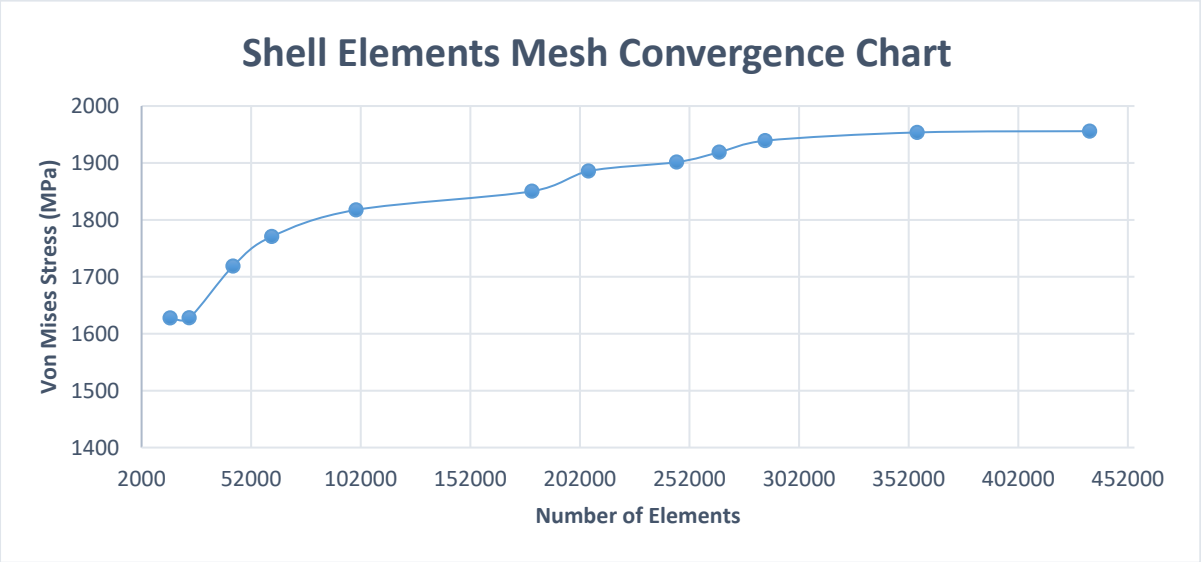

***Figure 5.5**:* Mesh convergence Study for Shell elements

5.1.5 Element Type

After getting results from the mesh study for both type of elements i.e. solid and shell. Both were used for analysis with the finer mesh and behaviour of the structure was closely monitored. When using solid elements, it was observed that distortion is arising around the parts of transition piece and substructure where they meet because of the complex geometry and concentration of stresses but for shell elements it was quite better. So a combination of element type is used for different part in whole assembly. **Table 5.5** summarizes the important data comprehensively relative to the mesh, including the number of finite elements and nodes.

***Table 5.5**:* Meshing Information for whole structure

Part	Element Type	Element Shape	Mesh Technique	Number of Elements	Number of Nodes
TP Flanges	C3D8R	Hexahedral	Structured	160928	195696
IR Flanges	C3D8R	Hexahedral	Structured	103040	127512
Covering Plates	C3D8R	Hexahedral	Structured	442624	511056
Internal Stiffener	S3	Triangular	Structured	145084	73416

Sub-Structure	S3	Triangular	Free	1075715	538347
Platform	C3D8R	Hexahedral	Structured	179944	227640
Transition Piece with Chords	S3	Triangular	Free	621736	311596
Tubular tower shell	S4R	Quad	Free	141075	141075
TOTAL				2,870,146	2,126,338

5.1.6 Material Model

For taking into account, the material non-linearity, the plasticity of the steel had to be introduced on the finite element model through property module in ABAQUS. Simple plasticity material model was used. **Figure 5.6** shows the material law for the high strength steel S690, S460 and for the mild structural steel S355.

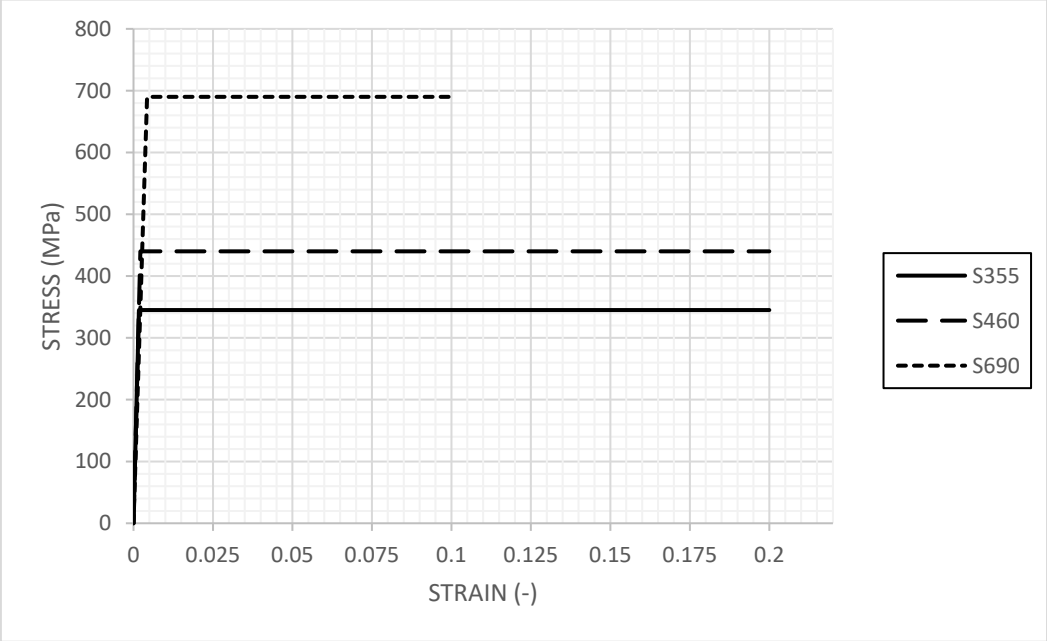

***Figure 5.6**:* Steel curve stress-strain for *S690, S460 & S355*

5.2 Ultimate Limit State

5.2.1 Plastic Limit State (LS1)

Plastic Limit State is verified according to the methodology explained in section 3.3.

5.2.1.1 Results for Case Study#1 (Hybrid TP with Internal Stiffener)

5.2.1.1.1 Transition Piece Shell

The Transition Piece Shell is composed by S460 steel, which has a least strength of 460 MPa.

$\sigma_{MISES,Ed} = 439 \leq f_{yd} = 460\ MPa$ → LS1 verified for Transition Piece Shell **Figure 5.7**.

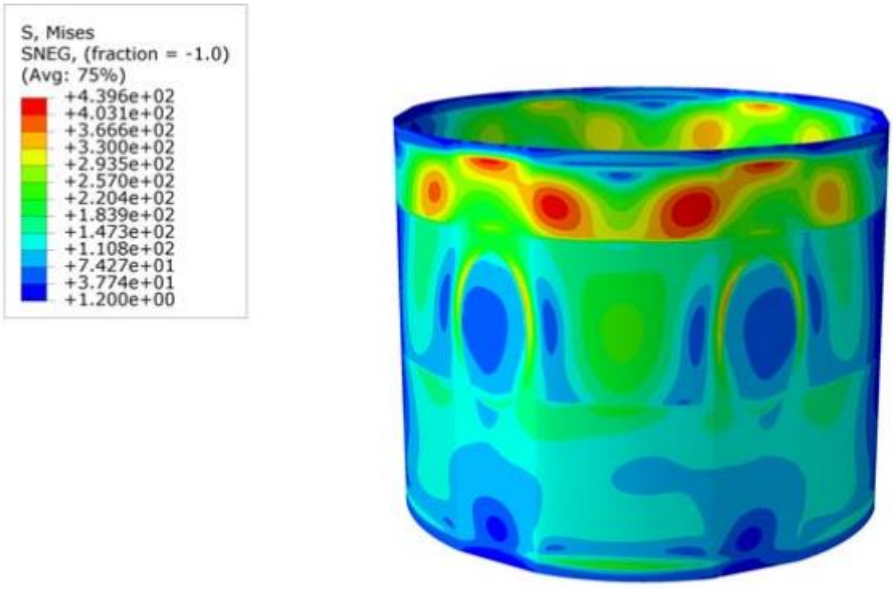

Figure 5.7: Stress distribution for Transition Piece Shell (GMNA) Solution#1

5.2.1.1.2 Internal Stiffener

The internal stiffener is composed by S690 steel, which has a least strength of 690 MPa.

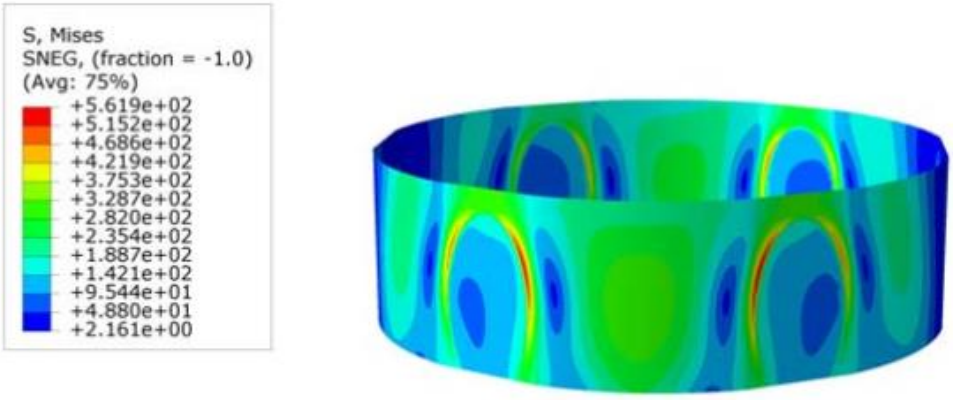

Figure 5.8: Stress distribution for Internal Stiffener (GMNA) Solution#1

$\sigma_{MISES,Ed} = 561.9 \leq f_{yd} = 690\ MPa$ verified for internal stiffener **Figure 5.8**.

5.2.1.1.3 Chord

The chord is composed by S690 steel, which has a least strength of 690 MPa.

$\sigma_{MISES,Ed} = 663.1 \leq f_{yd} = 690\ MPa$ verified for Chords **Figure 5.9**.

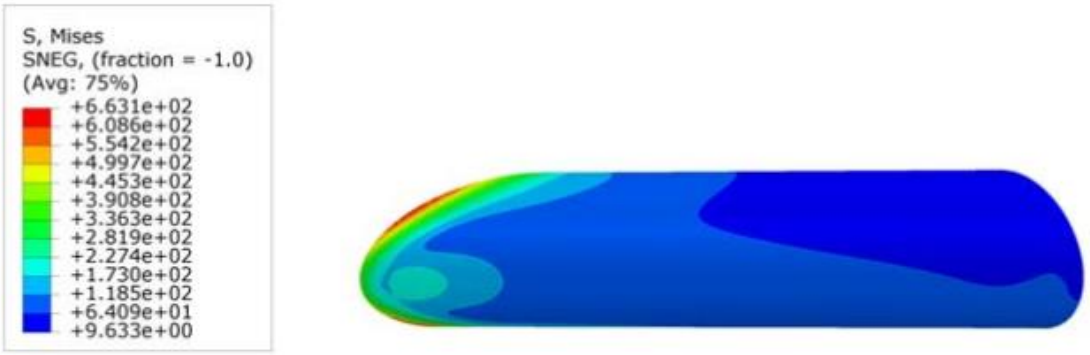

***Figure 5.9**:* Stress distribution for chords (GMNA) Solution#1

5.2.1.1.4 Tubular tower shell

Tubular tower shell is composed by S355 steel, which has a least strength of 345 MPa.

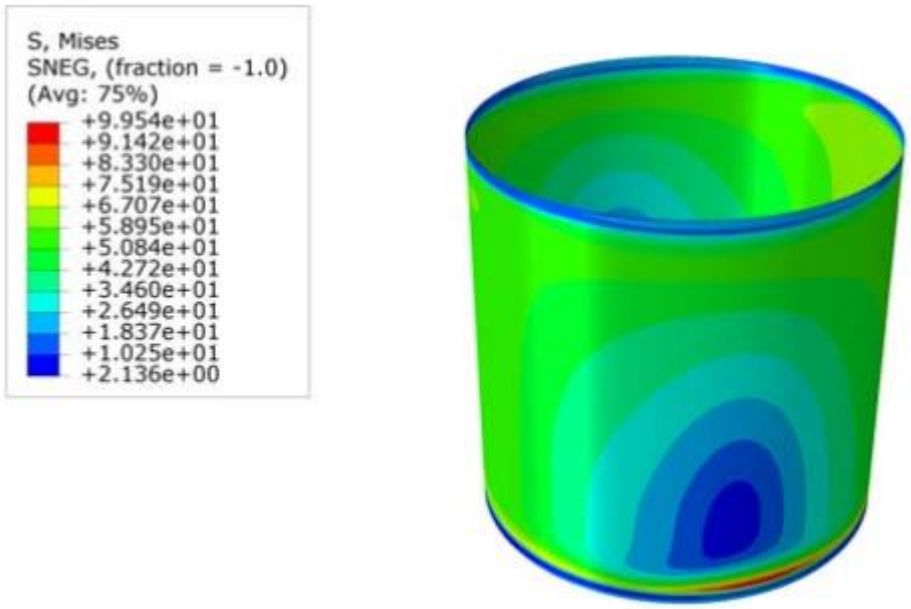

***Figure 5.10**:* Stress distribution for Tubular tower shell (GMNA) Solution#1

$\sigma_{MISES,Ed} = 99.5 \leq f_{yd} = 345\ MPa$ verified for Tubular tower shell **Figure 5.10**.

5.2.1.1.5 Substructure

Sub-structure is composed by S355 steel, which has a least strength of 345 MPa.

$\sigma_{MISES,Ed} = 262.5 \leq f_{yd} = 345\ MPa$ verified for Substructure **Figure 5.11**.

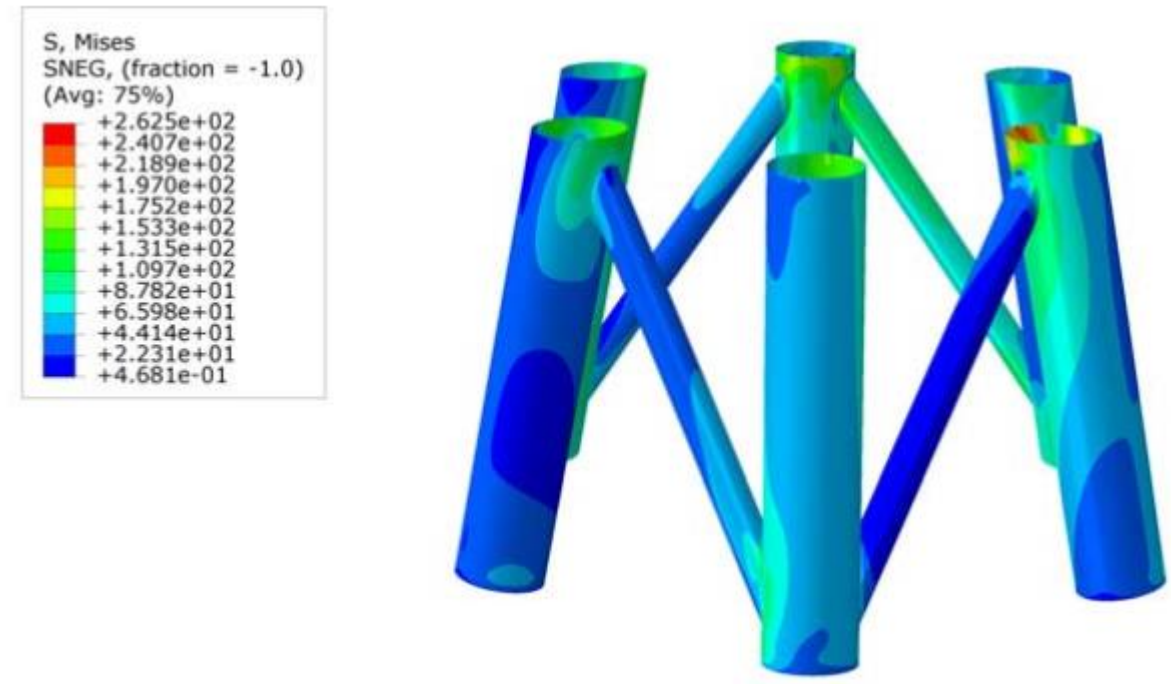

Figure 5.11: Stress distribution for Sub-structure (GMNA) Solution#1

5.2.1.2 Influence of Internal Stiffener

Once the design and modelling of the transition piece is done, it is important to estimate the contribution of the Internal Stiffener. Considering the complexity of the geometry of the transition segment, a geometrically non-linear analysis was performed with the load design values, not only for the model with the internal stiffener but also for the model without the internal stiffener reinforcement (**Figure 5.12** and **Figure 5.13**).

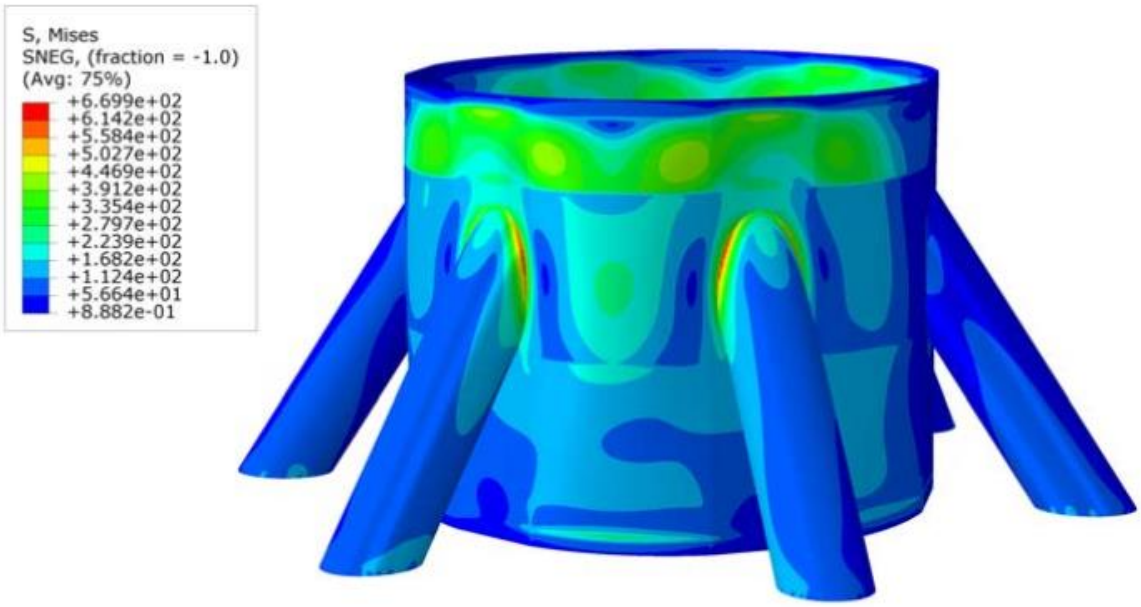

Figure 5.12: Stress distribution of Transition Piece including Internal Stiffener (GMNA) Solution #1

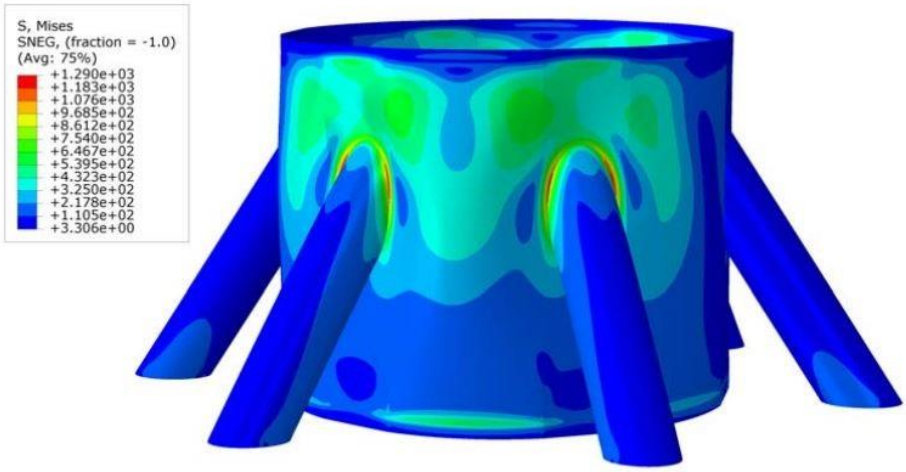

***Figure 5.13**:* Stress distribution of Transition Piece excluding Internal Stiffener (GMNA) Solution #1

The Von Mises stress distribution was compared for the two models. Although the stress distribution on the internal stiffener is significantly lower, but its presence causes a reduction of 50% on the stress distribution of the overall transition piece. Therefore, it was concluded that the internal stiffener has a key impact on the resistance of the transition segment for this solution.

5.2.1.3 Results for Case Study #2 (Circular TP using different grades of steel in Transition Piece Shell)

5.2.1.3.1 Transition Piece Shell

The Transition Piece Shell is composed of two steel grades S460 and S690, upper and lower section is assigned S460 steel while middle section has S690. The former has a least strength of 440 MPa while latter has 690 MPa **Figure 5.14**.

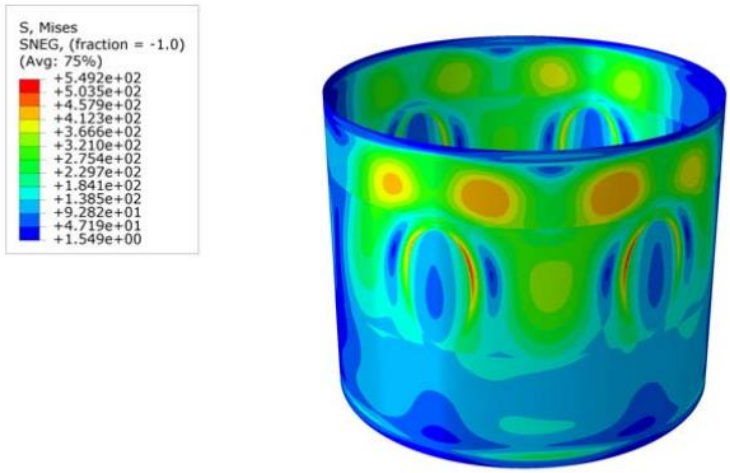

***Figure 5.14**:* Stress distribution of Transition Piece Shell (GMNA) Solution #2

$\sigma_{MISES,Ed} = 549.2 \leq f_{yd} = 690\ MPa$ verified for middle section;
$\sigma_{MISES,Ed} = 412.3 \leq f_{yd} = 440\ MPa$ verified for upper and lower section.

5.2.1.3.2 Chord

Six Chords with 40mm thickness and 800mm diameter made with S690 HSS steel are connected to the TP, which has a least strength of 690 MPa.

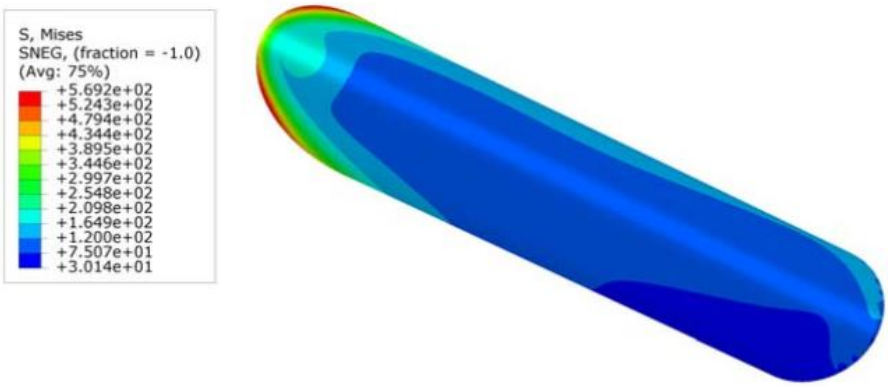

Figure 5.15: Stress distribution for chords (GMNA) Solution#2

$\sigma_{MISES,Ed} = 569.2 \leq f_{yd} = 690\ MPa$ verified for chord **Figure 5.15**.

5.2.1.3.3 Tubular tower shell

Tubular tower shell is composed by S355 steel, which has a least strength of 345 MPa.

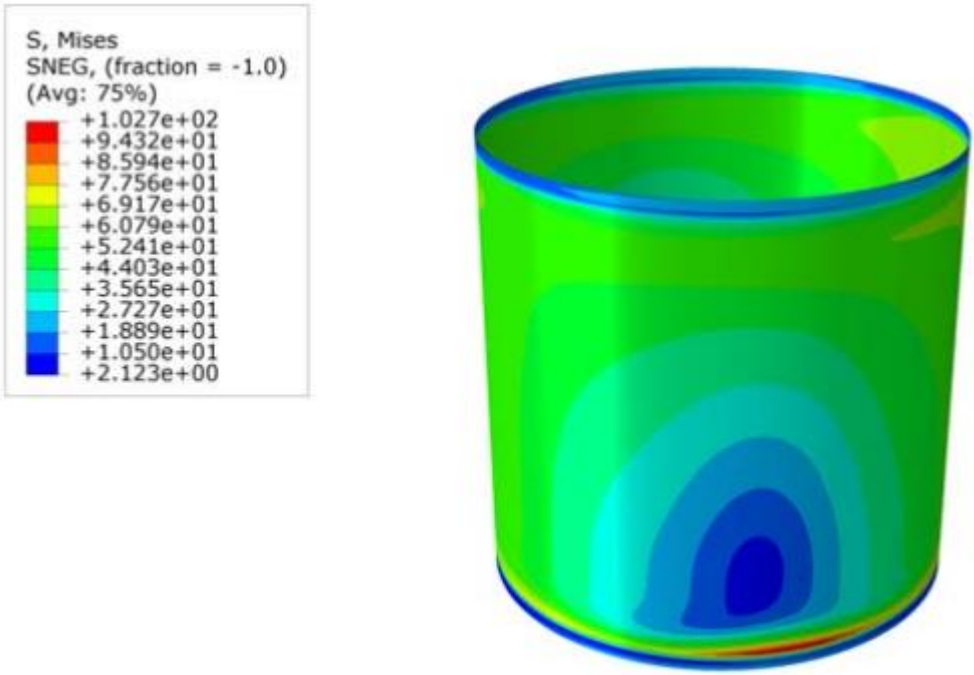

Figure 5.16: Stress distribution for Tubular tower shell (GMNA) Solution#2

$\sigma_{MISES,Ed} = 102.7 \leq f_{yd} = 345\ MPa$ verified for Tubular tower shell **Figure 5.16**.

5.2.1.3.4 Substructure

Sub-structure is composed by S355 steel, which has a least strength of 345 MPa.

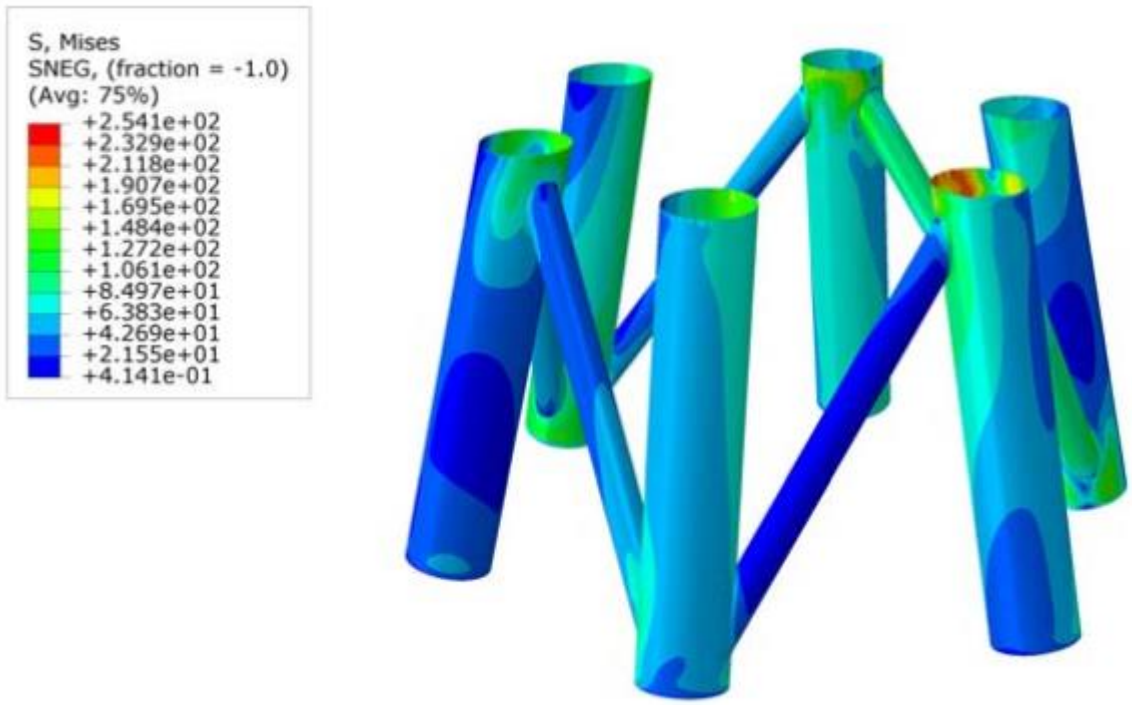

Figure 5.17: Stress distribution for Sub-structure (GMNA) Solution#2

$\sigma_{MISES,Ed} = 254.1 \leq f_{yd} = 345\ MPa$ verified for Substructure **Figure 5.17**.

5.2.1.4 Results for Case Study #3 (Circular TP using grade S690 steel in Transition Piece Shell)

5.2.1.4.1 Transition Piece Shell

The Transition Piece Shell is composed by S690 steel, which has a least strength of 690 MPa.

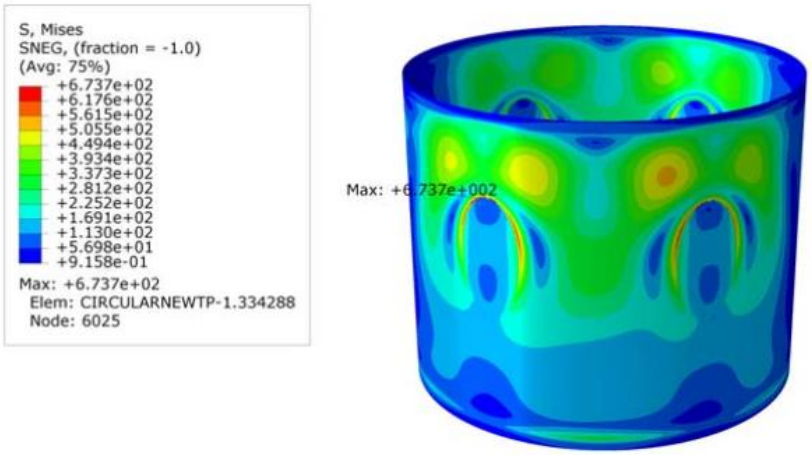

Figure 5.18: Stress distribution for Transition Piece Shell (GMNA) Solution#3

$\sigma_{MISES,Ed} = 637.7 \leq f_{yd} = 690\ MPa$ verified for Transition Piece Shell **Figure 5.18**.

5.2.1.4.2 Chords

6 Chords with 35mm thickness and 800mm diameter made with S690 HSS steel are connected to the TP, which has a least strength of 690 MPa.

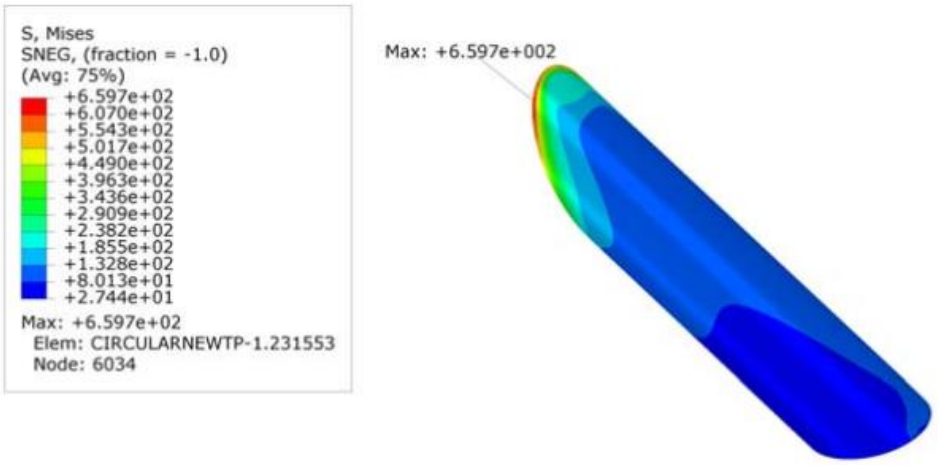

Figure 5.19: Stress distribution for chords (GMNA) Solution#3

$\sigma_{MISES,Ed} = 659.7 \leq f_{yd} = 690\ MPa$ verified for chord **Figure 5.19**.

5.2.1.4.3 Tubular tower shell

Tubular tower shell is composed by S355 steel, which has a least strength of 345 MPa.

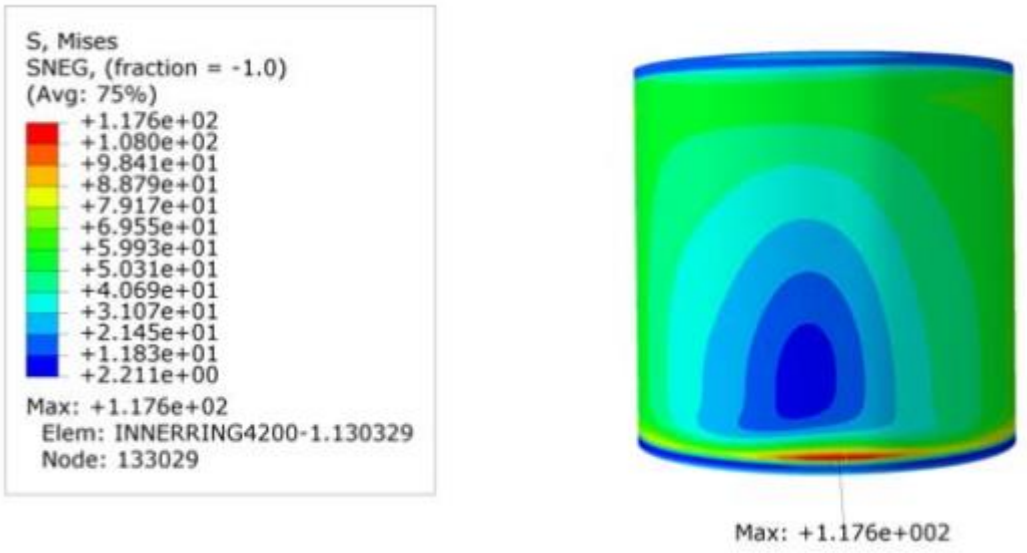

Figure 5.20: Stress distribution for Tubular tower shell (GMNA) Solution#3

$\sigma_{MISES,Ed} = 117.6 \leq f_{yd} = 345\ MPa$ verified for Tubular tower shell **Figure 5.20**.

5.2.1.4.4 Substructure

Sub-structure is composed by S355 steel, which has a least strength of 345 MPa.

$\sigma_{MISES,Ed} = 280.7 \leq f_{yd} = 345\ MPa$ verified for Substructure **Figure 5.21**.

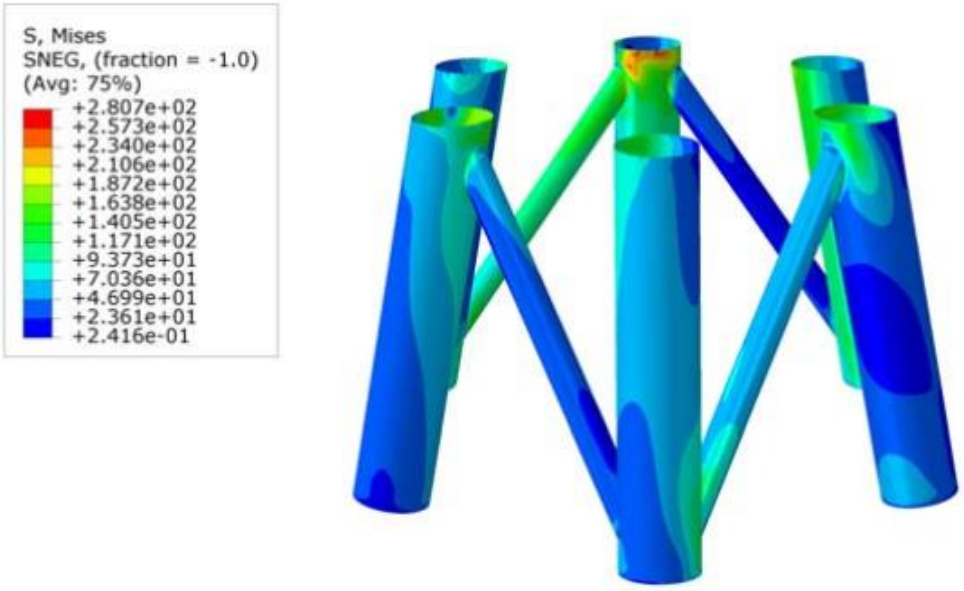

Figure 5.21: Stress distribution for Sub-structure (GMNA) Solution#3

5.2.1.5 Results for Case Study #4 (Circular TP using mild steel S355 in Transition Piece Shell)

5.2.1.5.1 Transition Piece Shell

The Transition Piece Shell is composed by S355 steel, which has a least strength of 335 MPa.

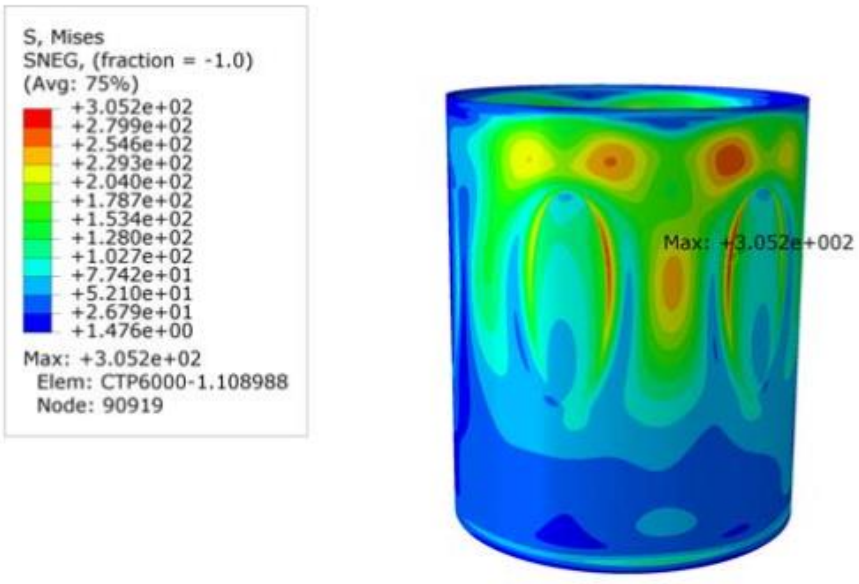

Figure 5.22: Stress distribution for Transition Piece Shell (GMNA) Solution#4

$\sigma_{MISES,Ed} = 305.2 \leq f_{yd} = 335\ MPa$ verified for Transition Piece Shell **Figure 5.22**.

5.2.1.5.2 Chords

6 Chords with 35mm thickness and 1000mm diameter made with S355 steel are connected to the TP, which has a least strength of 345 MPa.

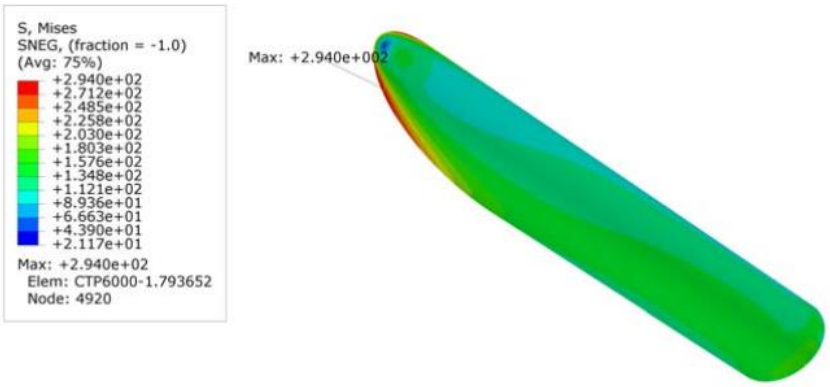

Figure 5.23: Stress distribution for chords (GMNA) Solution#4

$\sigma_{MISES,Ed} = 294 \leq f_{yd} = 335\ MPa$ verified for chord **Figure 5.23**.

5.2.1.5.3 Tubular tower shell

Tubular tower shell is composed by S355 steel, which has a least strength of 345 MPa.

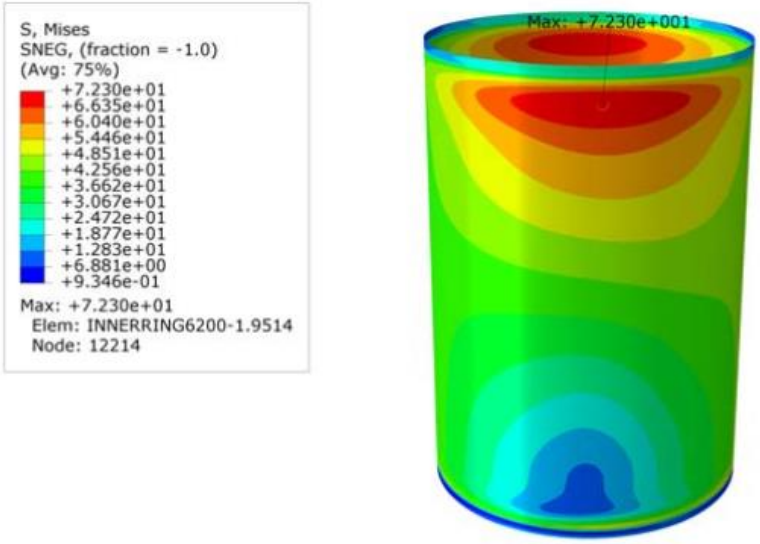

Figure 5.24: Stress distribution for Tubular tower shell (GMNA) Solution#4

$\sigma_{MISES,Ed} = 72.3 \leq f_{yd} = 345\ MPa$ verified for Tubular tower shell **Figure 5.24**.

5.2.1.5.4 Substructure

Sub-structure is composed by S355 steel, which has a least strength of 345 MPa.

$\sigma_{MISES,Ed} = 183.9 \leq f_{yd} = 345\ MPa$ verified for Substructure **Figure 5.25**.

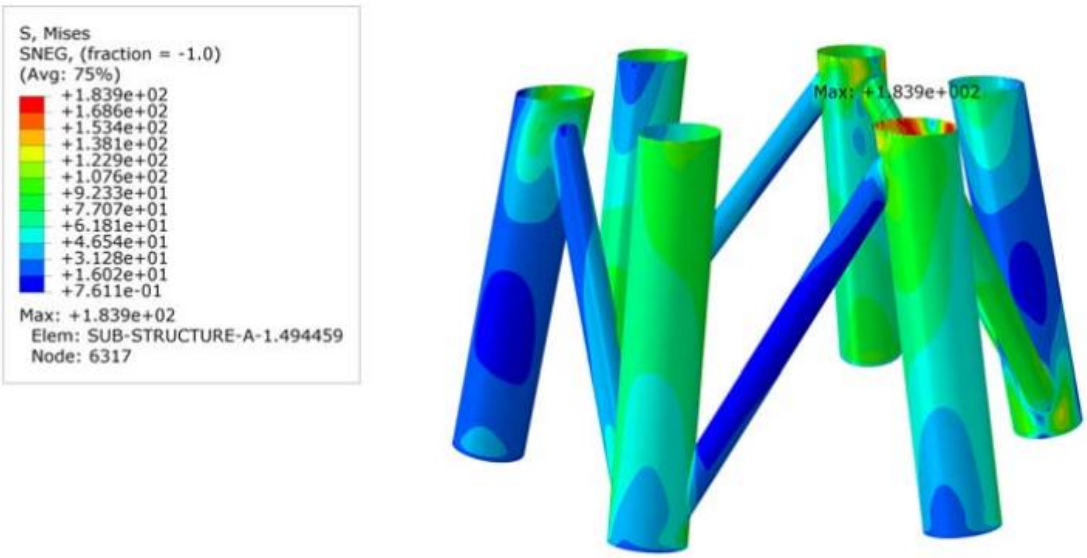

***Figure 5.25**:* Stress distribution for Sub-structure (GMNA) Solution#4

5.2.2 Buckling Limit State (LS3)

The buckling limit state (LS3) was verified according to the standard EN1993 Part 1-6 section 8.7 [27]. The same load cases as LS1 were considered to verify LS3.

Methodology is performed as explained in section 3.3. Nonlinear buckling analysis with effect of the steel plasticisation was used to investigate the post buckling behaviour and find if the yield transforms the stable post buckling behaviour into unstable, since, after the yield, an increase in the deformation causes a decrease of the corresponding load.

Since the post buckling behaviour may become unstable when the elasto-plastic deformations occur, it is very important to investigate the influence of imperfections on the structure loading capacity. A numerical study shall consider buckling and post buckling problems with the influence of imperfections in engineering structures in order to find out the most accurate, reliable and realistic numerical method for complex structures, such as this novel conceptual model of transition segment for onshore hybrid lattice-tubular steel wind towers.

For post buckling analysis due to convergence issues standard static RIKS solver was used to assess LS3 using previous boundary conditions and design value of loads. Standard static RIKS solver is based on arc-length method; the load proportionality factor at each iteration is modified so that the solution follows some specified path until convergence is achieved. The arc-length is kept fixed for current increment, whereas in the latter case, new arc-length is evaluated at the beginning of each load step to ensure the achievement of the solution procedure. For further increments the load-factor is computed according to the rate of convergence of the solution process. In case of divergence from the solution path, the arc-length is reduced and computations are performed once again. Moreover, RIKS method is able to find solution during unloading process. As GMNIA approach is a post buckling

analysis which requires a lot of computational effort and time, only solution 3 and 4 will be studied further for this type of analysis.

5.2.2.1 GMNIA Analysis of Case Study #4 (Mild steel S355 in Transition Piece Shell)

In order to obtain the Eigen mode-affine shapes, a linear elastic bifurcation analysis was performed to the model with real loads, see figure. The critical buckling load of the ideal structure (Eigenvalue) for the first mode is 3.9518E6 N. The first five Eigen mode-affine values are given in following **Table 5.6**.

***Table 5.6**:* Eigen Modes from LBA analysis for Solution#4

Eigen Modes	Values
1	13.627
2	-15.183
3	15.864
4	16.795
5	17.031

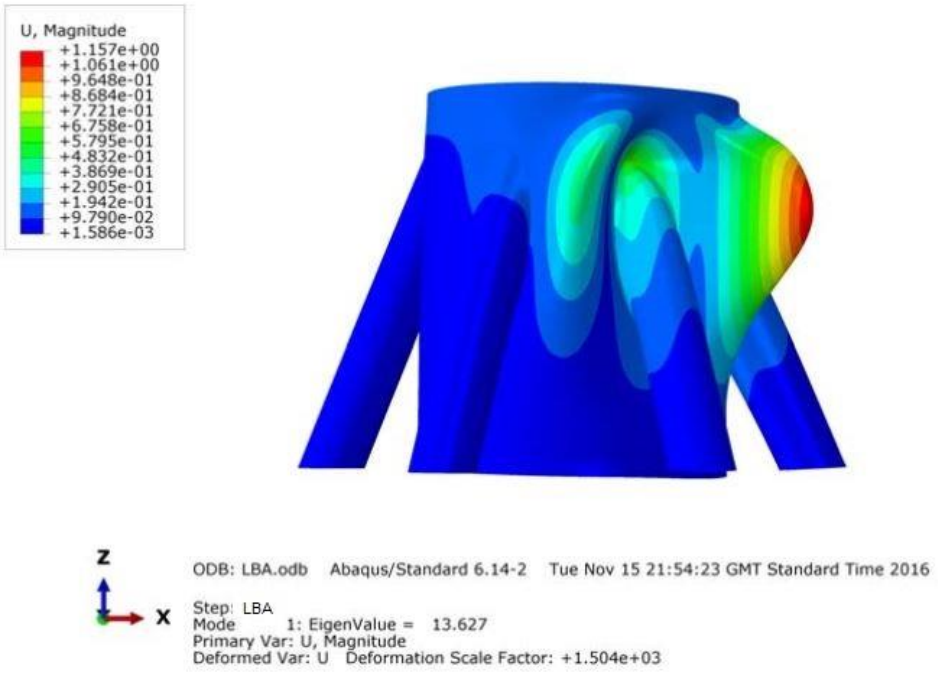

***Figure 5.26**:* Eigen mode shape for Solution#4

Once obtained the Eigen mode shape for the critical mode **Figure 5.26**, it is then necessary to estimate the magnitude of the imperfections to apply for the following model to determine the imperfect elastic-plastic buckling load. For both different steels it was considered a fabrication tolerance quality class B, values are shown in **Table 3.1** taken from Euro code.

Gauge length is calculated by using equation. The maximum deviation; $\Delta w_{0,eq}$ of the imperfection from the perfect structure shape should be estimated by the equation 3.1.

$$l_{gx} = 4 . \sqrt{r} . t = 4 . \sqrt{2500} . 45 = 1341.64mm \qquad 5.1$$

According to EN1993 Part 1-6 the recommended value of n_i is 25. Putting the value of l_g, U_{n1}, U_{n2} and n_i in equation 3.1.

$$\Delta w_{0,eq} = max\left\{\begin{matrix}\Delta w_{0,eq,1} = l_g \times U_{n1} \\ \Delta w_{0,eq,2} = n_i \times t \times U_{n2}\end{matrix}\right\} = max\left\{\frac{21.466}{18}\right\} \qquad 5.2$$
$$= 21.466mm$$

Therefore, it was considered a magnitude of 21.46 mm for the imperfections to analyse the most unfavourable situation. In order to introduce the imperfections on the succeeding model for the post-buckling analysis, the keywords had to be changed. The procedure was done according to ABAQUS documentation for post-buckling analysis.

Due to convergence issues, the numerical problem was solved using standard static RIKS procedure. As mentioned previously, this method increases the load until obtaining the maximum load amplification factor.

The curve obtained after post buckling analysis of this solution is presented below:

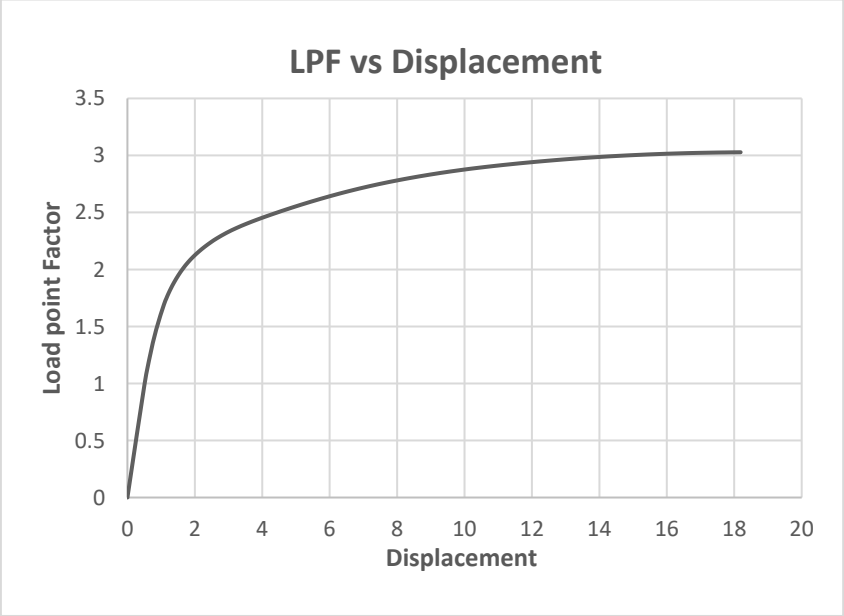

Figure 5.27: Post buckling curve from Global GMNIA analysis for solution#4

As it is evident from the **Figure 5.27** that the curve closely resembles with the criterion C3 defined in the Euro code **Figure 3.3** so the factor $r_{R,GMNIA}$ can be taken as C3 (largest tolerable deformation) or C4 (First yield safe estimate).

So, for having more precise results the author use factor C4 which is the first yield estimate because if it validates with first yield estimate automatically the solution will be validated for any largest tolerable deformation defined, which will be in plastic zone and these kind structures mostly operate in elastic zone so it would be better to validate it on first yield estimate.

To get more refined results the author decreased the increment size from one to 0.01 and stop the solution early by defining maximum LPF factor of 2 to relax the computational effort and time. The result is as follow **Figure 5.28**:

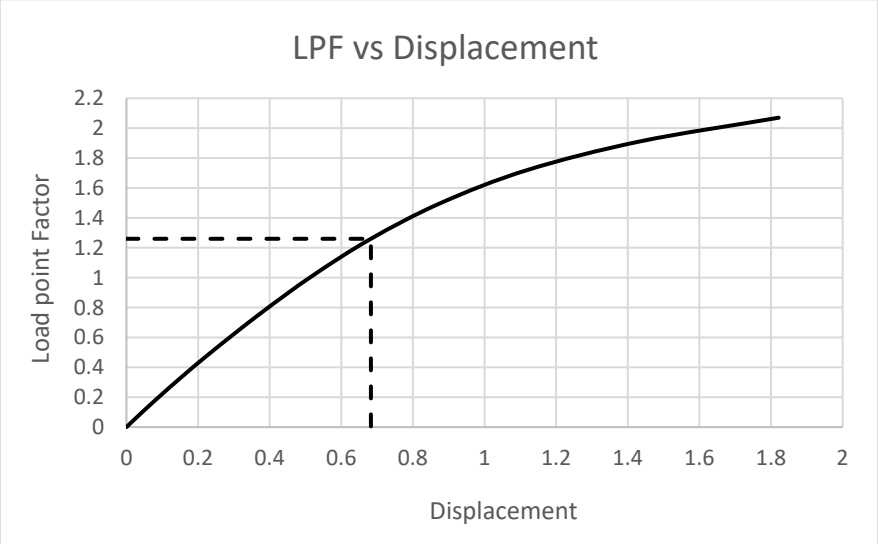

***Figure 5.28**:* Post Buckling curve resulting from smaller increment

So from the plot;

$$r_{R,GMNIA} = 1.26012 \qquad 5.3$$

A calibration factor was used to verify the buckling strength. However, to estimate its value a close comparison against test results on a shell structure with appropriately similar features has to done. Since this is a novel conceptual model, there are no similar test results; therefore, this calibration requirement is very challenging. Nevertheless, the values of calibration factor are within the range $0.8 \leq K_{GMNIA} \leq 1.2$. Therefore, to consider the most unfavourable case, it was assumed a calibration factor of 0.9. The summary of the buckling strength verification is shown on the table presented below in **Table 5.7**.

***Table 5.7**:* Buckling strength verification (LS3) for Solution#4

K_{GMNIA}	0.9
$r_{R,GMNIA}$	1.26012

r_{Rk}	1.134108
γ_{M1}	1.1
r_{Rd}	1.031

As the design buckling resistance is ≥ 1 so buckling strength is verified for solution#4.

5.2.2.2 GMNIA Analysis of Case Study #3 (HSS grade S690 in Transition Piece Shell)

In order to assess the buckling limit state, for the solution circular transition piece using high strength steel S690, the same procedure done on 5.2.2.1was performed once again. A linear elastic bifurcation analysis was performed to the model with real loads, see **Figure 5.29**. The critical buckling load of the ideal structure (Eigenvalue) for the first mode is 5.7579E6 N. The first five Eigen mode-affine values are given in following **Table 5.8**.

***Table 5.8**:* Eigen Modes from LBA analysis for Solution#3

Eigen Modes	Values
1	8.8584
2	9.0453
3	9.3153
4	-9.6471
5	9.7729

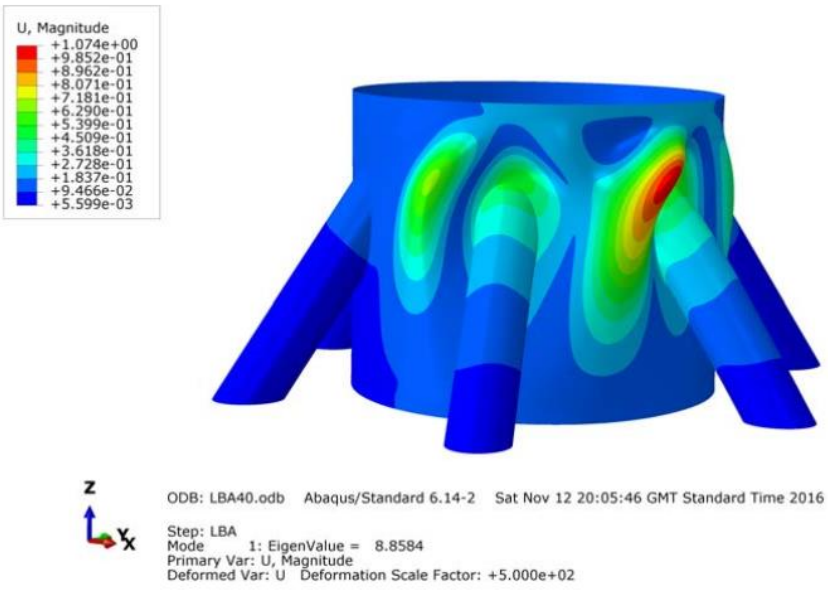

***Figure 5.29**:* Eigen mode shape for Solution#3

Since the Eigen mode shapes are determined, the next step was to estimate the magnitude of the imperfections, the following expressions from equation (3.1 & 3.2) were used:

$$\Delta w_{0,eq} = max\left\{\begin{matrix}\Delta w_{0,eq,1} = l_g \times U_{n1} \\ \Delta w_{0,eq,2} = n_i \times t \times U_{n2}\end{matrix}\right\} \quad 5.4$$
$$= max\left\{\begin{matrix}\Delta w_{0,eq,1} = 1264.91 \times 0.016 \\ \Delta w_{0,eq,2} = 25 \times 40 \times 0.016\end{matrix}\right\}$$
$$= max\left\{\begin{matrix}\Delta w_{0,eq,1} = 20.23 \\ \Delta w_{0,eq,2} = 16\end{matrix}\right\} = 20.23\ mm$$

$$l_{gx} = 4\,.\sqrt{r}.t = 4\,.\sqrt{2500}.40 = 1264.91mm \quad 5.5$$

Therefore, it was considered a magnitude of 21.46 mm for the imperfections to analyse the most unfavourable situation. In order to introduce the imperfections on the succeeding model for the post-buckling analysis, the keywords had to be changed. Due to convergence issues, the numerical problem was solved using standard static RIKS procedure. As mentioned previously, this method increases the load until obtaining the maximum load amplification factor.

The curve obtained after post buckling analysis of this solution is presented in the **Figure 5.30**:

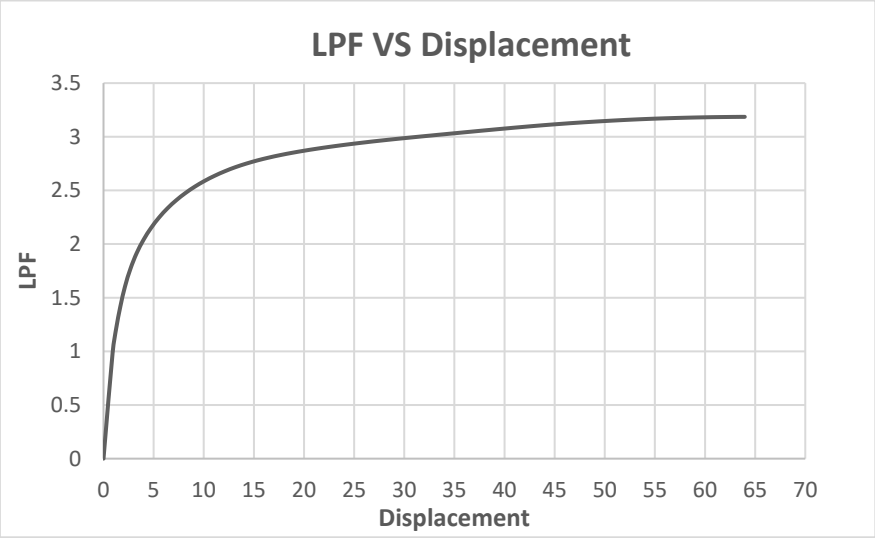

***Figure 5.30**:* Post buckling curve from Global GMNIA analysis for solution#3

Using the same procedure as defined in section 3.3, obtaining the value from the plot;

$$r_{R,GMNIA} = 1.30164 \quad 5.6$$

The characteristic buckling resistance ratio $r_{R,k}$ should be found from the imperfect elastic-plastic buckling resistance ratio $r_{R,GMNIA}$, adjusted by the calibration factor K_{GMNIA}. The design buckling resistance ratio $r_{R,d}$ should then be assessed using the partial factor γ_{M1}, according with the following equations 3.3 and 3.4. A calibration factor same as before was used to verify the buckling strength. The values of calibration factor are within the range

$0.8 \leq K_{GMNIA} \leq 1.2$. Therefore, to consider the most unfavourable case, it was assumed a calibration factor of '0.9.' The summary of the buckling strength verification is shown on the table presented below.

Table 5.9: Buckling strength verification (LS3) for Solution#3

K_{GMNIA}	0.9
$r_{R,GMNIA}$	1.30164
r_{Rk}	1.17147
γ_{M1}	1.1
r_{Rd}	1.064

As the design buckling resistance is ≥ 1 so buckling strength is verified for solution#3.

5.3 Fatigue Life Prediction

Fatigue life is calculated for the transition piece according to the methodology explained in section 3.4.

5.3.1 Cyclic properties of S355 mild steel and S690 HSS

5.3.1.1 Experimental Data for S355 mild steel

The fatigue behaviour of the S355 mild steel was evaluated by De Jesus et al. [29], [30], based on experimental results from fatigue tests of smooth specimens and fatigue crack propagation tests.

The fatigue tests of smooth specimens were carried out according to the ASTME606 standard under strain-controlled conditions. ***Table 5.10*** and ***Table 5.11*** summarizes the elastic (**E**: Young modulus) and monotonic strength properties ($\mathbf{f_y}$: yield strength; $\mathbf{f_u}$: tensile strength) as well as the cyclic elastoplastic constants (**K'**: cyclic strain hardening coefficient; **n'**: cyclic strain hardening exponent) and the strain-life constants. Figure illustrates the resulting experimental strain-life fatigue data.

Table 5.10: Monotonic and cyclic elastoplastic properties of the S355 mild steel

E	f_u	f_y	***K'***	***n'***
GPa	*MPa*	*MPa*	*MPa*	-
211.60	*744.80*	*422*	*595.85*	*0.0757*

Table 5.11: Morrow constants of the S355 mild steel

σ'_f	***b***	ε'_f	***c***
MPa	-	-	-
952.2	*-0.0890*	*0.7371*	*-0.6640*

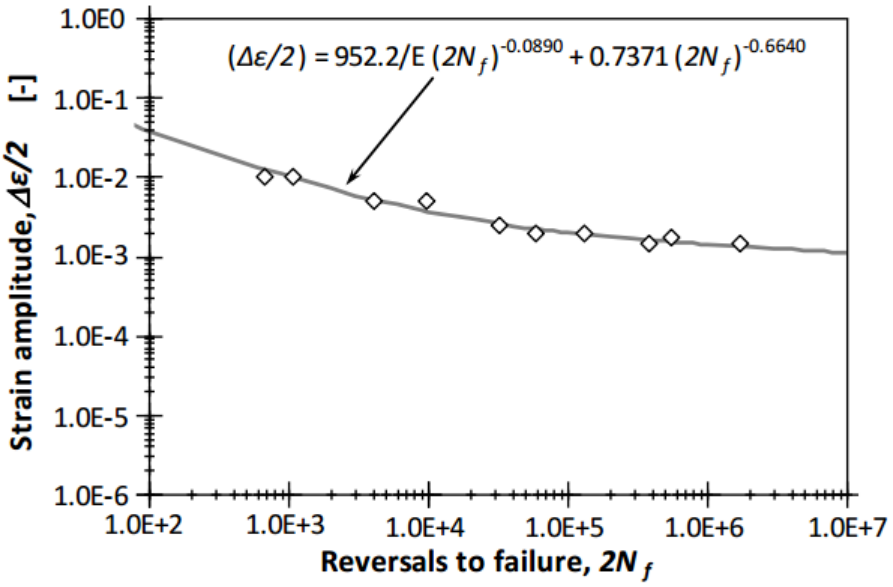

***Figure 5.31**:* Strain-life curves for the S355 steel, $R_\varepsilon = -1$ [30]

5.3.1.2 Estimated fatigue data for S690 HSS steel

If no experimental data are available, an estimation of the cyclic and fatigue behaviour of a material will be helpful at the design stage. Reference [31], [32] contains published results of the study that was undertaken by the American Iron and Steel industry to obtain and compare strain-controlled deformation and fatigue properties. The material properties approximation Equations for the strain based method was published in this article.

The calculated material properties[32] estimations for used materials in this thesis have been tabulated in the **Table 5.12** and **Table 5.13**.

***Table 5.12**:* Monotonic and cyclic elastoplastic properties of the S690 high strength steel

E	f_u	***HB***	***K'***	***n'***
GPa	*MPa*	-	*MPa*	-
211.60	*1000*	*275.4*	*1650*	*0.164*

***Table 5.13**:* Morrow constants of the S690 high strength steel

σ'_f	***b***	ε'_f	***c***
MPa	-	-	-
1396	*-0.09*	*0.392*	*-0.56*

5.3.2 Fatigue Loads

The basic environmental conditions considered to obtain the fatigue loads are the same that were used for the Onshore Wind Turbine analysis. The load history in this analysis is also calculated by the *OWT* simulation software ***ASHES***.

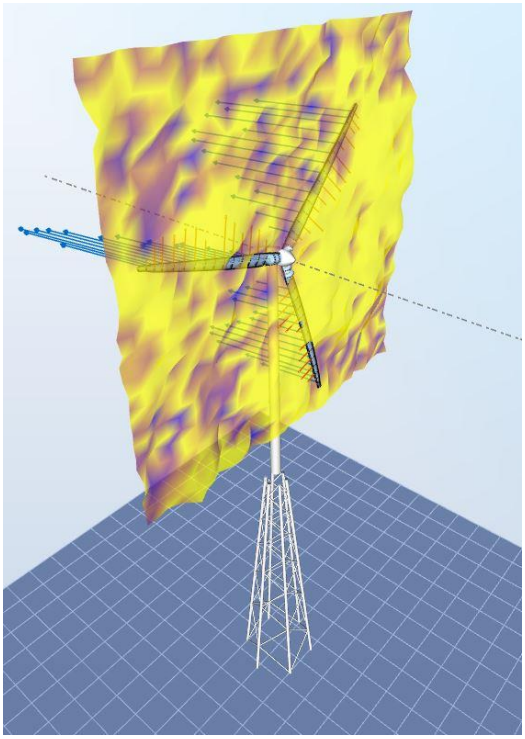

***Figure 5.32**:* Three-dimensional turbulent wind applied to wind turbine model in *ASHES*

To proceed with the fatigue analysis, time series of loads coming from the aero-elastic simulation **Figure 5.32** were recorded for periods of 10 min by the interval of 0.03 seconds for the wind speed 12m/s, 25m/s and 42.5m/s respectively. Which to be later applied as external forces and moments to the finite element model of the transition piece and proportional load histories for *Fe-Safe*. One of the load histories for force '***Fx***' calculated for 12m/s wind speed is shown in the **Figure 5.33**.

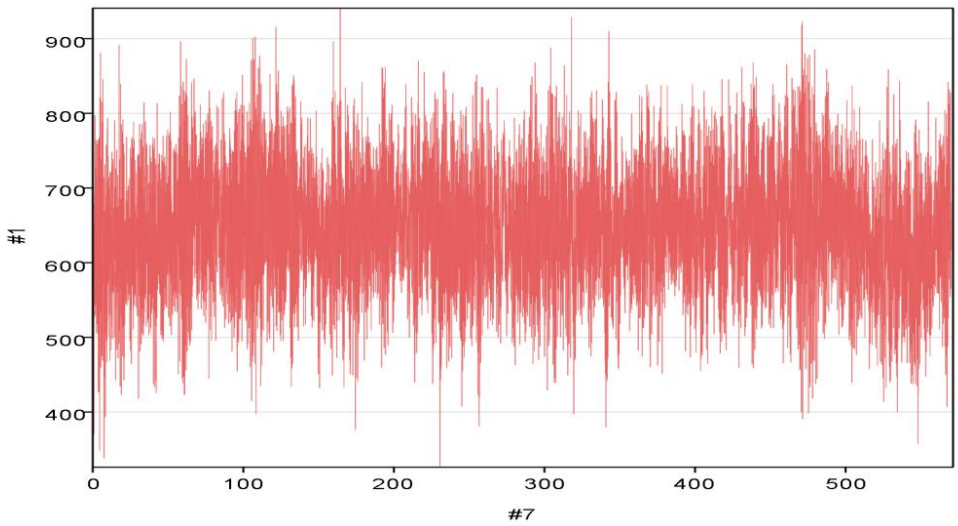

***Figure 5.33**:* Load history for signal *'Fx'* recorded for 10 minutes duration from aero-elastic simulation in *ASHES*

The highest forces and moments are taken out from the time series of load calculated from wind speed 12m/s and 25m/s shown in the **Table 5.14** are applied to the finite element model of the transition piece to calculate stresses at each node.

***Table 5.14**:* Design fatigue load values

Fatigue Loads in ABAQUS				
Wind Speed 12m/s		Wind Speed 25m/s		
Load vector	Magnitude	Load vector	Magnitude	Units
Fx	9.408E+05	Fx	1.080E+06	N
Fy	1.616E+05	Fy	3.959E+05	N
Fz	9.1815E+06	Fz	9.842E+06	N
Mx	1.5595E+10	Mx	3.6454E+10	N*mm
My	7.4268E+10	My	6.3014E+10	N*mm
Mz	6.7370E+10	Mz	5.4560E+10	N*mm

Similarly, all the load series are divided by the highest data point to make the proportional load history which will be eventually applied as a fatigue loading into the *Fe-Safe* to the respective data sets, example see **Figure 5.34**.

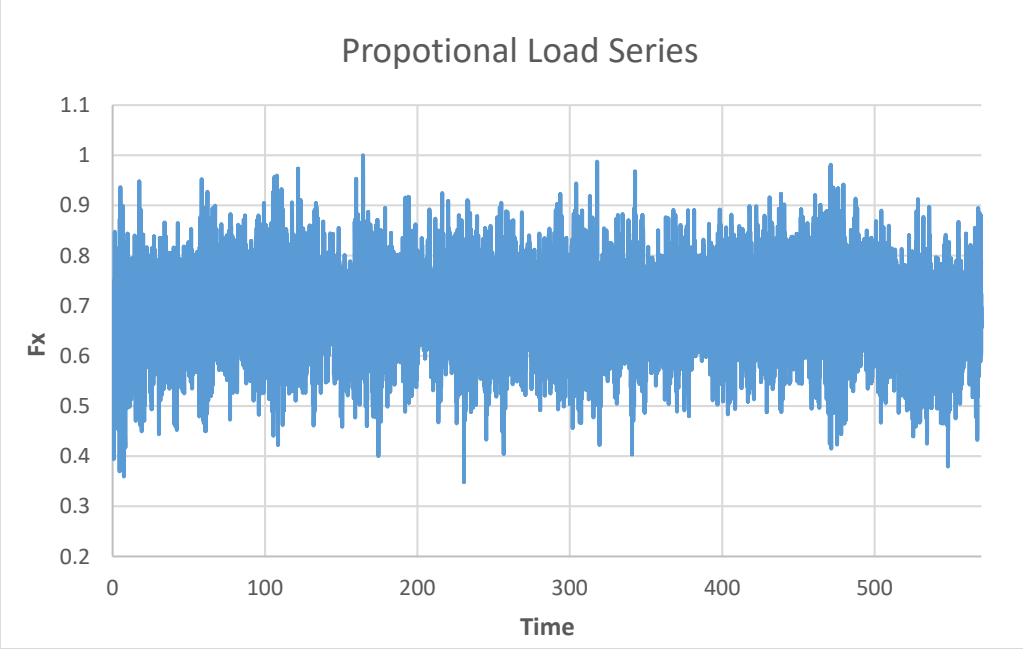

***Figure 5.34**:* Proportional Load history of signal *'Fx'* applied in fatigue prediction software *FE-SAFE*

5.3.3 Fatigue Analysis for Case Study#4 (S355)

The numerical model for this Case study is same as described previously in section 5.1 with same boundary condition, load point, mesh elements, assembly and interactions. Fatigue loads are introduced separately in each step for external forces and moments into the *ABAQUS.* An elastic analysis is performed, as an output from the FEM analysis we get the elastic stresses at each node of the elements. This stress at each node serves as input into the *Fe-Safe* software for the fatigue calculations.

The cyclic and fatigue properties explained in section 5.3.1 for S355 are entered into the *Fe-Safe* and are assigned to the groups which are to be analysed. Proportional load histories are applied over stress data sets of external forces and moments. Fatigue analysis will be carried out for wind speeds 12 and 25m/s.

5.3.3.1 Analysis utilizing data for wind speed 12m/s

To proceed with the fatigue analysis, time series of loads coming from the aero-elastic simulation recorded for periods of 10 min by the interval of 0.03 seconds for the wind speed 12m/s is evaluated on the basis of two algorithms.

1) Uniaxial Stress: Stress life with Goodman mean stress correction
2) Biaxial Strain Life: Strain based Brown Miller (CP) with Morrow mean stress correction.

Firstly, uniaxial analysis is carried out on FE stress data sets with the loads applied separately as *Fx, Fz & My* using Stress based Uniaxial Method with Goodman Mean Stress Correction. The results are illustrated in **Table 5.15**:

Table 5.15*:* Fatigue life prediction using Stress based Uniaxial Method for wind speed 12m/s

Uniaxial Force/Moment	Fatigue Life
Fx	No Damage
Fz	No Damage
My	No Damage

As from the table, it is evident that applying uniaxial case on transition piece gives no damage or in other words infinite life to the structure. As it's a uniaxial stress based algorithm the results from rainflow cycle counting for the force '*Fx*' are shown in the **Figure 5.36**.

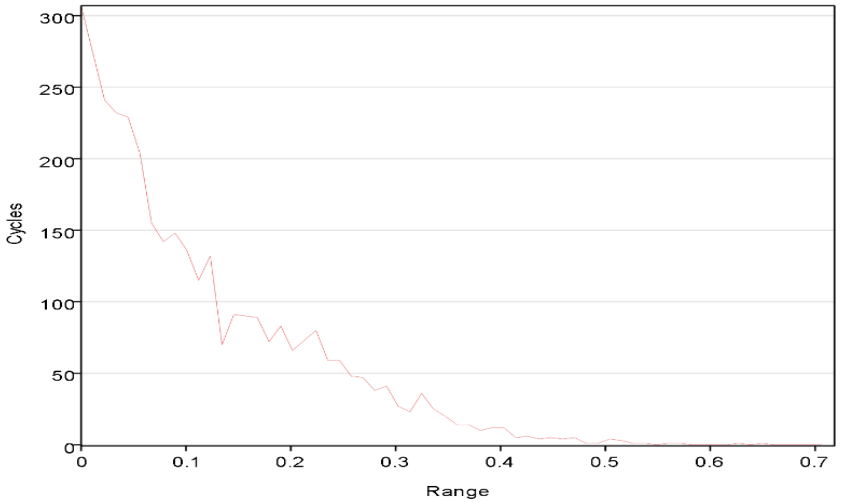

***Figure 5.35**: Range only rainflow cycle histogram*

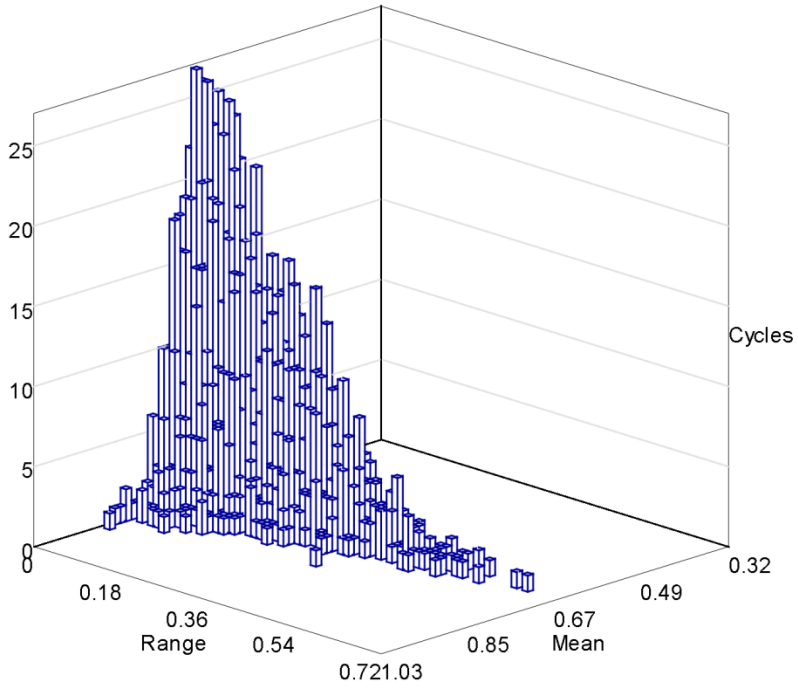

***Figure 5.36**:* Range-mean rainflow cycle histogram

Secondly for implementing multiaxial scenario in the present study, *Fe-safe's* multiaxial Brown–Miller algorithm with the Morrow mean stress correction is used to calculate the fatigue life as hours to failure. For steel, *Fe-safe* recommends using the multiaxial Brown–Miller algorithm described in section 2.5.4.4 for ductile steel and the principle strain algorithm for brittle steels, both with the Morrow mean stress correction. The Brown–Miller algorithm uses a critical plane analysis to determine the life in reversals to failure $2N_f$ see section 2.5.4.5.

In this method firstly each load history was applied separately to stress data sets (e.g. proportional loading of only signal '*Fx*' over stress data set) and then all loads are applied to have a multiaxial fatigue situation using scale and combine method. The results are as under:

Figure 5.37: Fatigue life prediction using Multiaxial Brown–Miller algorithm for wind speed 12m/s

Load History	Fatigue Life
Fx	No Damage
Fz	No Damage
My	No Damage
Fx, Fy, Fz, Mx, My & Mz	No Damage

So, for the case study using S355 mild steel fatigue results of the transition piece reveals that, if the wind speed is less or equal to 12 m/s over the complete service life there is no damage.

5.3.3.2 Analysis utilizing data for wind speed 25m/s

Same procedure is followed for wind speed 25m/s. Time series of loads coming from the aero-elastic simulation recorded for periods of 10 min by the interval of 0.03 seconds for the wind speed 25m/s is evaluated on the basis of two algorithms.

1) Uniaxial Stress: Stress life with Goodman mean stress correction
2) Biaxial Strain Life: Strain based Brown Miller (CP) with Morrow mean stress correction

Firstly, uniaxial analysis is carried out on FE stress data sets with the loads applied separately as *Fx, Fz & My* using Stress based Uniaxial Method with Goodman Mean Stress Correction. The results can be seen in **Table 5.16**:

Table 5.16: Fatigue life prediction using Stress based Uniaxial Method for wind speed 25m/s

Load History	Fatigue Life
Fx	No Damage
Fz	No Damage
My	No Damage

Multi-Axial Fatigue Analysis is carried by Strain based Brown Miller with Morrow mean stress correction as described earlier. In this method firstly each load history was applied

separately to stress data sets and then all loads are applied collectively to have a multiaxial fatigue situation. The results are in **Table 5.17**:

***Table 5.17**:* Fatigue life prediction using Multiaxial Brown–Miller algorithm for wind speed 25m/s

Load History	Fatigue Life
Fx	No Damage
Fz	No Damage
My	No Damage
Fx, Fy, Fz, Mx, My & Mz	151532.406 Hours

The summary from last multiaxial analysis carried out in Fe-Safe is shown in **Table 5.18**:

***Table 5.18**:* Summary for fatigue life using multiaxial state in Fe-Safe

Summary		
Worst Life-Hours	At element #595444	151532.406 Hours
Largest(+ or -) SMAX	At element #561110	423.74MPa
Largest Damage	At element #595444	6.599E-6

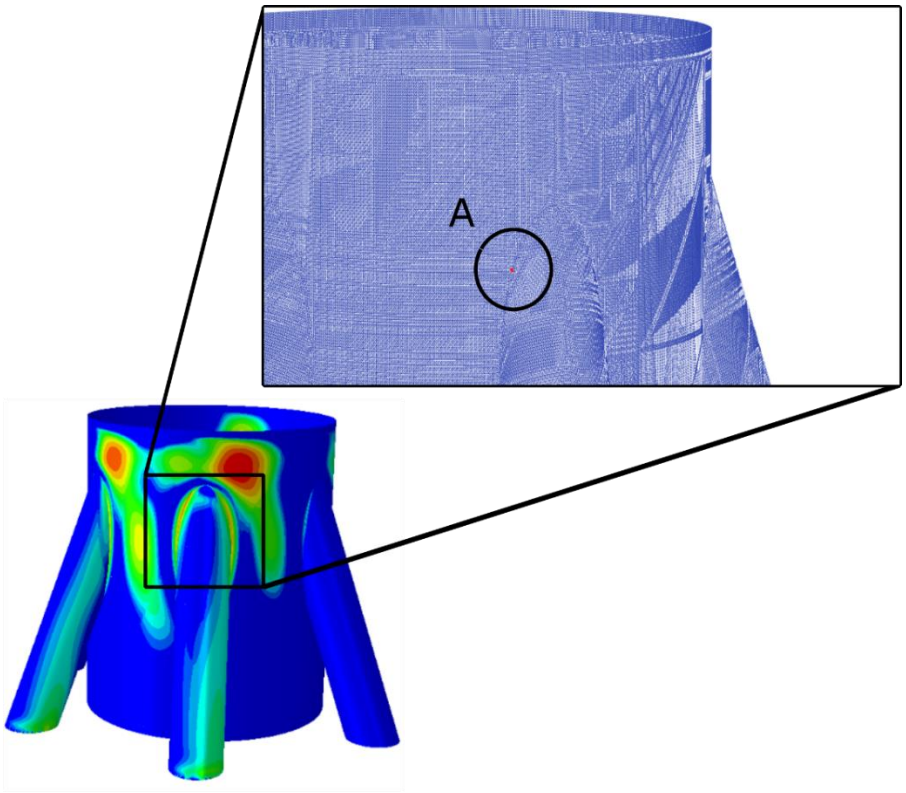

***Figure 5.38**:* Contours of fatigue life in transition piece. The point of lowest life (point A) is located in a lateral weld of the brace to tower joint.

So, for the case study using S355 mild steel fatigue results of the transition piece reveals that, if the wind speed is equal to 25 m/s constantly over the service life, it can sustain for 17.286 years. Originally on site the conditions are not that harsh i.e. wind speed is variable in time and constantly changing between 7m/s to 15m/s. It merely goes up to 25m/s. In **Figure 5.40** a Weibull probabilistic curve is shown which shows that probability of wind speed going up to 25m/s is mere 0.001% mostly the probability is between 7 to 12m/s of the wind so, if we consider the service life of 25 years the transition piece will be secure for fatigue loads as it is overdesigned in this case.

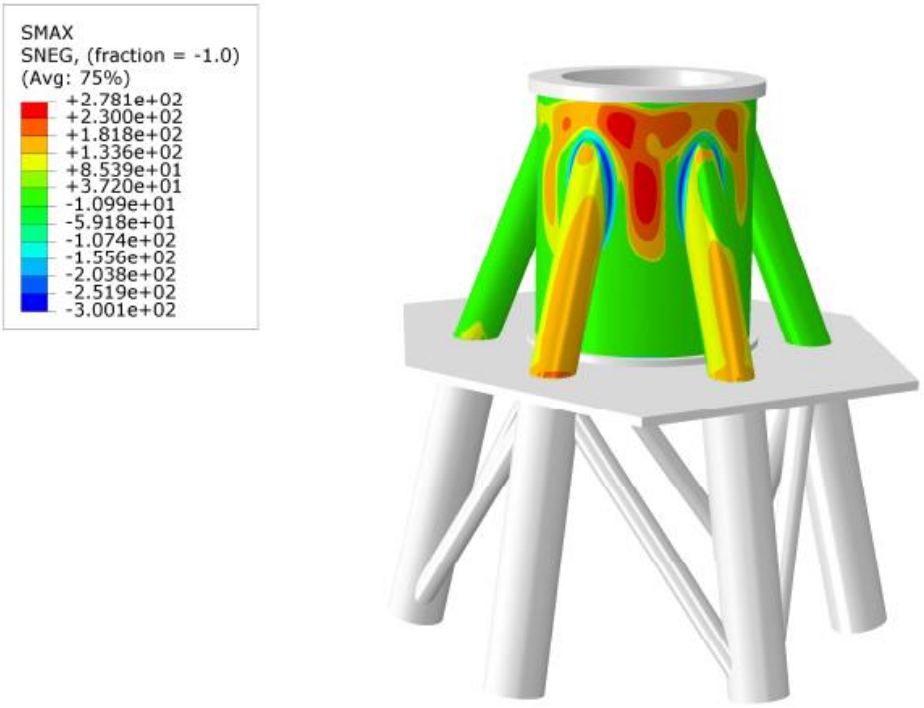

Figure 5.39: Average Stresses on transition piece resulting from fatigue loading

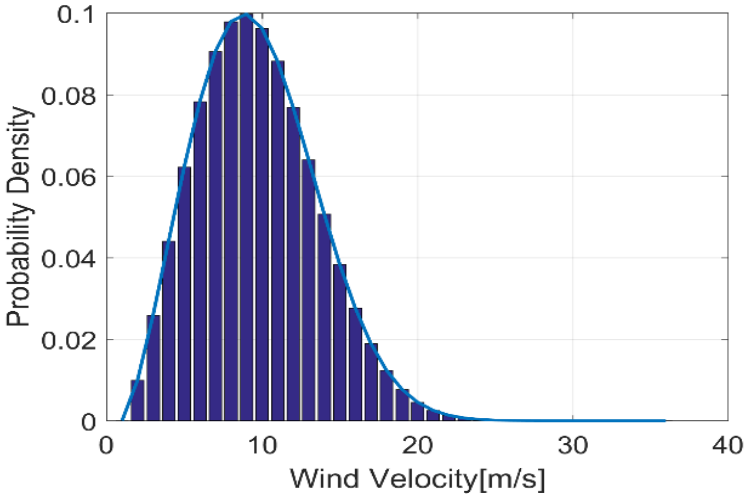

Figure 5.40: Weibull distribution according to the altitude [33]

5.3.4 Fatigue Analysis for Case Study#3 (HSS S690)

In order to access the fatigue life estimation for the case study using high strength steel, same procedure done before was performed again. Numerical model for this Case study is same as described previously with same conditions. Fatigue loads are introduced separately in each step for external forces and moments into the *ABAQUS*, resulting in elastic stresses at each node of the elements. This stress at each node serves as input into the *Fe-Safe* software for the fatigue calculations.

The cyclic and fatigue properties listed in **Table 5.12** for S690 are entered into the Fe-Safe and are assigned to the groups which are to be analysed. Proportional load histories are applied over stress data sets of external forces and moments. Fatigue analysis will be carried out for wind speeds 12 and 25m/s.

5.3.4.1 Analysis utilizing data for wind speed 12m/s

Same load histories for wind speed 12m/s is evaluated on the basis of Biaxial Strain Life: Strain based Brown Miller (CP) with Morrow mean stress correction algorithm.

In this case all the loads are applied collectively to have a multiaxial fatigue situation. The results are as under:

Table 5.19*:* Fatigue life prediction using Multiaxial Brown–Miller algorithm for wind speed 12m/s

Load History	Fatigue Life
Fx, Fy, Fz, Mx, My & Mz	448395.094 Hours

The summary from last multiaxial analysis carried out in Fe-Safe is shown below:

Table 5.20*:* Summary for fatigue life using multiaxial state in Fe-Safe

Summary		
Worst Life-Hours	At element #400961	448395.094 Hours
Largest(+ or -) SMAX	At element #400961	839.491MPa
Largest Damage	At element #400961	2.2E-6

For case study using S690 high strength steel fatigue results of the transition piece reveals that, if the wind speed is equal to 12 m/s constantly over the service life, it can sustain for 51.152 years.

5.3.4.1.1 Analysis utilizing data for wind speed 25m/s

Same procedure is followed for wind speed 25m/s. Load histories are evaluated on the basis of Biaxial Strain Life: Strain based Brown Miller (CP) with Morrow mean stress correction algorithm.

In this case all the loads are applied collectively to have a multiaxial fatigue situation. The results are as under:

Table 5.21: Fatigue life prediction using Multiaxial Brown–Miller algorithm for wind speed 25m/s

Load History	Fatigue Life
Fx, Fy, Fz, Mx, My & Mz	19998.227 hours

The summary from last multiaxial analysis carried out in *Fe-Safe* is shown below:

Table 5.22*:* Summary for fatigue life using multiaxial state in *Fe-Safe*

Summary		
Worst Life-Hours	At element #400961	19998.227 hours
Largest(+ or -) SMAX	At element #400961	848.185MPa
Largest Damage	At element #400961	5E-5

So, after the multi-axial fatigue analysis of case study using S690 high strength steel fatigue results of the transition piece reveals that, if the wind speed is equal to 25 m/s constantly over the service life, it can sustain just for 2.3 years. This as earlier described is not the original condition on site but comparing to case study#4 it gives a very low fatigue life due to exposure of higher stresses.

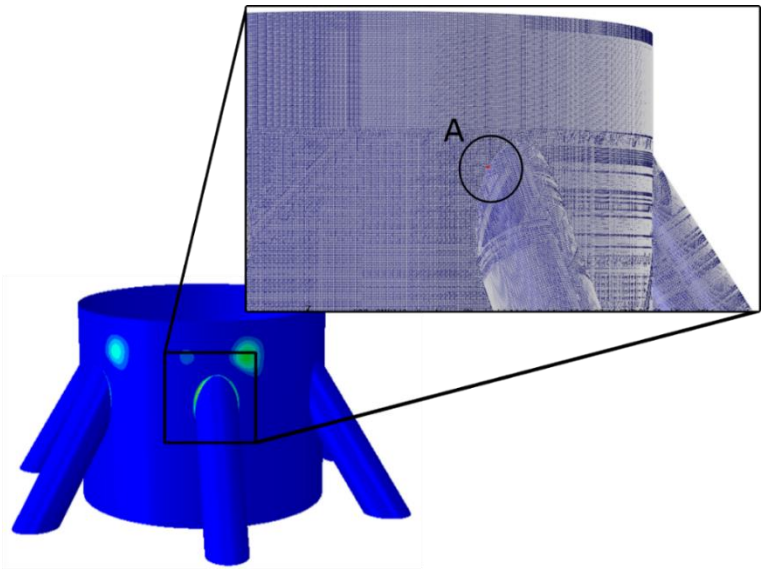

Figure 5.41*:* Contours of fatigue damage in transition piece. The point of maximum fatigue damage (point A) is located in a lateral weld of the brace to tower joint.

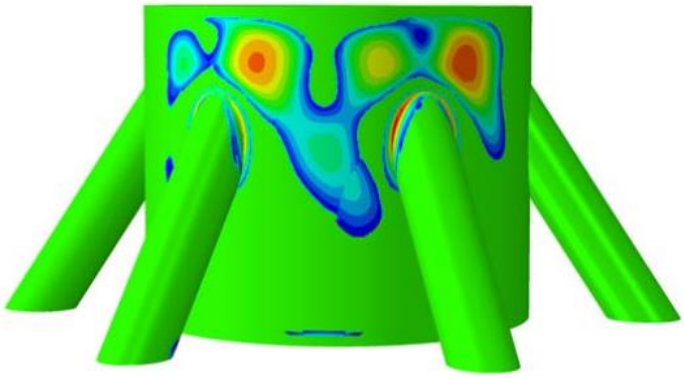

***Figure 5.42**:* Contours of log life in transition piece

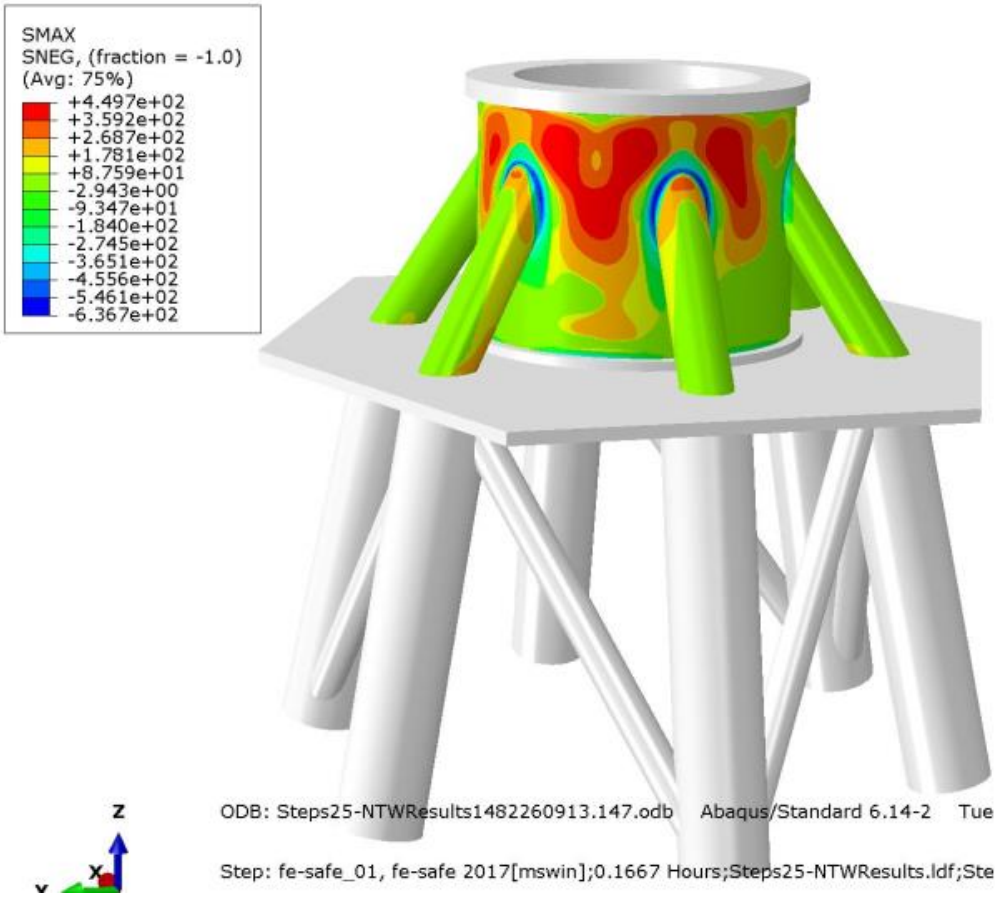

***Figure 5.43**:* Contours of Average Stresses experienced by the elements during fatigue loading

5.3.4.2 Impact of Internal Stiffener on Fatigue life

As the fatigue life for case study#3 comes out to be very low which not a good situation is for the design purposes. An internal stiffener is added on the inside of transition piece as proposed in Case study#1 for an alternative solution to the fatigue life problem to see how it affects to the overall life of structure.

So, for that purpose an internal stiffener of thickness 30mm and 1600mm height is added to the same numerical model, on the inside of transition piece covering the hotspots where the stress concentrations tend to be higher to decrease the stress magnitude.

Load histories for wind speed 25m/s are evaluated on the basis of Biaxial Strain Life: Strain based Brown Miller (CP) with Morrow mean stress correction algorithm. All the loads are applied collectively to have a multiaxial fatigue situation. The results are as under:

***Table 5.23**:* Fatigue life prediction using Multiaxial Brown–Miller algorithm for wind speed 25m/s

Load History	Fatigue Life
Fx, Fy, Fz, Mx, My & Mz	114708.492 hours

The summary from last multiaxial analysis carried out in *Fe-Safe* is shown below:

***Table 5.24**:* Summary from *FE-SAFE*

Summary		
Worst Life-Hours	At element #10692	114708.492 hours
Largest(+ or -) SMAX	At element #10692	774.865MPa
Largest Damage	At element #10692	8.71E-6

It is evident for the outcome of the results that including an internal stiffener increases the fatigue life of transition piece exponentially from approximately 2 years to 13 years.

5.3.4.3 Increasing thickness of the shell

Another solution that can be proposed for increasing the fatigue life of Solution#3 is by increasing the overall thickness of the shell of the transition piece and compare with the stiffener solution given in section 5.3.4.2 on the basis of mass of the structure.

So, for that purpose, the thickness of Transition Piece Shell is increased by 10 mm (form 40mm to 50mm). Load histories for wind speed 25m/s are evaluated on the basis of Biaxial Strain Life: Strain based Brown Miller (CP) with Morrow mean stress correction algorithm. All the loads are applied collectively to have a multiaxial fatigue situation. The results are as under:

***Table 5.25**:* Fatigue life using Multiaxial conditions for wind speed 25m/s

Load History	Fatigue Life
Fx, Fy, Fz, Mx, My & Mz	105805.977 hours

The summary from last multiaxial analysis carried out in *Fe-Safe* is shown below:

***Table 5.26**: Summary from FE-SAFE*

Summary		
Worst Life-Hours	At element #10692	105805.977 hours
Largest(+ or -) SMAX	At element #10692	773.388MPa
Largest Damage	At element #10692	9.451E-6

The outcome of the results with increasing thickness of the Transition Piece Shell is similar to that of including stiffener i.e. fatigue life increases from approximately 2 years to 12.5 years but if we compare the mass of the transition piece from both solution, it proves to be a lighter solution and doesn't require any welding complications as required in stiffener solution. The mass of the transition piece for high strength steel including stiffener is approximately 37 tones and on the other hand with increasing thickness to 50mm comes out be 36 tones so, it's a lighter solution than using a stiffener.

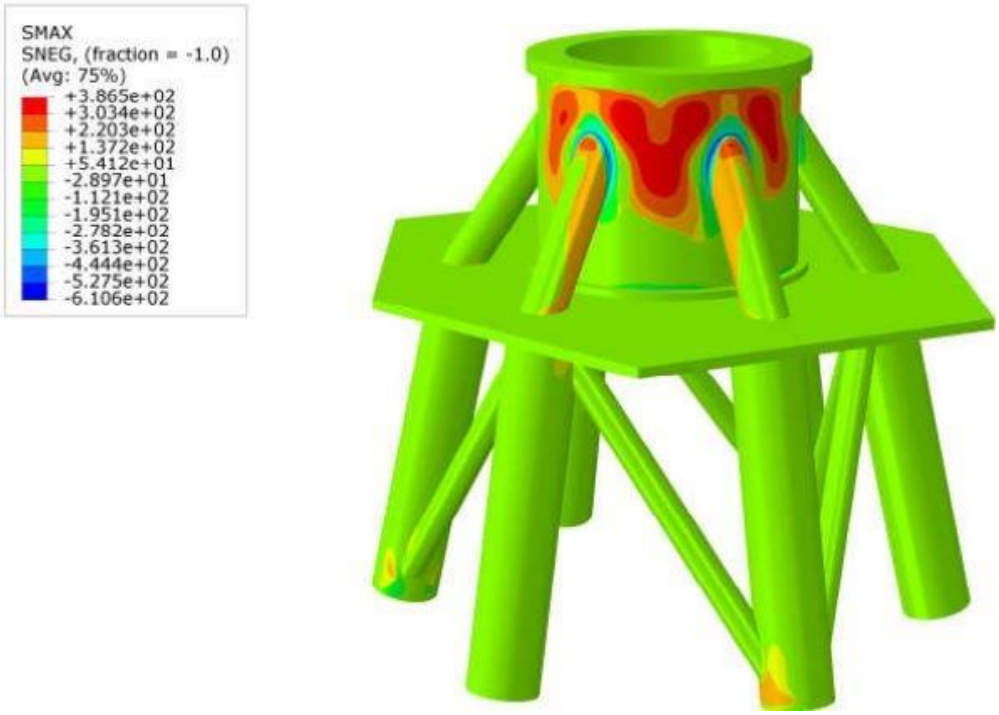

***Figure 5.44**:* Contours of Average Stresses experienced by the elements during fatigue loading

Chapter 6 DISCUSSION AND CONCLUSIONS

In context of global environment change and increasing deficiency of conventional energy sources, wind industry is progressively developing with a promising future even seen from now. Under this background, onshore wind industry is aiming for higher production turbines which could be possible by seizing higher wind speeds at higher altitudes with less turbulence in the wind. So, reaching to the higher heights makes new challenges for further mass production of onshore wind turbines in future.

The conventional onshore wind turbines compromise of a tubular tower as a support structure. As the height increases the tubular section at the bottom consequently got bigger in diameter and in weight, making it difficult for transportation and assembly of the sections. These local factors can tip the balance in the favour of the Hybrid solution comprising of a lattice structure in bottom and tubular section at the top. Hybrid structure could become a sound solution as wind turbine support structure because of its robustness in structural strength and efficiency in cost reduction.

This thesis work is based on experience learnt from existing hybrid offshore wind turbine support structures and further proposes this concept in onshore industrial application. Under this concept, transition piece which connects lattice support structure and tubular tower becomes an important aspect which deserves detailed consideration and analysis second to none. Existing research and practice sees a lack of study of this transition piece concept and in this thesis the critical subject is investigated with much effort.

After introduction of existing hybrid support structure consisting of the lattice structure and transition piece components, a conceptual model of transition piece is built which takes into consideration of various aspects including its geometrical requirement, functional requirement and mechanical connection requirement. A novel concept of the transition piece is established depicting its boundary relation with the lattice support structure. Preliminary design process analyses two different transition piece concepts, namely, frame-cylinder and cone-strut, mostly based on existing hybrid support structure experience in a comparative manner. In this thesis only frame-cylinder type of transition piece is studied deeply on the basis of using different steel grades in the design of transition piece. Four case studies were presented and analysed by ultimate limit state design according to EN 1993-1-6.

In first case study a hybrid solution of transition piece is presented which is made of six plates and six arc plates which when connected together makes an approximate perfect cylinder of 5m diameter, 4m high and 35mm thickness comprised of S460 steel grade. A GMNA analysis was performed to see the stress behaviour of transition piece, after analysis

the maximum stress came out to be way higher than the yield strength of the material. Solution to this, an internal stiffener of 50 mm thickness made of high strength steel S690 was added in the vicinity of high stress fields consequently the maximum stress came out to be 50% less than the solution without stiffener. In conclusion, applicability of thinner hybrid transition piece with an internal stiffener was achieved in this case study of frame type cylinder using different grades of steel.

In second case study a conventional circular transition is presented with three different sections i.e. upper, middle and bottom. Upper and bottom sections are made up with S460 steel grade having thickness of 35mm while middle section is comprised of S690 HSS steel having thickness of 50mm. Joining all sections make a perfect cylinder of 4 m high with 5m diameter. A GMNA analysis was perform to comply with Plastic limit state. In conclusion, the applicability of different grades of steel in transition piece by avoiding additional stiffener with less thickness was achieved.

In third case study circular transition piece is presented by using only high strength steel S690 in whole transition piece, which is 4m high with 40mm thickness. This solution was further analysed by plastic limit state, buckling limit state and for fatigue life calculations. A GMNA analysis was performed first, after complying with plastic limit state the solution was further analysed for GMNIA analysis for buckling check by performing an LBA analysis for Eigen modes and imperfections were calculated according to EN1993-1-6. The solution was verified for the design buckling resistance according to EN1993-1-6. Fatigue life calculations were based on elastic FEA stress analysis; these stresses were imported into fatigue analysis software to calculate the fatigue life distribution in the structure using multiaxial strain life criteria. Fatigue loads were calculated using aero-elastic simulations for wind speed 12m/s and 25m/s respectively. The solution was firstly run for uniaxial method for both wind speeds but there was no damage recorded in the structure. After that a multiaxial method was applied on combine forces and moments coming from wind speed 12m/s and a finite life of 51 years were recorded. The same multiaxial method was applied on loading resulting from 25m/s wind speed and ensued only in 2.5 years of finite life which is not a good design life for these kinds of structures. So, two solutions were proposed again for improving fatigue life of this transition piece. One by putting 30mm stiffener inside and second by increasing overall thickness of the shell by 10mm. Multiaxial fatigue analysis was performed again for both of these solution as a result fatigue life was improved to 13 years. Moreover, the mass of the structure with stiffener comes out to be 37 tones and for increased thickness 36 tones. Comparing both these alternatives on the basis of weight criteria the latter is much lighter solution so it will be adopted for this case study. In conclusion, a simple light weight transition piece with utilization of high strength steel was achieved.

In the last case study circular transition piece is presented by using only mild structural steel S355 in whole transition piece, which is 6m high with 45mm thickness. This solution was

further analysed by plastic limit state, buckling limit state and for fatigue life calculations. A GMNA analysis was performed first, after complying with plastic limit state the solution was further analysed for GMNIA analysis. Fatigue life calculations were based on elastic FEA stress analysis; these stresses were imported into fatigue analysis software to calculate the fatigue life distribution in the structure using multiaxial strain life criteria. Fatigue loads were calculated using aero-elastic simulations for wind speed 12m/s and 25m/s respectively. The solution was firstly run for uniaxial method for both wind speeds but there was no damage recorded in the structure. After that a multiaxial method was applied on combine forces and moments coming from wind speed 12m/s and again structure was safe with no damage recorded. The same multiaxial method was applied on loading resulting from 25m/s wind speed and a finite life of 17 years was recorded. In conclusion, a simple transition piece utilization mild structural steel was achieved.

6.1 Conclusions

The purpose of this study was to design a transition piece with different steel grades, investigate different stability criteria with ultimate limit state and calculating fatigue life time of the concepts using the loads from aero-elastic simulations. According to the work performed certain conclusions can be drawn:

A conceptual model of transition piece is achieved by taking into consideration of various aspects including its geometrical, functional and mechanical connection requirement. A novel concept of the transition piece is established depicting its boundary relation with the lattice support structure.

Different case studies are presented for the Transition segment with the aim to exploit more possibilities and broader the concept of research. In this research mainly the focus was to analyse the solution using a stiffener, transition piece using different grades of steel in different sections and transition piece using only one grade of steel also utilizing high strength steel.

It was shown that the design with normal mild steel grade leads to very large dimensions and proper fatigue life time. On the other hand, using high strength steel in the transition piece reduces the overall dimensions but lead to poor life time in terms of fatigue resistance, which can be cater by adding external stiffener or increase the overall shell thickness to have the proper life time. In comparison of last two case studies, the weight of the mild steel transition piece is approximately 54 tones but weight of high strength steel solution is 36 tones which is much lighter solution and it’s a crucial parameter concerning transportation of the structure and assembling so application of high strength steel is effective in design of transition piece. But it may cause a problem due to current difficulties in high strength steel rolling and part manufacturing in which the less thickness is more favourable. Both concepts had proper

buckling behavior; however, the transition piece with S355 was in the closer threshold with buckling resistance.

The influence of an internal stiffener is discussed which helps to decrease the stress level in the stress concentration spots and move the stress concentration in other parts of the shell to utilize other parts of the shell effectively. It also helps to increase the fatigue life of the transition piece. But it is envisaged that a more detailed study should be carried out for the behaviour of stiffener due to additional welding required for the connection with the shell and effects to the overall dynamics of the transition piece due to additional stiffener.

In brief, different transition piece concepts were proposed and the influence of the internal stiffener was discussed. The high strength steel concept led to smaller dimensions; however, an increase of the thickness is required in order to have the standard 25 years' life time. Fatigue limit State comes out to be major failure mode in these kind of structures.

6.2 Recommendation for future work

In this thesis, an overview of support structure for wind turbines is provided to an extent and the more extensive attention is placed on design and analysis of the transition piece. Conceptual model of transition piece which takes into consideration of multiple requirements and mechanical model including boundary condition and load condition have covered the principal and critical aspects for transition piece modelling, which can be referred to with reasonable amount of adequacy. Nevertheless, not all miscellaneous aspects are included and in fact for practical model computation purpose, they should rather not be.

Design models are from experience of hybrid support structure and the transition piece concepts are more suitable for this type of support structure. Analysis of the design transition piece model is majorly focusing on the frame cylinder type but for having more options other types of shapes should also be studied for comparison perspective. Cost reduction can be further achieved through regional redesign according to more compact design parameters but this should be dealt with carefully. An integrated design cycle including topology optimization in the design process should be performed, in order to decrease its weight and consequently decrease the ratio cost/effectiveness.

As the transition segment is fully welded. And in this thesis the connections were not main part of the study. A comprehensive study for the connections should be carried out. As from the fatigue analysis it was obvious that the stress concentration was more at the location of connection of chords with transition piece. So, a numerical study should be done by adding welds and calculating stresses on that location. After that fatigue life should be calculated again on the welds location which will definitely increase the fatigue life of the structure then by defining a detail category of the connection fatigue life can be compared with the standard procedure explained in Euro code 1993 Part 1-9 [34]. Also welding effect of addition of

internal stiffener as proposed in case study#1 should studied in more depth. The upper connection of the Transition Piece Shell with inner tubular ring is a crucial connection for the transmission of forces which should be indicated how it will be connected to both sides of ring.

Moreover, as the fatigue calculations were done on the basis of loads coming from wind speed 12 and 25m/s, which are just the extreme conditions due to which the solution can be overdesigned, as in reality the wind speed is constantly changing over the period of time. So, a probabilistic study of fatigue calculations should be done on the basis of Weibull distribution over the service life of transition piece to get more realistic and cost effective results.

Finally, this thesis work endeavours to provide solution and reference for future relevant research or practical purpose at the maximum capacity within its scope. Due to physical and temporal limitations, further verification and correction will be very much appreciated from interested readers.

REFRENCES

[1] E. Hau, *Wind turbines: Fundamentals, technologies, application, economics*, vol. 9783642271. Springer-Verlag Berlin Heidelberg, 2013.

[2] Ewea, "Wind in power," 2016.

[3] GWEC, "Global Wind Report 2015 | Gwec," 2016.

[4] T. S. Engstrom, Lyrner, M. Hassanzadeh, T. Stalin, and J. Johansson, "Tall towers for large wind turbines Tall towers for large wind turbines Report from Vindforsk project V-342 Höga," Stockholm August 2010, 2010.

[5] NORDEX, "Turbines INSTALLED on 120 meter high hybrid towers," 2013. [Online]. Available: http://www.nordex-online.com/en/products-services/hybrid-towers.html.

[6] Y. S. Lee, J. A. González, J. H. Lee, Y. Il Kim, K. C. Park, and S. Han, "Structural topology optimization of the transition piece for an offshore wind turbine with jacket foundation," *Renew. Energy*, vol. 85, pp. 1214–1225, 2016.

[7] M. Seidel, "Jacket substructures for the REpower 5M wind turbine," *Eur. Offshore Wind 2007*, pp. 1–8, 2007.

[8] W. Gong, "Lattice Tower Design of Offshore Wind Turbine Support Structures," 2011.

[9] G. Figueiredo, "Structural Behaviour of Hybrid Lattice-Tubular Steel Wind Tower," University of Coimbra, 2013.

[10] "Geodome Transition Piece." [Online]. Available: http://www.geodome.co.uk.

[11] "SeaPlace transition Piece." [Online]. Available: http://www.seaplace.es/projects/offshore-renewable-energy/proyecto-seamar/.

[12] Ambau GmbH, "AMBAU Press information," 2013.

[13] STL, "Fe-Safe 6 Fatigue Theory Reference Manual," vol. 2, Dassault Systems, 2014.

[14] S. B. and R. Patibandla, "Metal Fatigue and Basic Theoretical Models: A Review," *Alloy Steel - Prop. Use*, pp. 203–236, 2011.

[15] J. A. F. de O. Correia, "an Integral Probabilistic Approach for," University of Porto, 2014.

[16] O. Basquin, *The exponential law of endurance tests. Proc Am Soc Test Mater 1910;10:625–30. .*

[17] J. Schijve, *Fatigue of structures and materials*. Springer Netherlands, 2009.

[18] J. Morrow, "Cyclic plastic strain energy and fatigue of metals. In Africa Damp Cyclic Plast ASTM STP 1965; 378:45–87.," in *Cyclic plastic strain energy and fatigue of metals.*, 1965, pp. 45–87.

[19] I. Stephens, Ralph, A. Fatemi, R. Stephens, Robert, and O. Fuchs, Henry, "Metal Fatigue in Engineering," *Journal of Engineering Materials and Technology*. p. 472, 2001.

[20] W. Ramberg and W. R. Osgood, "Description of stress-strain curves by three parameters," *Natl. Advis. Comm. Aeronaut.*, p. Technical Note No. 902, 1943.

[21] J. (LF) Coffin, *A study of the effects of the cyclic thermal stresses on a ductile Metal*. 1953.

[22] K. N. Smith, P. Watson, and T. H. Topper, "Stress-Strain Function for the Fatigue of Metals," *Journal of Materials*, vol. 5. pp. 767–778, 1970.

[23] G. Sines, "Behaviour of metals under complex stresses," *Sines G, Waisman JL, Ed. fatigue. New York McGraw-Hill; 1959.*, pp. 145–69, 1959.

[24] T. Matake, "An explanation on fatigue limit under combined stress," *Bull JSME 1977*, vol. 20, no. 257–63, 1977.

[25] STL, "Fe-Safe 6 User Manual," 2014.

[26] J. P. Martins, L. Simões da Silva, and A. Reis, "Eigenvalue analysis of cylindrically curved panels under compressive stresses--Extension of rules from EN 1993-1-5," *Thin-Walled Struct.*, vol. 68, pp. 183–194, 2013.

[27] D. D. Env, Bsi, and D. D. Env, "Eurocode 3 : Design of steel structures —," *Design*, vol. 3, no. April, 2001.

[28] J. P. Almeida, "Hybrid Lattice-Tubular Steel Onshore Wind towers: Conceptual Design of Tower and Transition segment," University of Coimbra, 2016.

[29] A. M. P. de Jesus, R. Matos, B. F. C. Fontoura, C. Rebelo, L. S. da Silva, and M. Veljkovic, "A comparison of the fatigue behavior between and steel grades," *J. Constr. Steel Res.*, vol. 79, no. 0, pp. 140–150, 2012.

[30] J. A. F. O. Correia, A. M. P. de Jesus, A. Fernández-Canteli, and R. A. B. Calçada, "Modelling probabilistic fatigue crack propagation rates for a mild structural steel," *Frat. ed Integrita Strutt.*, vol. 31, pp. 80–96, 2015.

[31] S. K. Koh and R. I. Stephens, "Mean Stress Effects on Low Cycle Fatigue for a High Strength Steel," *Fatigue Fract. Engng Mafer. Strucl*, vol. 14, no. 4, 1991.

[32] J. Peippo, “A modified nominal stress method for fatigue assessment of steel plates with thermally cut edges,” 2015.

[33] S. Velázquez, J. A. Carta, and P. Ramírez, “A review of wind speed probability distributions used in wind energy analysis: Case studies in the Canary Islands,” *Renew. Sustain. Energy Rev.*, vol. 13, no. 5, pp. 933–955, 2009.

[34] EN 1993-1-9, “Eurocode 3: Design of Steel Structures: Fatigue,” *Eur. Commitee Stand.*, vol. 3, 2005.